DEVELOPMENTS IN THE UNDERSTANDING OF THE DINITROSYL IRON UNIT: ITS STABILIZATION, REACTIVITY, AND NITRIC OXIDE RELEASE

A Dissertation

by

RACHEL BETH CHUPIK

Submitted to the Office of Graduate and Professional Studies of
Texas A&M University
in partial fulfillment of the requirements for the degree of

DOCTOR OF PHILOSOPHY

Chair of Committee,	Marcetta Y. Darensbourg
Committee Members,	Paul Lindahl
	Michael Nippe
	Alice Villalobos
Head of Department,	Simon North

December 2017

Major Subject: Chemistry

ABSTRACT

Dinitrosyl iron complexes (DNICs), as well as S-nitrosothiols (RSNOs), form endogenously to provide a stable means of storage and transport for the highly reactive signaling molecule, nitric oxide. Through the development of biomimetic complexes, the fundamental chemistry of such DNICs is established within a range of ligand sets as anionic and neutral donors that stabilize the dinitrosyl iron unit, DNIU, in oxidized $\{Fe(NO)_2\}^9$ and reduced $\{Fe(NO)_2\}^{10}$ (Enemark-Feltham notation) redox levels. This amorphous electronic characteristic is readily accommodated by amino acid residues, cysteinyl S- and histidine N-donors, and their surrogates, as ligands to iron. My research targets a greater understanding of DNIC reactivity with components of cellular environments, the possible connections between the electronically similar d^9, Cu(II) and d^{10}, Cu(I), redox couple, the DNIC/Copper/RSNO connections, structural studies of aggregates of DNICs with metallodithiolates, as well as design strategies for NO-release therapeutic development of DNICs.

A stable, reduced, $\{Fe(NO)_2\}^{10}$ DNIC containing a bipyridyl ligand, [(neo)Fe(NO)$_2$] (neo = 2,9-dimethyl-1,10-phenanthroline) was used to explore redox switches and N_2 ligand exchange between copper and the Fe(NO)$_2$. Both Cu^I and Cu^{II} sources were found to promote neo ligand transfer from the DNIU with concomitant NO release. With Cu^{II}, redox processes were also involved, as evidenced by the formation of a mixture of oxidized $\{Fe(NO)_2\}^9$ DNICs, in addition to both Cu^I- and Cu^{II}-neo

complexes. Copper is known to catalyze the release of NO from RSNOs, and our discoveries found here are the first biomimetic investigation of copper's reactivity with DNICs.

Reaction of an RSNO with reduced, $\{Fe(NO)_2\}^{10}$ DNICs, $[(L)_2Fe(NO)_2]$ (L = CO or neo), results in NO release and the formation of a unique $(\mu\text{-S})(SR)_2[Fe(NO)_2]_4$ cluster, containing an interstitial sulfide. Such a cluster can be visualized as a plausible intermediate in the known conversion of DNICs to FeS clusters. The NO released showed complete scrambling with ^{15}N-labeled RSNO.

Although DNICs are promising NO-delivery candidates, the lack of biocompatible examples has hindered their development into useful therapeutics. We reported the first DNICs with pendant thiosugars, isolated in both monomeric and dimeric form. Cytotoxicity towards endothelial cells was low and steady NO release over several hours was observed in aqueous media.

DEDICATION

To my Lord and Savior, Jesus Christ to whom belongs all the glory, to my beloved parents, siblings and boyfriend who have shown me such unfailing love and support.

ACKNOWLEDGEMENTS

It has been a great privilege and honor to have had Marcetta Y. Darensbourg as my advisor. She is an accomplished and outstanding chemist who truly cares about her students. She has been so supportive and encouraging, and has challenged me to do my very best. I greatly admire her dedication to her research and to teaching, qualities that I desire to emulate in my own career. I also appreciate her humble attitude and eagerness to credit others for even their smallest accomplishments. Thank you again, Marcetta, for your guidance and mentorship, and for inspiring me to become a better scientist and teacher.

Thank you to my committee members, Professors Paul Lindahl, Alice Villalobos, and Michael Nippe for serving on my committee and for providing help when needed. The classes I took from you, Dr. Lindahl, were some of my favorites in graduate school, and provided me with an excellent foundation on which to build my career in chemistry. Dr. Villalobos, you were always so encouraging and it was a pleasure having you as part of my committee. I would also like to thank Dr. Soon-Mi Lim for the wonderful collaboration and all her guidance as we entered an area of research with which we were not very familiar. Finally, I would also like to thank Dr. Amber Schaefer for her mentorship, guidance and friendship throughout graduate school.

Thank you also to all the current and former Darensbourg group members. Pokhraj, thank you for always being a listening ear, for helping me with any and

everything, and for just being a good friend. Jason and Danielle, thank you both for training me, answering my many questions, and guiding me, especially when I first began graduate school. I also want to thank Mark (Chung-Hung Hsieh) for being an excellent undergraduate mentor and for teaching me so many essential synthetic skills. Thanks also to my other current group members, Chris, Chase, Xiemue, Shengda, Nick, and Debangsu for your support and for all the good times we've had.

My dear parents also deserve many thanks for loving and supporting me, and for instilling in me the values of hard work and serving others. Thank you, Mom and Dad for all you have taught me, most importantly to seek God first. And my amazing, loving siblings, Jon, Becky, Joe, Liz, Josiah, Joshua, Esther, Jeremy, and Jacob, you all are the best siblings anyone could ask for and I thank each one of you for loving me and always being there for me. Nanny, thank you for teaching me during my homeschool years and for your wonderful advice that slow and steady wins the race.

I also want to thank my precious boyfriend Zach for his unfailing support, selfless love and constant encouragement. You are such a blessing and I appreciate your help with the references and in formatting my dissertation. Thank you also to my sweet friend Pearl for her assistance in getting all my references formatted for the dissertation.

Finally, I would also like to thank Dr. Sharon Hoffman for her friendship, for all that she taught me in freshman chemistry and beyond, and for being the inspiration for me to pursue my Ph.D. in chemistry.

CONTRIBUTORS AND FUNDING SOURCES

Contributors

The work reported within this dissertation was supported by a dissertation committee consisting of Professor Marcetta Y. Darensbourg, advisor, Professors Paul Lindahl and Michael Nippe, both of the Department of Chemistry, and Professor Alice Villalobos, of the Department of Nutrition and Food Sciences.

The data presented in Chapter III was done in collaboration with Didjay Bruggeman, a visiting scholar from Leiden University, and Magy Mekhail, an undergraduate student in the Department of Chemistry. The work reported in Chapter V was done in collaboration with Dr. Randara Pulukkody of the Department of Chemistry, and was published in 2017. The Griess assays reported in Chapter V were carried out by Professor Soon-Mi Lim of the Department of Chemistry, and the cell viability assays were performed by Sarosh Khan of the Department of Chemistry. Portions of the work reported in Chapter VI were carried out in collaboration with Drs. Pokhraj Ghosh and Chung-Hung Hsieh, both of the Department of Chemistry.

All other work reported in this dissertation was completed independently, under the supervision of Marcetta Y. Darensbourg of the Department of Chemistry.

Funding Sources

TABLE OF CONTENTS

LIST OF FIGURES

xiii

xiv

xvi

LIST OF TABLES

CHAPTER I

INTRODUCTION AND LITERATURE REVIEW

Nitric Oxide: the Essential Free Radical

The area of nitric oxide chemistry has exploded in the thirty years since Ignarro, Furchgott, and Murad made the Nobel Prize winning discovery that nitric oxide was actually the endothelial-derived relaxing factor responsible for vascular relaxation in smooth muscle cells.[1] Since that time, we have learned that in addition to vascular relaxation, endogenous nitric oxide also plays a seminal role in other essential biological processes including platelet aggregation and adhesion, the immune response to infection and wound repair.[2] Additionally, NO is also involved in cancer biology and pathology, serving as a "two-edged sword" in which low concentrations of NO actually promote cell growth, whereas higher concentrations induce apoptosis.[2]

The fundamental basis of understanding how living organisms use NO involves triggers for regulation of its biosynthesis. Nitric oxide is generated in vivo via a five-electron oxidation of L-arginine to L-citrulline, catalyzed by the nitric oxide synthase (NOS) (Figure I-1).[3]
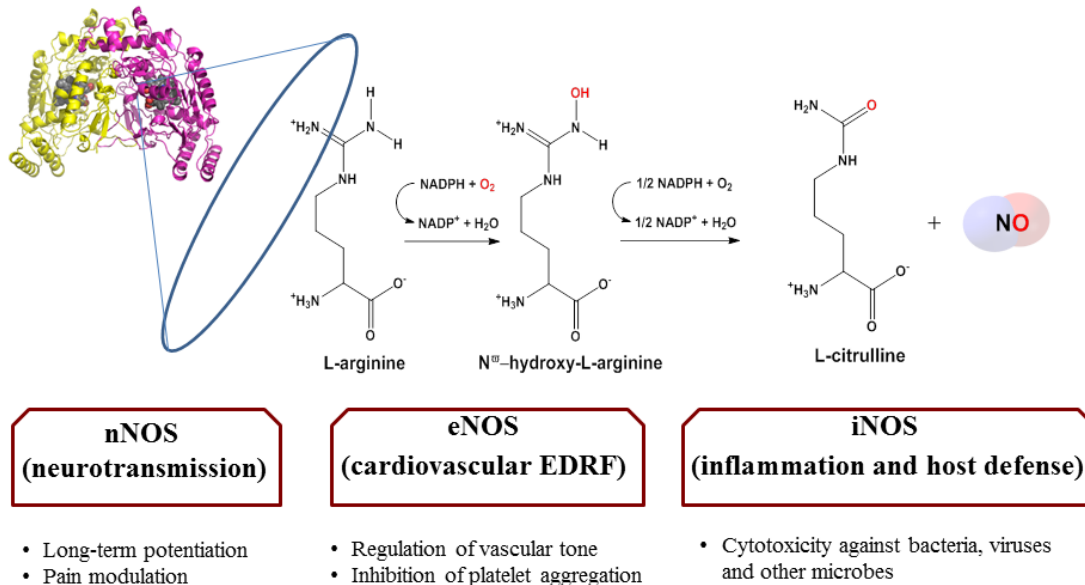
Figure I-1. Nitric oxide synthase (NOS) catalyzes the NADPH-dependent conversion of L-arginine to L-citrulline, in the process producing nitric oxide. The NOS exists in three different isoforms (shown in the boxes) each of which fulfills specific and distinct functions.

This family of heme-containing enzymes exists in three isoforms, namely neuronal (nNOS), endothelial (eNOS), and inducible (iNOS), each of which is encoded by a separate gene. These three isoforms can be classified into two broad classes of NOS based on the concentration of NO produced. Both nNOS and eNOS produce low concentrations of NO and are associated with signaling functions. The nNOS is responsible for cell communication and is expressed in both nerve cells and skeletal muscle, while eNOS is located in the endothelium and is responsible for vasodilation. The iNOS, on the other hand, catalyzes the production of large amounts of NO in response to immune system triggers, thus acting as an integral part of the immune

2

system.[4] From this, it can be seen that the concentration of NO released determines its function. At concentrations in the picomolar to low nanomolar range, NO plays a protective role. However, at concentrations above 400 nanomolar, its cytotoxic and regulatory effects predominate.[5] This concentration dependent function is displayed in Figure I-2.[6] As a reactive, free radical species, NO must be highly regulated and cannot be recognized by proteins via the weak intermolecular interactions that typify the recognition of other secondary messengers.[7] Hence, NO signals primarily by binding to the ferrous heme of soluble guanylate cyclase, an entirely novel signaling mechanism at the time of its discovery.[7] Additionally, because of the highly reactive nature of NO, it is tightly regulated with a lifetime of no more than 2 s as a free molecule in the biological milieu.

Thus, other forms of NO must exist to facilitate its storage and transport; these have been identified as S-nitrosothiols (RSNOs) and dinitrosyl iron complexes (DNICs).[8] S-nitrosothiols form upon reaction of nitric oxide with thiols present in the plasma. In the cardiovascular system, RSNOs, as the carriers of NO, are responsible for promoting vasodilation, inhibiting platelet aggregation, and regulating Ca^{2+} channel function that influences myocyte contractility and electrophysiologic stability.[9] The mechanism by which RSNOs release NO is discussed in detail in the section titled "RSNOs and the interplay of Cu and Fe in NO Release."
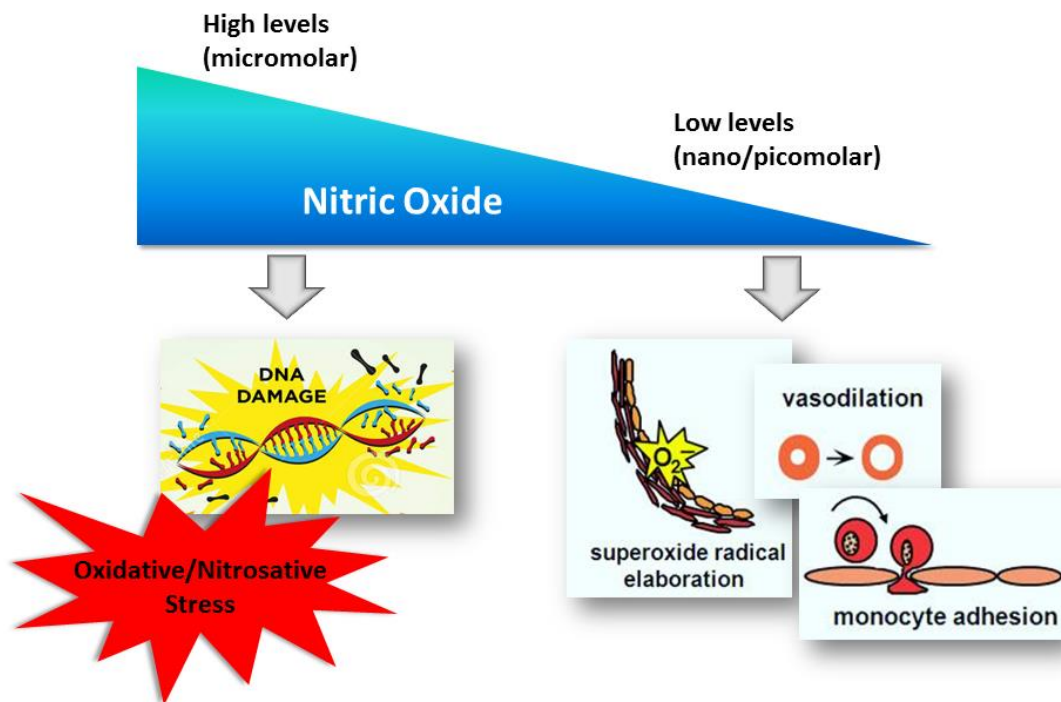
Figure I-2. Nitric oxide can be described as a two-edged sword, depending upon concentration. As depicted above, at micromolar concentrations, NO induces DNA damage and cell death, while at lower nano- and picomolar concentrations, NO serves protective roles such as vasodilation or even as part of the immune system (right hand side). Images within this figure were adapted from Arginine Cardio. Science of Nitric Oxide-What Nitric Oxide does for the health and wellness of our cardiovascular system, according to Dr. Rainer Böger, M.D. https://www.argininecardio.com/science-of-nitric-oxide.php (access July 21, 2017).[6]

Dinitrosyl Iron Compounds (DNICs): Discovery and Biological Presence

Biological DNICs (Figure I-3) were discovered in the mid-1960s from their characteristic EPR signal with g ~ 2.03 that arises from a single tetrahedral iron center coordinated by two nitrosyl ligands and two thiol/thiolate ligands.[10] These paramagnetic DNICs have been shown to exist in both protein-bound[11] and low molecular weight

(LMW)[12] forms; however, there is also evidence for the formation Roussin's red ester type complexes as well as Roussin's black salts upon exposure of iron sulfur clusters to NO.[13,14]
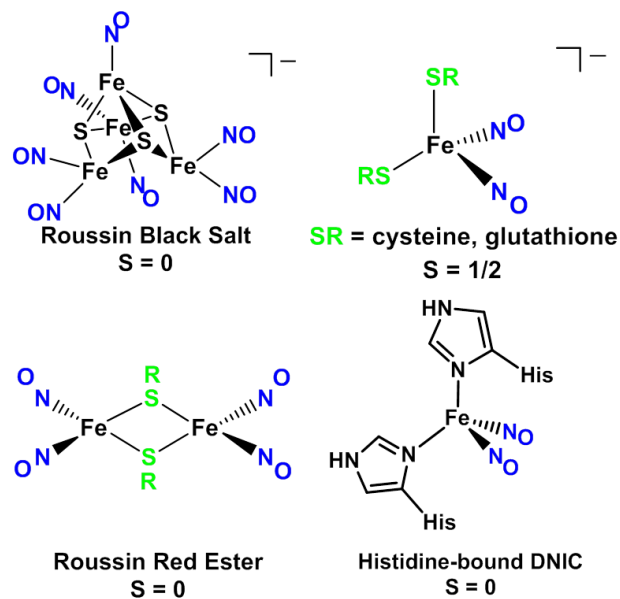
Figure I-3. Various forms of DNICs proposed to be present in biological systems.

As such, it is generally understood that these naturally occurring DNICs most likely contain thiol ligands, given the abundance of glutathione (GSH) present in the cell, coupled with the high affinity of thiol ligands for the dinitrosyl iron unit (DNIU). Many studies have been conducted to elucidate the mechanism of formation of DNICs, revealing that nitrosylation of both [2Fe-2S] and [4Fe-4S] clusters produce DNICs.[15] In

addition, the LMW-DNICs are thought to form as a result of thiol ligand exchange with the protein-bound form.[12]

Iron-sulfur cluster degradation is not the only pathway by which DNICs are formed. Work by Toledo *et al.*[16] and Hickok *et al.*[17] report that the chelatable iron pool (CIP) also plays a major role.[17] The CIP is a small, dynamic reservoir of iron utilized in the movement of iron between cellular compartments and metalloproteins.[16] Treatment of macrophages with NO resulted in DNIC formation with concentrations of DNIC equal to or greater than the concentration of the chelatable iron.[17] Concurrent cell treatment with the metal chelator, desferrioxamine, resulted in no DNIC formation, confirming the source of iron in the DNICs formed when the chelator was not present was indeed the CIP.[17] Evidence also exists for DNIC formation from the iron-catalyzed decomposition of RSNOs; this report will be discussed in detail in the section addressing RSNOs, vide infra.[18]

Key to the mutual affinities of NO and iron are their electronic characteristics. Delocalization between the valence orbitals of iron and those of NO arises from similar energy levels between the Fe 3d and low-lying NO π^* orbitals, which renders oxidation state assignments for Fe ambiguous; the term "non-innocent' ligand is epitomized by NO.[19] In an attempt to avoid this ambiguity, Enemark and Feltham proposed a notation wherein the electronic structure is denoted as $\{Fe(NO)_2\}^n$, where n refers to the number of d electrons plus the number of NO π^* electrons.[20] However, this notation simply avoids the issue of the actual electron distribution, especially in interpretation of spectroscopies that might reflect physical and reactivity properties. For a more explicit

description of electron distribution, computations and advanced spectroscopic techniques are needed.

Synthetic Analogs

The complexities of the biological environment render detailed cellular studies of DNICs extremely challenging. Hence chemists have built a library of synthetic DNICs in order to define spectroscopic signals, compare structures, and understand their chemical reactivity. As outlined in an extensive review by Liaw *et al.* DNICs can be categorized into two broad categories: mononuclear (including both the classical four-coordinate and non-classical five- and six-coordinate DNICs) and dinuclear (also referred to as Roussin's red esters).[21] The typical four-coordinate DNICs of general form $[L_2Fe(NO)_2]^{0/-1/-2}$ have been isolated in both redox levels and with a wide range of ligands, some examples of which are shown in Figure I-4.[15,22-24]
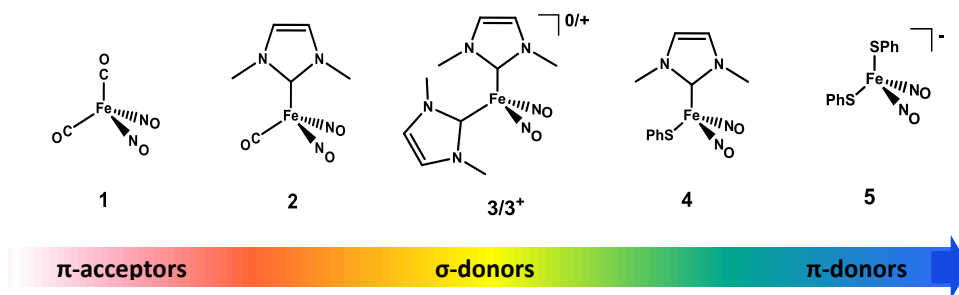
Figure I-4. Examples of DNICs that have been synthesized (**1-5**)[15,22-24] that incorporate a range of donor ligands as well as different oxidation states $\{Fe(NO)_2\}^{10}$ (**1** and **2**), both $\{Fe(NO)_2\}^{10/9}$ (**3/3⁺**) and $\{Fe(NO)_2\}^9$ (**4** and **5**).

The EPR active, oxidized $\{Fe(NO)_2\}^9$ DNICs exist as both neutral and anionic species with S-, N-, O- and C-donor ligands.[21] Liaw *et al*. have also investigated the exchange of biologically relevant S-, N-, O- and C-donor ligands with the $\{Fe(NO)_2\}^9$, $[X_2Fe(NO)_2]^-$ motif, finding the binding affinity to be thiolate (SR^-) > imidazolate (Im^-) > phenolate (OPh^-) > carboxylate (COO^-) > nitrite (NO_2^-) > nitrate (NO_3^-).[25] [We note that this order might not hold for DNICs in a biological system, considering that one of the glutathione ligands of the bis-glutathione DNIC is replaced by an active site tyrosine upon addition of the glutathione S-transferase (GST) to the bis-glutathione DNIC (See section on GST for further discussion)]. The EPR silent, reduced $\{Fe(NO)_2\}^{10}$ DNICs, on the other hand, prefer the neutral N- and C-donor ligands, although there is at least one example of a dianionic DNIC in the $\{Fe(NO)_2\}^{10}$ oxidation state where the Fe of the DNIU is coordinated by two ethanethiol ligands.[21,26]

Mononuclear DNICs with expanded coordination numbers have only been isolated in the oxidized, $\{Fe(NO)_2\}^9$ state with S-, N- and O-donor ligands, and adopt square pyramidal and trigonal bipyramidal geometries for the five-coordinate DNICs and octahedral geometry for the six-coordinate DNICs.[27] For the dinuclear or Roussin's red ester DNICs, the two DNIUs are bridged by S-donor (or in one case, O-donor) ligands and exist in the anitferromagnetically coupled, EPR silent, neutral $[\{Fe(NO)_2\}^9\text{-}\{Fe(NO)_2\}^9]$ state, the anionic mixed valent, EPR active, $[\{Fe(NO)_2\}^9\text{-} \{Fe(NO)_2\}^{10}]$ state, or the dianionic $[\{Fe(NO)_2\}^{10}\text{-} \{Fe(NO)_2\}^{10}]$ state, which is EPR silent.[28-30]

X-ray absorption spectroscopy, Fe/S K-edge XAS,[25,30,31] and X-ray emission spectroscopy, valence to core (V2C) Fe Kβ XES,[32] supported by *ab initio* DFT

calculations, in addition to direct probing of the Fe-NO and N-O bond strengths through IR, resonance Raman and Nuclear Resonance Vibrational Spectroscopy studies, have provided more definitive insights into the Fe-NO bonds.[11,33,34] The Fe K-edge XAS pre-edge energies of various tetrahedral $\{Fe(NO)_2\}^9$ DNICs were reported to be $\sim 7113.4 - 7113.9$ eV, placing them between the Fe^{II} and Fe^{III} standards.[35] On this basis, the electronic state of the $\{Fe(NO)_2\}^9$ DNICs is assigned as a resonance hybrid of $\{Fe^{II}(\bullet NO)(NO^-)\}^9$ and $\{Fe^{III}(NO^-)_2\}^9$ electronic states.[35] Liaw *et al*. further report that ligation by hard O-containing ligands polarizes the $\{Fe(NO)_2\}^9$ core to possess more $\{Fe^{III}(NO^-)_2\}^9$ character that DNICs coordinated by soft S-containing ligands, as confirmed by both DFT calculations and a combination of S K-edge pre-edge and thiolate energy peaks.[32] Furthermore, the reduced $\{Fe(NO)_2\}^{10}$ DNICs are assigned as $\{Fe^{II}(NO^-)_2\}^{10}$ in which high spin Fe^{II} (S = 2) is antiferromagnetically coupled with two triplet NO^- ligands.[20,23]

All such studies highlight the $Fe(NO)_2$ as a singular unit, with considerable covalency in the Fe-NO bond and likely quite resistant to NO exchange with classical two-electron donor, diatomic ligands such as CO or CN^-. The next section reviews NO release from DNICs, factors that promote NO release, and assays that may be used to characterize the process.

NO Release from DNICs
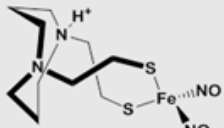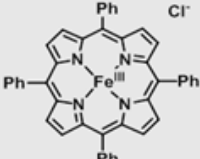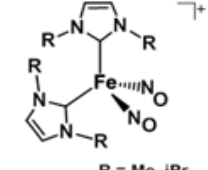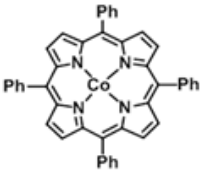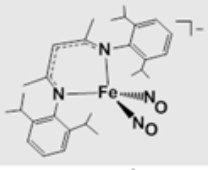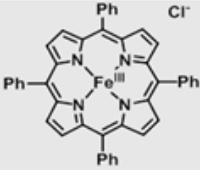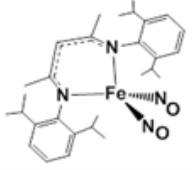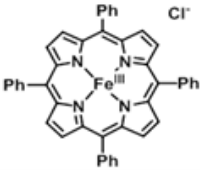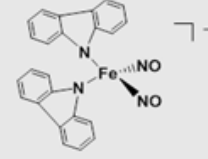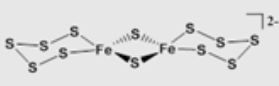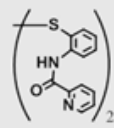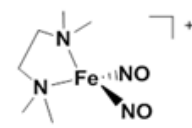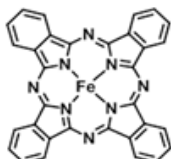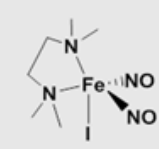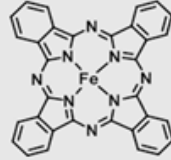
With the numerous vital roles played by NO and the therapeutic potential for NO-bearing species, understanding the process of NO release is of great importance. Ford *et al*. have done outstanding work in this area by developing a water-soluble, dye-

derivatized dimeric DNIC $Fe_2(\mu\text{-}RS)_2(NO)_4$ (RS = 2-thioethyl ester of fluorescein) that uses both single and two-photon excitation to sensitize NO release.[36,37] As measured by an NO electrode, $Fe_2(\mu\text{-}RS)_2(NO)_4$ releases ~3.2 mol of NO per mol of compound.[37] Although this is a promising strategy for NO therapy, the applications are limited to sites that are readily penetrated by the light source. Additionally, the use of light to promote NO release fails to explain the transfer of NO from naturally occurring DNICs within a biological system. The following section will review those studies that have examined other stimuli to encourage NO release/transfer from DNICs.

Considering the importance of understanding the mechanism for NO release from DNICs, surprisingly few studies have been devoted to this area of DNIC chemistry. Table I-1 summarizes the studies that have examined NO release from DNICs. A structure of the DNIC used in each study, along with the NO trapping agent and the stimuli used to induce NO release are provided in the table. Most of the NO release studies reported to date utilize an NO-trapping agent to promote transfer of NO from the DNIC. In 2006, the M. Y. Darensbourg laboratory reported NO transfer from a unique dithiolate DNIC to an iron porphyrin, entry 1, Table I-1.[38] Even when performed in the dark, NO transfer still occurred, suggesting that the associative process could derive from either protonation from the ligand or through a bimolecular interaction of the two reagents.[38] Additionally, the rate dependence on acid implies that NO is transferred to the Fe^{III} porphyrin as HNO. This is one of the few studies that identified the iron product following removal of one NO. A role for protonation in NO release is also supported by work from Vanin *et al*. that demonstrated that acidic pH enhances the NO release rate.[39]

The M. Y. Darensbourg laboratory has carried out NO release studies with bis-N-heterocyclic (NHC) DNICs.[22] N-heterocyclic carbene ligands have become a standard of organometallic chemistry for their strong σ-donating capabilities and ability to bind to and stabilize a wide range of transition metal complexes.[22] It should also be noted that the NHC can be viewed as a mimic for imidazole which in turn is a surrogate for histidine.[40] The $\{Fe(NO)_2\}^9$ NHC-DNICs were found to release (or transfer) NO in the presence of Co(TPP), while no NO release was observed for the $\{Fe(NO)_2\}^{10}$ DNICs (entry 2, Table I-1). Clearly, with organometallic-like DNICs, oxidation leads to destabilization and NO release.

Table I-1. Summary of the DNICs that have been investigated for NO release, along with the promoter for the NO release.

	Complex	NO Receiver	Trigger	Reference
1			Addition of the porphyrin	Inorg. Chem. 2006, 11, 359–370. (MYD)
2	R = Me, iPr		Addition of the porphyrin	Inorg. Chem. 2011, 50, 8541-8552. (MYD)
3			Addition of the porphyrin	Inorg. Chem. 2011, 50, 157. (Lippard)
4			Addition of the porphyrin with light or heat	Inorg. Chem. 2011, 50, 157. (Lippard)
5				Inorg. Chem. 2005, 44, 5872-5881. (Liaw)
6			Spontaneous Decomposition	Chem. Sci., 2014, 5, 2374. (Kim)
7			Addition of AgPF$_6$	Chem. Sci., 2014, 5, 2374. (Kim)

In 2011, Lippard *et al.* also reported reductive nitrosylation of Fe(III)(TPP)Cl (where TPP = 5,10,15,20-Tetraphenyl 21H,23H-porphine) by an $\{Fe(NO)_2\}^9$ DNIC [Fe(NO)$_2$(Ar-nacnac)] (where Ar-nacnac = anion of [(2,6-diisopropylphenyl)NC(Me)]$_2$CH) with dissociation of either NO or NO$^-$ (entries 3 and 4, Table I-1).[41] When this DNIC is reduced to the $\{Fe(NO)_2\}^{10}$ state, it displayed rapid electron transfer to the Fe(III)(TPP)Cl. The $\{Fe(NO)_2\}^9$ DNIC resulting from the electron transfer then nitrosylated the Fe(II)(TPP).[41]

Liaw *et al.* ventured from the use of porphyrins and showed that addition of different chelating ligands to a carbazolate DNIC triggers the release of either NO$^+$, NO$^{\cdot}$, or NO$^-$, depending upon the incoming substitution ligand (entry 5, Table I-1).[42] Following the idea that incoming substitution ligands promote NO release, biological studies have shown that the rate of NO release is dependent upon the free thiol concentration, with an increase in NO release in the presence of thiols.[43] Additionally, Vanin *et al.* claim that the glutathione-DNIC only demonstrated NO release in the presence of iron chelators, suggesting that the chelator is needed to promote the NO release.[44]

Kim *et al.* reported an interesting NO release strategy (entry 7, Table I-1) in which loss of the iodide from the stable five-coordinate DNIC [Fe(TMEDA)(NO)$_2$I] generates the metastable $\{Fe(NO)_2\}^9$ species [Fe(TMEDA)(NO)$_2$]$^+$ that spontaneously decomposes and releases NO, as confirmed by NO capture by an iron porphyrin.[45] Considering that the intracellular chloride ion concentration is much lower than the extracellular concentration, Kim *et al.* proposed that the labile halide would be lost upon

13

entering the cell, yielding the active species $[Fe(TMEDA)(NO)_2]^+$.[45] Indeed, the activation of cisplatin is known to occur in this same manner, namely loss of Cl^- upon entering the cell.[46] Gene expression levels of heme oxygenase-1 increased significantly upon treatment of cells with $[Fe(TMEDA)(NO)_2I]$, while the inducible nitric oxide synthase expression was downregulated.[45] Both these results were consistent with what is expected when cells are treated with NO.

Understanding the chemistry of these DNICs and factors affecting their NO release is essential towards developing such complexes into NO-releasing pharmaceuticals. The most promising NO release agent in therapeutic development is the water soluble bis-glutathione DNIC reported by Vanin *et al*. Under the name Oxacom®, this NO-releasing drug is currently in phase II clinical trials.[47,48] It has shown a host of biological activities including prolonged hypotension, attenuated platelet and erythrocyte aggregation, promotion of skin wound healing and effects on penile erection.[48] In addition, Shamova *et al*. demonstrated that this glutathione containing DNIC blocks early stage cell aggregation in HeLa cells.[49]

RSNOs and the Interplay of Cu and Fe in NO Release

Unlike the rather unexplored area of NO release/transfer from DNICs, this process has been well studied in RSNOs, the other biological carrier of NO. The RSNOs are readily made from the electrophilic nitrosation of thiol groups on biomolecules ranging from sugars to amino acids or simple peptides. Within the plasma, the low molecular weight forms, for example S-nitrosoglutathione, are present in submicromolar concentrations.[50] As a reservoir of NO, RSNOs participate in the post-translational

modification of proteins via S-nitrosation of cysteine residues, and are reported to protect against myocardium, lung and airway injuries.[9]

Early kinetic studies of the rate of decomposition of RSNOs yielded conflicting and inconsistent results. Rate expressions of zero-, half-, first-, and intermediate-order were reported for aqueous solutions.[51] These puzzling results were finally deconvoluted with the suggestion that trace metal ions were present in the media solutions used in these studies and could be promoting the RSNO decomposition. Indeed, addition of the metal chelator, EDTA, stopped the decomposition reaction, leading to the major finding that trace metal ions present in the media were responsible for the decomposition of RSNOs.[52] Further studies in which Williams *et al*. added a slight excess of metal ions (over the amount of EDTA added) revealed that Cu^{2+}, even at concentrations as low as 10^{-6} mol dm^{-3} promoted the release of NO from the RSNOs.[53] Ferrous ions also facilitated the reaction, albeit to a much lesser extent, while Mg^{2+}, Zn^{2+}, Ca^{2+}, Ni^{2+}, Co^{2+}, Mn^{2+}, Cr^{3+} or Fe^{3+} had no measurable effect.[53]

Although copper was clearly the main catalyst for this decomposition reaction, in subsequent kinetic studies some findings, i.e. zero-order kinetics under some circumstances and an induction effect in many experiments, pointed to Cu^+ rather than Cu^{2+} serving as the true promoter. Indeed, addition of neocuproine, known for its high affinity for and selective binding to Cu^+, virtually stopped the decomposition reaction.[54] Subsequent studies by Williams, Payne, and Warren have further supported the fact that copper effectively catalyzes the decomposition of RSNOs, thereby releasing NO.[55]

15

Two catalytic pathways are suggested for the RSNO decomposition reaction, both of which are shown in Figure I-5, as adapted from an excellent review by Szaciłowski and Stasicka.[56] Path (a) is proposed by Williams *et al*. in which Cu^{2+} is first reduced to the active Cu^+ before reacting with the RSNO, thus producing NO gas and half an equivalent of RSSR.[55]
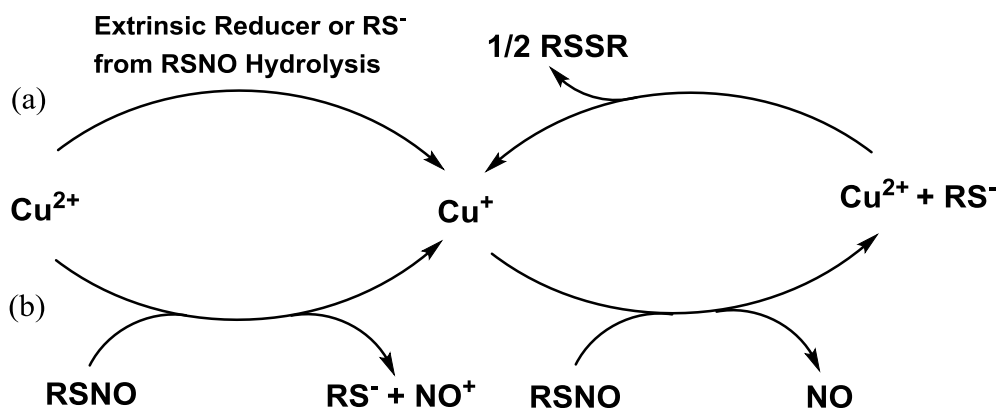
Figure I-5. The catalytic cycle involving Cu^+ for the decomposition of RSNOs *in vivo*. Pathway (a) is proposed by Williams *et al*. and pathway (b) by Szaciłowski and Stasicka. Figure adapted from a similar figure from Szacilowski, K.; Stasicka, Z. *Prog. React. Kinet.* **2000**, *26*, 1-58.[56,58]

In pathway (b), as proposed by Szaciłowski and Stasicka, the RSNO binds to the Cu^{2+} forming a Cu^+-RSNO adduct through an intramolecular electron transfer.[56] This adduct then decomposes to the radical RS·, NO^+, and the catalytically active Cu^+ species can then react with a second RSNO and produce NO.

16

The binding modes of the RSNO to a metal center can be envisioned in four different ways, as proposed by Richter-Addo (Figure I-6).[57] Experimentally, only S- and N-bonded coordination modes have been observed.[56]
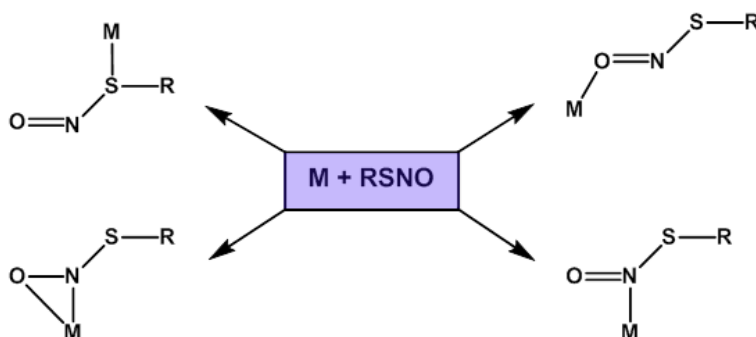
Figure I-6. Four different binding modes are possible for the RSNO to a metal center. Working clockwise starting from the top right, there can be binding through the oxygen, through the nitrogen, through both the oxygen and the nitrogen, or through the sulfur. Adapted from a similar figure by Szaciłowski and Stasicka.[56]

Electron rich metal ions, such as Cu^I would be expected to coordinate through the sulfur, which allows the occupied metal orbitals to engage in back donation. The S→M σ bonding coupled with π back donation weakens the S-N bond. For those metal ions with unoccupied d-orbitals, bonding through the nitrogen would be preferred. However, Warren *et al*. recently reported RSNO binding to a Cu^I center, with bonding through the nitrogen.[58]

17

In 2001, Vanin *et al*. questioned the conclusion that Cu^+ was the primary catalyst for NO release from RSNOs by reporting that nitric oxide initiates the binding of neocuproine to Fe^{II}.[59] This study merits consideration since Williams *et al*. used the selectivity of neocuproine for Cu^+ as part of the evidence that Cu^+ (rather than iron) was the primary catalyst.[54]

In a subsequent study, Vanin *et al*. showed that addition of either Fe^{2+} or Fe^{3+} ions accelerated the degradation of RSNO (where R = cysteine) concomitant with the appearance of a DNIC, where the RSNO was the source of the NO in the DNIC.[18] The DNICs were identified by the appearance of the prototypical EPR signals centered near g = 2.03, and assigned to either cysteine-containing (in the case where L-cysteine was also added) or to phosphate-containing DNICs (when in phosphate buffer).[18]
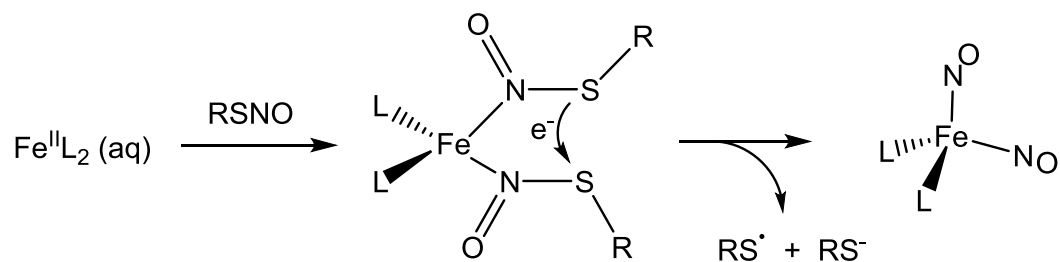
Figure I-7. Proposed mode of interaction between iron and RSNOs, which results in the formation of a DNIC as opposed to releasing free NO, as is seen in the copper catalyzed system.

As shown in Figure I-7, these DNICs are thought to form when each iron ion binds two RSNOs through the nitrogen of the NO, providing for the mutual oxidation-reduction of the RSNO molecules.[18] Disulfide is then eliminated and the remaining NO and NO^+ maintain their connection to the iron center thereby forming a DNIC.

Although Vanin's main claim is that iron rather than copper is the primary catalyst for RSNO decomposition, the studies by Williams and others discussed above are both thorough and extensive and provide compelling evidence for a seminal role of copper. The significance of Vanin's work is not that iron instead of copper catalyzes RSNO decomposition, but rather that the role played by iron is intertwined with the formation of DNICs. Early discoveries by Williams support Vanin's findings that ferrous ions do indeed catalyze RSNO decomposition, albeit not as effectively as do copper ions.[52,55] What Vanin has highlighted, perhaps unrecognized, is a fascinating correlation between copper and the DNIU.

Correlation Between Cu and DNIU

The correlation between copper and the DNIU is not confined to the story regarding the decomposition of RSNOs. In fact, examples abound in both biological and chemical studies. Glutathione S-transferase (GST) is known to strongly bind copper.[60-63] Interestingly, the very first crystal structure of a protein-bound DNIC featured the GST protein.[64] The electronic similarity of copper and the $Fe(NO)_2$ unit is demonstrated in thiolate/disulfide interconversion reactions which involve the redox couples, $\{Fe(NO)_2\}^{9/10}$ and Cu^{II}/Cu^{I}.[65-68] Furthermore, Cu and $Fe(NO)_2$ in their two redox levels can form structurally analogous complexes as showcased by tetramolecular and cluster

compounds wherein the Cu and Fe(NO)$_2$ units occupy analogous sites.[15,69-71] This section will explore this correlation in depth.

Glutathione S-Transferase (GST)

Maintaining the redox balance of the cell is essential for survival. The balance is achieved by a tripeptide consisting of a glutamate, cysteine and glycine called glutathione (GSH), which exists at millimolar concentration in the cell.[72] Glutathione serves as substrate for glutathione-S transferase (GST), in which capacity it facilitates the removal of species known to form reactive oxygen species (ROS) such as free radicals, peroxides, lipid peroxides and metal ions.[73]

Glutathione-S transferases (GSTs) represent a family of enzymes, both cytosolic and membrane-bound, that serve as part of the cell detoxification mechanism by binding toxins and functioning as transport proteins.[73,74] These enzymes, found predominately in the liver, protect the cell from harmful toxins such as carcinogenic metabolites and metal ions, by catalyzing the nucleophilic attack of glutathione (GSH) on electrophilic substrates.[73] Foreign elements such as arsenic and lead are well known to be highly toxic to living organisms, but even those metals that are essential for life, such as iron and copper, must be tightly regulated.[63] Unregulated metals in the cytosol damage cells by participating in Fenton chemistry which forms reactive oxygen species (ROS). Metals are also linked to improper protein folding and induce protein aggregation, as seen in Alzheimer's and Parkinson's disease.[75] Hence, it is proposed that one of the roles played by GST is to bind and remove metal ions from the cell, as discussed in the following paragraphs.

Although not extensively explored, it is well established that GST binds metal ions.[60-63] Early work linked the inhibition of tumor specific human GST activity to GST binding of mercury, cadmium and copper (II).[76] A *Caenorhabditis elegans* GSTπ homologue, GST-1, inhibited Mn-induced dopamine neurodegeneration, providing strong proof of GST interaction with Mn, albeit not direct evidence of binding.[77]

In 1997, Neuefeind *et al*. solved an X-ray structure of apo-GST from maize, providing structural proof of metal binding. The structure contained several Cd^{2+} ions bound to the protein surface, and one Cd^{2+} bound to the GSH-binding site where N59 and Q72 from one monomer and D106 from the partner chain formed the coordination sphere (Figure I-8).[62,78] The $CdSO_4$ from the crystallization buffer was the source of Cd in this study.

When crystallized in the presence of zinc, three different crystal types were identified in three different crystal systems. One was a homo-dimeric GST with Asp26 and His79 of one monomer and His46 from a neighboring molecule forming the coordination sphere of the zinc ion. In the second crystal type, the zinc ion is coordinated by Asp26, His79 and a water molecule in the place of the His46. When Asp26 is mutated with His, the zinc adopts the more typical biological binding environment comprised of four histidines that derive from two different dimers. Hence, the zinc connects two different GST dimers.
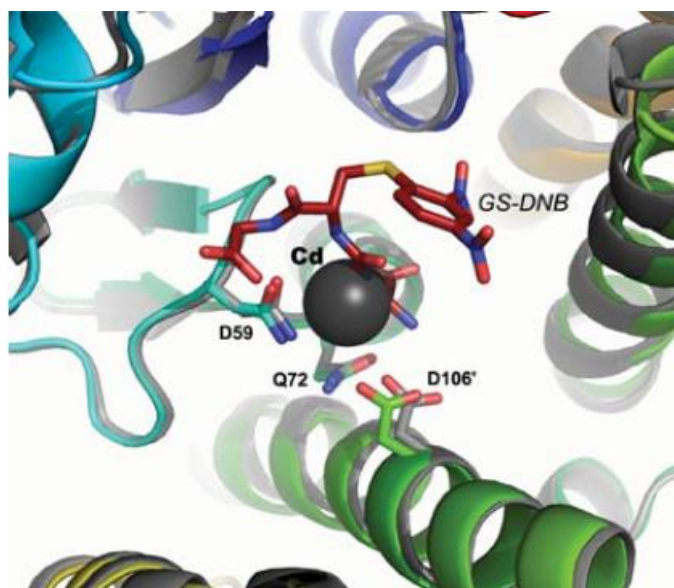
Figure I-8. Overlay of the X-ray crystal structure of the cadmium binding site of *L. vannamei* GST with the molecular model of GST with the product GS-DNB. Reprinted with permission from "Inhibition by Cu^{2+} and Cd^{2+} of a mu-class glutathione S-transferase from shrimp Litopenaeus vannamei" by Salazar-Medina, A. J.; Garcia-Rico, L.; Garcia-Orozco, K. D.; Valenzuela-Soto, E.; Contreras-Vergara, C. A.; Arreola R.; Arvizu-Flores, A.; Sotelo-Mundo, R. R.. *J. Biochem. Molec. Tox.*, **2010**, *24*, 218-222, Copyright **2010** by John Wiley & Sons, Inc.[62]

Each of these studies employed apo-GST and thus do not present a realistic representation of what the binding modes would be in the cellular environment, primarily because the actual substrate, GSH, was not present. Considering that the function of GST is to catalyze the binding of GSH to metal ions (or other xenobiotic substrates), the question remains whether a structure obtained in the presence of both GSH and a metal ion would have the GSH bound. It is possible, though, that *in vivo* the GSH does not remain bound to the metal (or other xenobiotic substrates) and merely acts

to facilitate the binding to GST, which in turn delivers the toxic substance to the membrane-bound multidrug resistant protein-1 (MRP-1) for removal from the cell.

The first realistic view of GST binding a metal ion in the presence of the GSH substrate was reported by Lo Bello *et al*. in 2005.[64] An exogenously prepared bis-glutathione DNIC, $[(GS)_2Fe(NO)_2]^-$, i.e. the oxidized, $\{Fe(NO)_2\}^9$ form, was introduced to the GST, resulting in replacement of one of the GS ligands with the tyrosine of the GST active site (Figure I-9).[64] Not only does this work model how the GST functions *in vivo*, but it also constitutes the first, and only, example of a protein-bound DNIC.
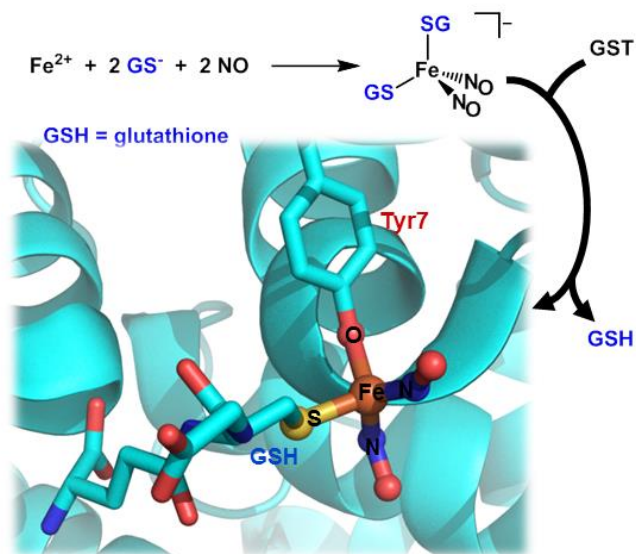
Figure I-9. Exogenously prepared DNIC, $[(GS)_2Fe(NO)_2]^-$ was introduced to GST, resulting in the loss of one of the GS⁻ ligands as GSH and incorporation of the $Fe(NO)_2$ unit into the GST active site via binding through the active site tyrosine residue.[64]

This study also provides yet another example of the similarities between the DNIU and copper, in this case $\{Fe(NO)_2\}^9$ and Cu^{2+}. It should be noted that the GST-DNIC experiences a loss of GST activity, confirming that the DNIC tightly binds the active site of GST.[64]

In studies assessing GST binding affinity for various metal ions, most find that Cu^{2+} binds GST with higher affinity than any other metal ion. Michibata *et al*. investigated the metal-binding affinity of GST from the vanadium-rich ascidian *Ascidia sydneiensis samea*.[60] Immobilized metal ion affinity chromatography revealed the binding affinity of this particular GST was Cu(II) >V(IV) > Fe(III) with Co(II), Ni(II), and Zn(II) showing low binding affinities.[60] However, GST activity was only inhibited by Cu(II). The same analysis performed on GST from an entirely different species also revealed that only Cu(II) inhibited GST activity.[60]

In 2016, Ahmed *et al*. reported the effects of a range of metal ions (NaCl, KCl, $FeCl_2$, $LaCl_2$, $MnCl_2$, $CaCl_2$, $MgCl_2$, $NiCl_2$, $ZnCl_2$, $CdCl_2$, $CoCl_2$, $CuCl_2$, $FeCl_3$, and $AlCl_3$) on camel liver GST.[63] Of all the metals tested, Cu^{II} displayed the greatest inhibition of enzyme activity, readily attributed to the strong binding affinity of Cu^{II} for the thiol groups on GST. The high affinity of Cu^{II} for GST has also been shown in studies using GST from rat liver cells.[61] Nevertheless, no structural evidence for the binding of Cu to GST has been reported to date.

In summary, although the GST can bind many different metal ions, the highest affinity binding is for Cu^{II}. Additionally, when the $Fe(NO)_2$ unit is introduced to GST, as

opposed to just iron ions, the binding affinity is also high. From this, it can be concluded that there is indeed a strong case for the similarity between copper and $Fe(NO)_2$.

Dithiolate Compounds

An important artifact in the studies involving GST with copper and DNICs is the affinity of both the Cu ions and the $Fe(NO)_2$ for sulfur donors. Some prominent endogenous thiol environments in which iron exists include iron sulfur clusters and the Cys-Gly-Cys binding motif of nitrile hydratase. Nitrous oxide reductase and cytochrome c oxidase both house copper in a Cu_A binding site that utilizes methionine and cysteine. Additionally, both the $Fe(NO)_2$ and Cu have a high affinity for glutathione.

Structural Analogy Between Cu and Fe(NO)$_2$

Nitrogen donor environments are also prevalent for both of these moieties as exhibited in the active sites of catechol oxidase and tyrosinase that contain copper coordinated by three histidine residues or the bis-histidine DNIC that has been spectroscopically observed. Accordingly, chemists have developed a vast library of both DNICs and Cu complexes with N- and S-donor ligands, many of which have already been mentioned. Amongst them, our group and others have extensively explored the N_2S_2 ligands, where N_2S_2 is predominately bis-mercapto-diazacycles, and the reactivity and properties of their metalated forms.

The following paragraphs highlight structural similarities between the $\{Fe(NO)_2\}^{10}$ and Cu^I incorporated into adamantane-like structures with N_2S_2, as well as tetramolecular structures that incorporate $\{Fe(NO)_2\}^9$ and Cu^{II} in a N-donor

environment. Furthermore, we consider the electronic similarities of the $\{Fe(NO)_2\}^{9/10}$ and Cu^{II}/Cu^{I} redox couples with regards to thiolate/disulfide interconversion.

Due to the high affinity of N_2S_2 ligands for divalent metals, a rather extensive library of complexes has been synthesized and characterized.[79] Moreover, the thiolate sulfurs show reactivity towards electrophiles such as metals and oxygen. The reactivity of these sulfurs towards both copper and $Fe(NO)_2$ provides an excellent example of structural similarity between complexes formed from these two units.

Reaction of $Cu(N_2S_2)$ (N_2S_2 = bis(N,N'-2-mercapto-2-methylpropyl)-1,5-diazocyclooctane) with $Cu^{I}Cl$ forms a cluster complex in which two $Cu(N_2S_2)$ metalloligands are bridged by $Cu^{I}Cl$ via attachment of the Cu to the thiolate sulfurs. This bridging core region was noted to bear a remarkable resemblance to adamantane as displayed in Figure I-10.[69]
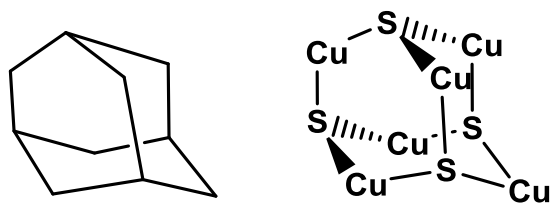
Figure I-10. The structure of adamantane (left) and the adamantane core of the $Cu(N_2S_2)$ cluster (right).

The major product isolated in this reaction was the cluster with a complete adamantane core, while the minor product was also analyzed and found to contain an "incomplete adamantane core". This incomplete core contains only three (instead of four) bridging Cu^ICls.

As will be discussed in detail in Chapter III, a similar cluster complex with an adamantane core was isolated when $[Ni(N_2S_2)Fe(NO)_2(CO)]$ (where $N_2S_2 = $ N,N′-bis (2-mercaptoethyl)- 1,4-diazacycloheptane) was reacted with $Fe(CO)_2(NO)_2$.[70] The resulting complex contained two $Ni(N_2S_2)$ units bridged by three $Fe(NO)_2$ units, which formed an incomplete adamantane core analogous to that seen in the copper case discussed above.
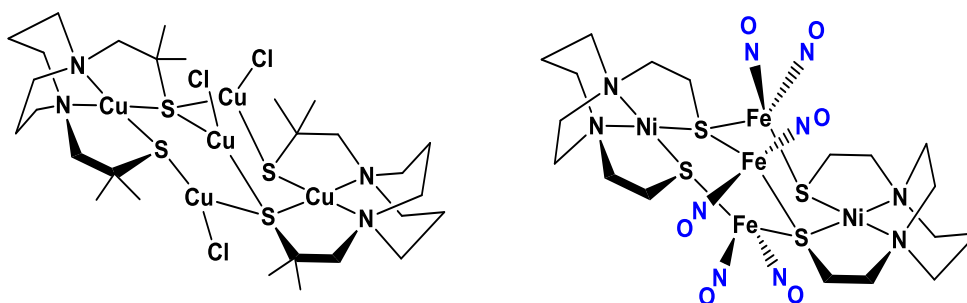
Figure I-11. Chemdraw depictions of the analogous incomplete adamantane structures in which either Cu^ICl (left) or $Fe(NO)_2$ (right) occupies equivalent sites within the core.

Figure I-11 shows a chemdraw sketches of both the Cu cluster and the $Fe(NO)_2$ cluster. The two incomplete adamantane cores overlay nearly perfectly when the

structures are overlaid, providing an excellent example of two structurally analogous compounds that can house either Cu^I or $\{Fe(NO)_2\}^{10}$ in equivalent positions.

M = Fe(NO)$_2$ or Cu^{II}L (L = 1,4,7-triazacyclononane)
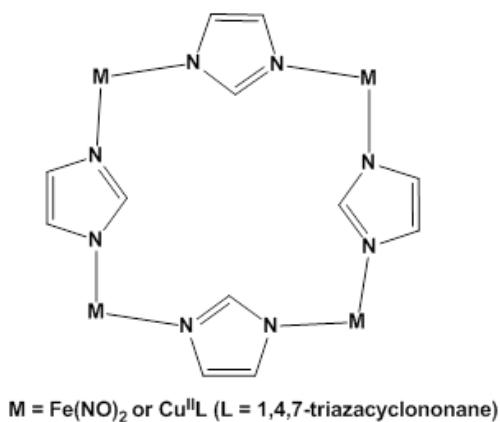
Figure I-12. Chemdraw depiction of tetramolecular squares with imidazole linkers in which either $\{Fe(NO)_2\}^9$ or $Cu^{II}L$ (L = 1,4,7-triazacyclononane) occupy the corners.

Structurally analogous complexes containing the d^9 Cu^{II} and $\{Fe(NO)_2\}^9$ have also been isolated. In this case, nitrogen donor ligands in the form of imidazoles form tetramolecular squares in which four imidazole ligands bridge either $Cu^{II}L$, where L = 1,4,7-triazacyclononane)[71] or $\{Fe(NO)_2\}^{9,22}$ which occupy the corners of the square (Figure I-12). Again, this example provides yet another insight into the similarity between copper and Fe(NO)$_2$.

Similarity Between $\{Fe(NO)_2\}^{9/10}$ and Cu^{II}/Cu^{I} Redox Couples with Regards to Thiolate/Disulfide Interconversion

The conversion interconversion between thiolates and disulfide is well known in biology, namely as was discussed with regards to the redox buffering activity of GSH in the section covering GSH/GST. We also note that conversion of thiolates to disulfide also occurs in RSNO decomposition reactions. Other systems, such as the metalloprotein that delivers Cu superoxide dismutase 1 (SOD1), forms disulfide bonds from cysteinyl thiolates as part of the Cu insertion process.[80] In this reaction, the Cu serves as the oxidant for disulfide formation.

Following the idea of copper involvement in thiolate/disulfide interconversion, Henkel *et al.* reported a chloride-induced conversion of a copper(I) disulfide cation $[Cu^{I}_2\{(NGuaS-)_2\}_2]^{2+}$ (NGuaS = o-SC$_6$ H$_4$ NC(NMe$_2$)$_2$) to the electrically neutral copper(II) thiolate species $[Cu^{II}_2\text{-}(NGuaS)_2Cl_2]$.[68] Our group noticed a similar thiolate/disulfide interconversion with a DNIC (instead of the Cu seen in the previous example).[65] Upon exposure to CO gas, the oxidized $\{Fe(NO)_2\}^9$ DNIC [(sIMes)(SPh)Fe(NO)2], (where sIMes = 1,3- bis(2,4,6- trimethylphenyl)- imidazole and SPh = thiophenol) converts to the $\{Fe(NO)_2\}^{10}$ species [(sIMes)(CO)Fe(NO)$_2$] concomitant with release of disulfide.

Summary and Overview

As discussed in this chapter, the vital importance of nitric oxide to living organisms has propelled a large number of studies regarding NO storage and transport agents, specifically the DNICs. Chemical and biochemical studies have elucidated the

basic chemistry of these complexes and have built an extensive library of biomimetic DNICs that provide scaffolds for further exploring the DNIC field, although the mechanism of NO release and development of viable pharmaceutical candidates is still lacking. The work reported in this dissertation addresses both of these lacking areas.

In Chapter III, the reactivity of DNICs with copper is explored. These reactions have implications in DNIC reactivity with components of the cellular environment, and further build the case for the correlation between copper and DNICs that was discussed in detail in this chapter. This study also exemplifies copper-initiated nitric oxide release, suggesting copper might serve as an endogenous trigger for NO release from DNICs.

Chapter IV examines the reactivity of RSNOs with DNICs, addressing the hypothesis that DNICs may play a role in NO release from RSNOs. While NO release is observed, this study also focuses on the formation of a unique cluster and its implications in iron-sulfur cluster repair.

New DNICs containing thioglucose ligands are presented in Chapter V and their application as biocompatible NO-releasing molecules is described. The use of the glucose ligands provides the potential for low cytotoxicity, water solubility and increased cell permeability over traditional inorganic ligand sets.

Finally, Chapter VI presents several structural examples of the $Fe(NO)_2$ unit bound to both metallodithiolate and phosphene ligands and provides insights into the various binding modes of each ligand.

CHAPTER II

EXPERIMENTAL SECTION FOR CHAPTERS III-V

Abbreviations

DNIU : Dinitrosyl iron unit

DNIC : Dinitrosyl iron complex

RRE : Roussin's red ester

Neo : 2,9-dimethyl-1,10-phenanthroline (neocuproine)

NHC : N-heterocyclic carbene

SGlu : 1-thio-β-D-glucose tetracetate

bme-dach : bis(N,N'-2-mercapto-2-methylpropyl)-1,5-diazocycloheptane

bme-daco : bis(N,N'-2-mercapto-2-methylpropyl)-1,5-diazocyclooctane

DCM : Dichloromethane

THF : Tetrahydrofuran

General Methods and Materials

All chemical reactions were carried out under air-free conditions using standard Schlenk techniques or in an argon-filled glovebox. Solvents were of reagent grade and were freshly purified by an MBraun manual solvent purification system packed with Alcoa F200 activated alumina desiccant. Tetrahydrofuran was further purified by distillation under N_2 from sodium-benzophenone. Many of the X-ray quality crystals obtained are described to have been grown from slow diffusion of a hexanes/ether mixture into a concentrated DCM or THF solution of the product. These crystallizations

were set up by first adding a small amount of the concentrated product solution to a test tube. A layer of hexanes (ca. twice as much as the volume of the product solution) was added next. Enough ether was then added as a top layer to fill the test tube, after which time the layered mixture was carefully placed in the freezer.

Physical Measurements

Infrared spectra were recorded on a Bruker Tensor 27 FTIR spectrometer using CaF_2 solution cells with a path length of 0.1 mm. Mass spectrometry (ESI-MS) was performed by the Laboratory for Biological Mass Spectrometry at Texas A&M University. Nanoelectrospray ionization in positive mode was performed on solution samples using an Applied Biosystems QSTAR Pulsar (Concord, ON, Canada) equipped with a nanoelectrospray ion source. Solution was flowed at 700 nL/min through a 50 μm ID fused-silica capillary that was tapered at the tip. Electrospray needle voltage was held at 1900 V. Elemental analyses of crystalline samples were determined by Atlantic Microlab, Inc., Norcross, GA. Electron Paramagnetic Resonance (EPR) spectra were recorded in frozen THF, DCM or DMSO using a Bruker ESP 300 equipped with an Oxford ER910 cryostat operating at 10 K. The SpinCount software was obtained from Prof. Mike Hendrich at Carnegie Mellon University and was used to simulate spectral parameters. UV-vis absorption spectra were collected on a Shimadzu UV-2450. Cyclic voltammograms were recorded on a BAS-100A electrochemical analyzer. All CV experiments were performed at room temperature under an Ar blanket in CH_3CN or DCM solution containing 0.1 M [t-Bu_4N][PF_6] as the electrolyte, with a 3.0 mm glassy

carbon working electrode, a $Ag/AgNO_3$ reference electrode, and a Pt coil counter electrode. All values have been internally referenced to Cp_2Fe/Cp_2Fe^+.

X-ray Crystallography

X-ray diffraction (XRD) studies were carried out using a Bruker APEX2 using MoKα radiation (0.7107 Å). Selected crystals were coated in paraffin oil, mounted on a nylon loop, and placed under streaming N_2 (110/150 K). The space groups were determined by systematic absences and intensity statistics, and structures were solved by direct methods and refined by full-matrix least-squares on F^2. Anisotropic displacement parameters were employed for all non-hydrogen atoms; H atoms were placed at idealized positions and refined with fixed isotropic displacement parameters. The following programs were used: cell refinement, data collection, data reduction, APEX2[81]; absorption correction, SADABS[82]; structure solutions, SHELXS-97[83]; and structure refinement, SHELXL-97.[83] The final data presentation and structure plots were generated in Mercury Version 3.8.[84] CIF files were prepared for publication using WinGX[85] and its included programs.

Experimental Details for Chapter III

Materials

Reagents, including nitrosonium tetrafluoroborate, 2,9-Dimethyl-1,10-phenanthroline, copper(I) chloride, copper(I) bromide, Tetrakis(acetonitrile)copper(I) hexafluorophosphate, copper(II) chloride, and copper(II) bromide were purchased from either Sigma-Aldrich Chemical Co. or VWR Chemical Co. and were used as received. Standard Schlenk-line techniques (N_2 atmosphere) and an Ar-filled glovebox were used

to maintain anaerobic conditions during preparation, isolation, and product storage. $Fe(CO)_2(NO)_2$[86] and [Na-18-crown- 6-ether][$Fe(CO)_3(NO)$][87] were prepared according to published procedures.

Synthesis of Complex 1

Sodium tetrafluoroborate (0.2 mmol, 0.023 g) and [Na-18-crown- 6-ether][$Fe(CO)_3(NO)$] (0.2 mmol, 0.091 g) were added to a Schlenk flask, dissolved in THF and stirred for 15 min. The resulting $Fe(CO)_2(NO)_2$ was vacuum transferred to a second Schlenk flask. Neocuproine (0.042 g, 0.2 mmol) was loaded into a round bottom flask, dissolved in THF, and then added to the freshly prepared $Fe(CO)_2(NO)_2$. During the 1 h stir, the color changed from orange red to dark brown, indicating the formation of the product [(neo)$Fe(NO)_2$] (**1**). This dark brown product solution was filtered through Celite and the solvent removed *in vacuo*. After drying, the dark brown solid was washed with hexanes (3x10 mL) to yield spectroscopically pure **1** as a dark brown powder (0.034 g, 52 %). X-ray quality crystals of **1** were obtained by slow diffusion of a hexanes/ether mixture into a DCM solution of **1** at -35 °C. IR (cm^{-1}): ν(NO): (1697, 1649). Cyclic Voltammetry: $E_{1/2}$: -0.36 V. UV-Vis: 802, 662, 373, 360, 328, 314, 273. Elem. anal. found (calc'd for $C_{14}H_{12}FeN_4O_2$) %: C, 46.03 (47.23); H, 4.66 (5.01), N, 11.18 (11.60).

Chemical Oxidation of 1 to Form 1$^+$

A round bottom flask containing a THF solution of ferrocenium hexafluorophosphate was cooled to -78°C using a dry ice/acetone bath. This cooled solution was then added slowly to a THF solution of **1**, also at -78°C. The reaction

mixture was stirred at -78°C for 1 h. The resulting light brown solution was stable upon warming to room temperature. IR spectroscopy confirmed complete conversion to 1^+. Following solvent removal, the light brown powder was washed with hexanes (3x10 mL) and dried. Due to thermal instability, an accurate yield was not determined. IR (THF, cm^{-1}): ν(NO): (1837, 1769). $^+$ESI-MS for $C_{28}H_{24}FeN_6O_2$ (MW=532 g/mol): m/z = 533.3 [M + H]$^+$. Instability prevented collection of reliable elemental analysis data.

Reactivity Studies with Cu^I

Three reactions were conducted to study the potential binding of Cu^I or the DNIU to neocuprione. All reactions with Cu^I were carried out at 22°C. In the first reaction, a 1:1 mixture of Cu^{I}Cl and **1** was dissolved in THF and left to stir overnight. A color change from brown red to orange-red occurred, and the resulting solution showed complete disappearance of the NO bands of **1** and no new bands appeared. IR (THF, cm^{-1}): ν(NO): none. $^+$ESI-MS for $CuC_{28}H_{24}N_4$ (MW=479 g/mol): m/z = 479 [M]$^+$, and UV-Vis (λ, nm): 454, 336, 324, 291, 274, 226 (indicates the formation of [Cu(neo)$_2$]Cl, a previously synthesized compound).[88]

In the second reaction, [Cu(CH$_3$CN)$_4$]PF$_6$ was dissolved in THF and added to a round bottom flask containing a THF solution of **1** (1:1). The reaction was allowed to stir overnight. A change of color to orange-red was again observed. The resulting solution was then characterized by IR, mass spectrometry and UV-Vis and all revealed the same results as the first reaction, indicating that the main product for both reactions is [Cu(neo)$_2$]$^+$.

The same reaction was again carried out but with CuBr. Results again showed disappearance of the IR NO bands and a mass spectrum and UV-vis spectrum that showed the only major product to be $[Cu(neo)_2]^+$.

Finally, in a round bottom flask, THF solutions of Cu^ICl (0.1 mmol, 0.010 g) and $Fe(CO)_2(NO)_2$ (0.1 mmol, 0.046 g) were mixed, and monitored for any reactivity. No change in color was observed, even after hours of stirring. IR spectroscopy confirmed the presence of unreacted $Fe(CO)_2(NO)_2$. A THF solution of neocuprione (0.1 mmol, 0.021 g) was then added to the round bottom flask containing the two compounds. After a 3 h stir, a color change to orange red was observed. The resulting major product was identified as $[Cu(neo)_2]^+$. IR (THF, cm^{-1}): ν(NO): none. $^+$ESI-MS for $CuC_{28}H_{24}N_4$ (MW=479 g/mol) : m/z = 479 $[M]^+$, and UV-Vis (λ, nm): 454, 336, 324, 291, 274, 226

Reactivity Study with Cu^{II} (1:1 Stoichiometry)

To a Schlenk flask containing a brown CH_3CN solution of **1** (0.02 mmol, 0.065 g) was slowly added a bright green CH_3CN solution of $CuBr_2$ (0.02 mmol, 0.045 g). Upon addition, there was an immediate color change to a dark red-brown. IR spectroscopy showed the disappearance of the NO bands of **1** and formation of two new bands at 1777 and 1716 cm^{-1}. The reaction was monitored by both IR spectroscopy and UV-vis spectroscopy for 5 h, in which time no additional changes occurred. The product mixture was dried *in vacuo*, dissolved in a minimal amount of DCM and precipitated with hexanes. The brown solid mixture was then washed with hexanes (3 x 10 mL), and filtered. X-ray quality crystals of one of the products, (neo)CuBr$_2$ (neo = 2,9-dimethyl-1,10-phenanthroline), complex **2**, were obtained by slow diffusion of a hexanes/ether

mixture into a DCM solution at -35 °C. Spectroscopic analysis of the dark red-brown product solution indicated the formation of two copper species, $[Cu(neo)_2]^+$ and **2** in addition to the iron nitrosyl products (one confirmed to be $Fe(NO)_2Br_2^-$). IR: $\nu(NO)$: 1777, 1716 cm^{-1}. $^+$ESI-MS for $CuC_{28}H_{24}N_4$ (MW = 479 g/mol): m/z = 479 [M]$^+$, and for $CuC_{14}H_{12}N_2Br_2$ (MW = 432 g/mol): m/z = 352 [M-Br]$^+$. UV-Vis (λ, nm): 277, 448, 567, 857.

The reactions with CuX_2 (X = Cl, Br) as detailed above, were also each carried out in a vial, which was placed in a larger sealed vial containing the NO trapping agent $[(bme\text{-}daco)Fe]_2$ (bme-daco = (N,N'-bis(2- mercaptoethyl)-1,4-diazacycloheptane)) dissolved in DCM. Nitric oxide evolution was confirmed by the formation of [(bme-daco)Fe(NO)], ν_{NO} = 1648 cm^{-1}.

Reactivity Study with Cu^{II} (2:1 Stoichiometry)

Using the same synthetic methods described above, THF solutions of **1** (0.04 mmol, 0.13 g) and $CuBr_2$ (0.02 mmol, 0.090 g) were mixed in a 2:1 stoichiometric ratio. The reaction occurred more slowly than with the 1:1 stoichiometry, with starting material remaining after 10 min of stirring. After stirring overnight, the IR spectrum of the dark red-brown solution showed only product bands ($\nu(NO)$: 1777, 1716 cm^{-1}). Mass spectrometry and UV-vis spectroscopy showed that the only copper product was $[Cu(neo)_2]^+$. IR: $\nu(NO)$: 1777, 1716 cm^{-1}. $^+$ESI-MS for $CuC_{28}H_{24}N_4$ (MW = 479 g/mol): m/z = 479 [M]$^+$. UV-Vis (λ, nm): 454, 336, 324, 291, 274, 226.

Synthesis of Complex 2 (and 3)

In a Schlenk flask, DCM (30 mL) was added to $CuBr_2$ (0.10 mmol, 0.022 g) and the solution sonicated for 30 min. Neocuprione (0.10 mmol, 0.020 g) was added to the $CuBr_2$ slurry and left to stir for 2 h. A change in color from the black slurry to yellow to brownish red was observed and the crude product was dried, washed with hexanes (3x10 mL), dissolved in DCM and then filtered. The solution was dried under a flow of N_2 gas to yield (neo)$CuBr_2$ (**2**) as a dark powder. X-ray quality crystals were obtained by slow diffusion of a hexanes/ether mixture into a DCM solution. Cyclic voltammetry: $E_{1/2}$: -0.17 V. UV-Vis (λ, nm): 802, 570, 465, 375, 350, 300. Elem. anal. found (calc'd for $C_{14}H_{12}N_2CuBr_2 \cdot C_2H_6O$) %: C, 40.23 (40.27); H, 3.80 (3.60), N, 5.86 (5.90).

Synthesis of Complex 4

Complex **4** was prepared in a similar manner to **2** but using $CuCl_2 \cdot H_2O$ as the copper source. In this case, the product solution was a green brown color. X-ray quality green crystals were obtained by slow diffusion of a hexanes/ether mixture into a DCM solution. Cyclic Voltammetry: $E_{1/2}$: -0.36 V. UV-Vis: 802, 662, 373, 360, 328, 314, 273. Elem. anal. found (calc'd for $C_{28}H_{24}N_4CuCl_2H_2O \cdot CH_2Cl_2$) %: C, 54.78 (55.32); H, 4.12 (4.24), N, 8.81 (9.10).

Synthesis of Complex 5

[Na-18-crown- 6-ether][Fe(CO)$_3$(NO)] (0.50 mmol, 0.240 g), $NOBF_4$ (1.0 mmol, 0.116 g) and NaBr (1.0 mmol, 0.103 g) were loaded into a Schlenk flask under an argon atmosphere, dissolved in approximately 30 mL of THF, and stirred for 2 h. A change of color from orange to brown was observed, and the crude product was dried, washed with

hexanes (3x10 mL), and filtered through Celite to yield spectroscopically pure **5** (yield). X-ray quality crystals of **5** were obtained by slow diffusion of a hexanes mixture into a THF solution. IR (cm^{-1}): ν (NO): (1783, 1715). UV-Vis (λ, nm): 701, 523, 463, 423.

Synthesis of Complex 6

[Na-18-crown- 6-ether][Fe(CO)$_3$(NO)] (0.25 mmol, 0.120 g), NOBF$_4$ (0.50 mmol, 0.058 g) and CuBr (0.50 mmol, 0.082 g) were loaded into a Schlenk flask under an argon atmosphere, dissolved in approximately 30 mL of THF and stirred for 12 h. A change of color from orange to brown was observed and the crude product was dried, washed with hexanes (3x10 mL); the product was redissolved in a minimal amount of THF and filtered through Celite to yield spectroscopically pure **6**. IR(cm^{-1}): ν(NO): (1793, 1793).

Synthesis of (μ-Br)$_2$[Fe(NO)$_2$]$_2$

In a Schlenk flask, Br$_2$ (0.30 mmol, 7.7 μL) was dissolved in THF, then added to freshly prepared Fe(CO)$_2$(NO)$_2$ and stirred for 90 min. A slight change of color from orange to dark brown was observed. The product solution was dried *in vacuo*, dissolved in hexanes, and then filtered through Celite. Attempts at crystallization via slow evaporation of the concentrated hexanes solution were unsuccessful. IR(cm^{-1}): ν(NO): (1816, 1712).

Quantification of NO Release

A small vial was charged with **1** (0.050 mmol, 0.016 g) and CuBr$_2$ (0.050 mmol, 0.011 g) and placed inside a larger vial containing [Co(bme-dach)]$_2$ (0.05 mmol, 0.030 g) and sealed under argon. The contents of each vial were dissolved in 5 mL of DCM

and stirred for 12 h. A color change was observed in the solution of the outer tube reaction and confirmed to be [Co(bme-dach)]NO by the appearance of a single NO band at 1601 cm^{-1}. The intensity was compared to a known intensity-concentration plot for [Co(bme-dach)]NO. The product of the inner vial was characterized by IR, which showed two main stretches at IR(cm^{-1}): v(NO): (1777, 1716). In a similar manner, the amount of NO released in the reactions with CuCl$_2$ and CuX (X = PF$_6$, Br, Cl) was also analyzed. The same molar scales and reaction times were also used.

Experimental Details for Chapter IV

Materials

Reagents, including nitrosonium tetrafluoroborate and tritylthiol, were purchased from either Sigma-Aldrich Chemical Co. or VWR Chemical Co. and were used as received. Standard Schlenk-line techniques (N$_2$ atmosphere) and an Ar-filled glovebox were used to maintain anaerobic conditions during preparation, isolation, and product storage. Fe(CO)$_2$(NO)$_2$ and [Na-18-crown-6-ether][Fe(CO)$_3$(NO)] were prepared according to published procedures.[86,87] The amylnitrite,[89] used in the synthesis of tritylthiol, as well as the trityl-S-nitrosothiol,[90] were prepared according to published procedures.

Synthesis of Complex 1 from Ph$_3$CSNO

A Schlenk flask was loaded with sodium tetrafluoroborate (0.10 mmol, 0.012 g) and [Na-18-crown- 6-ether][Fe(CO)$_3$(NO)] (0.10 mmol, 0.046 g), which were dissolved in THF and stirred for 15 min. The resulting orange-red Fe(CO)$_2$(NO)$_2$ was vacuum transferred to a second Schlenk flask immersed in liquid N$_2$. Upon warming the

Fe(CO)$_2$(NO)$_2$ solution to room temperature, a green THF solution (~ 5 mL) of Ph$_3$CSNO (0.10 mmol, 0.031 g) was added. IR spectroscopy revealed complete disappearance of the reactant IR bands concomitant with the appearance of two new bands (1787, 1752 cm^{-1}) following a 1 h stir. A color change to dark brown also occurred during this time, signaling the formation of complex **1**. The product solution was dried *in vacuo*, redissolved in hexane and filtered through Celite to yield spectroscopically pure complex **1**. X-ray quality crystals were grown from the slow evaporation of a concentrated hexanes solution. IR (cm^{-1}): ν(NO): (1787, 1752).

Synthesis of Complex 1 from Ph₃CSH

The reaction outlined above was again carried out but this time with Fe(CO)$_2$(NO)$_2$ (0.1 mmol, 0.017 g) and tritylthiol (Ph$_3$CSH) (0.1 mmol, 0.028 g). The THF mixture was stirred for 1 h, after which time a color change to dark brown and a shift in the IR bands to 1787 and 1752 cm^{-1} indicated formation of complex **1**. There was no nitric oxide release in this case. X-ray quality crystals were grown from the slow evaporation of a concentrated hexanes solution. IR (cm^{-1}): ν(NO): (1787, 1752).

Synthesis of Complex 2 from Ph₃CSNO

A Schlenk flask was loaded with (neo)Fe(NO)$_2$ (0.10 mmol, 0.032 g) and trityl-S-nitrosothiol (0.10 mmol, 0.031 g). The mixture was dissolved in THF and stirred for 1 h. The IR spectrum of the resulting product solution showed a shoulder at 1788 cm^{-1} and two major NO stretches at 1780 and 1747 cm^{-1}. The reaction mixture was dried *in vacuo*, and hexanes were added. Part of the dark brown product dissolved in the hexanes, which was identified by IR spectroscopy to be complex **1**. The hexane solution was removed,

leaving a dark brown hexane-insoluble solid. This solid was then washed with hexanes (3x10 mL), dissolved in DCM, and filtered through Celite to yield complex **2**. X-ray quality crystals of **2** were grown by slow diffusion of a hexanes/ether mixture into a DCM solution. IR (cm^{-1}): ν(NO): (1780, 1747).

NO Trapping Experiments

A small vial was charged with a THF solution of freshly prepared $Fe(CO)_2(NO)_2$ (0.050 mmol, 0.010 g) and placed in a larger vial containing $[Fe(bme-dach)]_2$ (0.02 mmol, 0.13 g). A THF solution of trityl-S-nitrosothiol (0.050 mmol, 0.015 g) was added to the inner vial and DCM was added to the $[Fe(bme-dach)]_2$ in the outer tube. Over the course of an hour stir, the solution in the inner vial changed from brown-green to dark brown. The solution in the outer tube changed from brown to dark green, indicating the formation of [Fe(bme-dach)NO]; a single NO band at 1648 cm^{-1} in the IR spectrum confirmed the presence of [Fe(bme-dach)NO]. The product of the inner vial was characterized by IR spectroscopy and confirmed to be complex **1**.

The exact experiment as above, using the same amounts and conditions, was carried out but with tritylthiol (0.050 mmol, 0.014 g) in the place of trityl-S-nitrosothiol. After an hour stir, the inner tube showed formation of complex **1**, as confirmed by IR spectroscopy. However, there was no change in the color of the outer vial (it remained brown). Additionally, IR spectroscopy of the solution from the outer vial revealed no nitrosyl band formation.

Again, the same experimental setup and amounts were used as outlined above, but with $(neo)Fe(NO)_2$ as DNIC. A small vial was loaded with $(neo)Fe(NO)_2$ (0.050

mmol, 0.016 g) and placed in a larger vial containing [Fe(bme-dach)]$_2$ (0.02 mmol, 0.13 g). Trityl-S-nitrosothiol (0.050 mmol, 0.015 g) was then dissolved in THF and added to the inner vial, while the [Fe(bme-dach)]$_2$ in the outer tube was dissolved in DCM. Following an hour stir, a color change from brown-green to dark brown was observed in the inner vial, which was confirmed by IR spectroscopy to be a mixture of **1** and **2**. A color change from brown to dark green, indicated the formation of [Fe(bme-dach)NO], which was confirmed by IR spectroscopy.

Experimental Details for Chapter V

Materials

All reagents, including 1,3-bis(2,4,6-trimethylphenyl)imidazolium chloride (IMesH$^+$Cl$^-$), sodium *tert*-butoxide (NaO^{t}Bu), sodium methoxide (MeONa) 1-thio-β-D-glucosetetraacetate, 1-thio-β-D-glucose sodium salt and CoTPP were purchased from Sigma-Aldrich Chemical Co. and were used as received. Air-free conditions were maintained during synthesis, isolation, and storage of products through the use of standard Schlenk-line techniques (N$_2$ atmosphere) and an Ar-filled glove box. The NHC stabilized IMes-TNIC, [(IMes)Fe(NO)$_3$]$^+$, [(bme-dach)Co]$_2$, and complex **3** were synthesized according to literature procedures.[70,91] Complex **4** was synthesized as described in Chapter III. Bovine coronary venular endothelial cells (CVECs) were kindly gifted by Professors Cynthia J. Meininger and Andreea Trache at Texas A&M Health Science Center. CVECs were cultured in GIBCO® Dulbecco's Modified Eagle Medium: Nutrient Mixture F-12 (DMEM/F-12) (Invitrogen, Carlsbad, CA) mixed with 10% fetal bovine serum (Sigma Aldrich, St. Louis, MS), 100 U/mL penicillin - 100

U/mL streptomycin - 0.25 mg/mL amphotericin B (Lonza, Walkersville, MD), and 20 units/mL heparin (Midwest Vet Supply, Lakeville, MN).

Synthesis of Complex 1

A 0.10 mmol (0.054 g) portion of [(IMes)Fe(NO)$_3$]$^+$ and 0.10 mmol (0.036 g) of 1-thio-β-D-glucosetetraacetate were weighed and dissolved in 10 mL of THF in a 100 mL Schlenk flask. A color change from green to brown resulted within time of mixing and the formation of complex **1** was confirmed by IR spectroscopy. The solution was filtered through Celite, and **1** (0.066 g, 83%) was isolated as a brown powder by recrystallization of THF solutions of **1** with cold hexanes or pentane. X-ray quality crystals of **1** were obtained from THF solutions layered by hexanes at -35 °C. IR (THF, cm^{-1}) υ(Me-C(O)O): 1759 (s), 1749 (sh) cm^{-1} υ(NO): 1768 (sh), 1718 (s) cm^{-1}. Elemental Anal. calculated for C$_{35}$H$_{43}$FeN$_4$O$_{11}$S (found) : C, 53.64 (53.21); H, 5.53 (5.42); N, 7.15 (6.73). C$_{35}$H$_{43}$FeN$_4$O$_{11}$S (MW = 783 g/mol) $^+$ESI-MS: m/z = 784 [M + H]$^+$. Room temperature EPR measurements showed an isotropic signal at g = 2.03. Upon exposure to air for 3 h, **1** converted to an unidentified species that has the appearance of a mononitrosyl iron complex. IR (DMSO, cm^{-1}) υ(NO): 1663.

Deprotection of Complex 1 to Give Complex 1' and the Direct Synthesis of 1'

In a 100 mL Schlenk flask, 0.040 g (0.05 mmol) of complex **1** was mixed with excess (0.40 mmol, 0.022 g) of MeONa and the solid mixture was dissolved in 20 mL of MeOH. The deprotection proceeded with changes in the IR pattern of complex **1**, and was complete in ca. 2 h. Direct synthesis of complex **1'** was achieved by reacting 0.10 mmol (0.054 g) of [(IMes)Fe(NO)$_3$]$^+$ and 0.10 mmol (0.022 g) of 1-thio-β-D-glucose

sodium salt in THF. The reaction was complete within time of mixing as confirmed by IR spectroscopy and a greenish brown product was obtained in powder form in good yield (crude yield > 75%). IR (THF, cm^{-1}) υ (NO): 1768 and 1716 cm^{-1}. $C_{27}H_{35}FeN_4O_7S$ (MW = 615 g/mol) $^+$ESI-MS: m/z = 638 [M + Na]$^+$.

Synthesis of Complex 2

The Roussin's Red Ester type dimeric complex **2**, $(\mu-(SR))_2[Fe(NO)_2]_2$, where R = acetylated thiosugar units, was synthesized by the room temperature reaction of 1 mmol of 1-thio-β-D-glucosetetraacetate with 1 mmol of freshly prepared $Fe(CO)_2(NO)_2$ (isolated by vacuum transfer to a flask immersed in liquid N_2) in ~ 30 mL THF solution. The reaction was complete in about 12 h as monitored by IR spectroscopy. A brown powdery product was obtained in good yield (0.36 g, 75.1%), by recrystallizing concentrated THF solutions (~ 5 mL) of **2** with cold hexanes (~20 mL). Room temperature EPR measurements showed no signal in DCM. However, a rhombic signal with g_x=2.043, g_y=2.030, g_z=2.013 appeared in DMSO solution. IR (THF, cm^{-1}) υ(NO): 1787, 1750 cm^{-1} υ(Me-C(O)O): 1759, 1749 cm^{-1}. Elemental Anal. calculated for $C_{28}H_{38}Fe_2N_4O_{22}S_2 \bullet$THF (found) : C, 37.30 (37.63); H, 4.50 (4.41); N, 5.44 (4.65). $C_{28}H_{38}Fe_2N_4O_{22}S_2$ (MW = 958 g/mol) $^+$ESI-MS: m/z = 959 [M + H]$^+$, 980 [M + Na]$^+$.

NO Trapping Experiments

Complex **1** was used in NO trapping experiments with Co(TPP). Into a 50 mL Schlenk flask, 0.060 mmol (0.050 g) of **1** was weighed out and dissolved in 10 mL of THF. This was transferred *via* cannula into a different flask containing 0.12 mmol (0.081 g) of CoTPP in 10 mL THF. Loss of NO bands was seen over 48 hours in the IR monitor.

In order to isolate the (TPP)Co(NO), the solution was concentrated to ca. 5 mL, and MeOH was added. Careful decanting of the red supernatant showed a dark purple precipitate. The residue was dried in *vacuo* and re-dissolved in dichloromethane. The IR spectrum of this dichloromethane solution showed a strong absorption peak at 1683 cm^{-1} for (TPP)Co(NO). $^+$ESI-MS: m/z = 671 [(TPP)Co]$^+$. UV-Vis (DCM): 410 nm, 534 nm.

Complex **1** (0.025 mmol, 0.019 g) and **2** (0.025 mmol, 0.023 g) were individually reacted with 0.10 mmol (0.056 g) of [(bme-dach)Co]$_2$ in THF solutions separately. Loss of NO bands in the IR monitor was seen over ~24 h for **1** and over ~12 h for **2**. The resulting solution was dried *in vacuo* and washed x2 with Et$_2$O. The remaining solid was re-dissolved in dichloromethane, of which the IR showed a strong, broad band at 1601 cm^{-1}, indicating the formation of (bme-dach)Co(NO). When the reactions were carried out in DCM, loss of the NO bands was seen over ~48 h for **1** and ~24 h for **2**. $^+$ESI-MS:m/z = 308 [M + H]$^+$, 277 [M-NO].

Quantification of NO Trapped by [(bme-dach)Co]$_2$

A series of DCM solutions of Co(bme-dach)NO were prepared with concentrations ranging from 3-14 mM. A calibration curve (below) was created using the intensities of the ν_{NO} band at 1601 cm^{-1} and the concentrations. Complex 1 (0.008 g, 0.008 mmol) and 2 (0.008 g, 0.01 mmol) were separately mixed with an excess of [Co(bme-dach)]$_2$ and stirred in DCM for 24 h. The reaction mixture was then dried *in vacuo* and the solid residue dissolved in 5 mL DCM. IR of **1** revealed the formation of Co(bme-dach)NO (0.002 g, 0.005 mmol) ca. 0.5 moles Co(bme-dach)NO per mole **1**,

while **2** showed the formation of Co(bme-dach)NO (0.007 g, 0.02 mmol) in a ratio of 2.7 moles Co(bme-dach)NO per mole **2**.

Griess Assay Analysis

The release of NO from the compounds under physiological conditions was quantitatively measured by the Griess assay (Invitrogen) following the manufacturer's protocol. For each measurement, compounds 1-4 were mixed with the media, which was taken from 96-wells with and without cells, and incubated at 37 ˚C with 5% CO_2. NO under physiological conditions converts to nitrite (NO^{2-}), which induces formation of the azo dye that absorbs at 548 nm. Specific absorbance at 548 nm was measured and corrected with blank measurement and with absorbance at 690 nm with a Spectra Max M5 plate reader.

Cell Viability Studies

Bovine coronary venular endothelial cells (CVECs) were cultured in GIBCO®Dulbecco's Modified Eagle Medium: Nutrient Mixture F-12 (DMEM/F-12) from Invitrogen (Invitrogen, Carlsbad, CA), along with 10% FBS, 100 U/mL penicillin - 100 U/mL streptomycin - 0.25 mg/mL amphotericin B (Lonza, Walkersville, MD), and 20 units/mL heparin (Midwest Vet Supply, Lakeville, MN). For cytotoxicity experiments, cells were trypsinized and quenched with media. Trypsin was removed after centrifugation at 250 G for 5 minutes. Resuspended cells were plated (10 x 10^3 cells/well) in a 96-well plate coated with 1.5 % bovine gelatin. Cells were incubated at 37 °C in a humidified atmosphere containing 5% CO_2 for 24 h to adhere. The medium was replaced with fresh medium 1 h prior to the addition of formulations at desired

concentrations. The cells were incubated with the formulations for 72 h. MTS combined reagent was added to each well (Cell Titer 96® Aqueous Non-Radioactive Cell Proliferation Assay, Promega Co., Madison, WI). The cells were then incubated with the reagent for 2 h at 37 °C in a humidified atmosphere containing 5% CO_2 protected from light. Absorbance was measured at 490 nm using SpectraMax M5 (Molecular Devices Co., Sunnyvale, CA). The cell viability was calculated based on the relative absorbance to the control-untreated cells.

Experimental Details for Chapter VI

The various structures reported in Chapter VI were prepared according to known procedures[69,70,91-93] and modified as necessary. Crystals were obtained in general by the three layer technique. All structures have been deposited into the Cambridge Crystallographic Database and ascension numbers are given. Short descriptions of properties are given with each structure.

CHAPTER III

COPPER (II/I)-PROMOTED LIGAND EXCHANGE AND NO RELEASE FROM

DINITROSYL IRON COMPLEXES (DNICs)

Introduction

The discovery of dinitrosyl iron complexes, DNICs, as potential NO storage and delivery agents, has prompted the development of a distinct field in the DNIC area.[21,94,95] Although much is known about the synthesis, reactivity, and, to a lesser extent, the biochemistry of these complexes, the goal of developing their physiological or therapeutic potential requires an understanding of the interaction of the $Fe(NO)_2$ unit with components of the physiological milieu. As more results accumulate regarding the interactions of the $Fe(NO)_2$ unit, an interesting correlation between this unit and copper has been revealed. Such is highlighted by their respective interactions with glutathione-S transferase (GST) and S-nitrosothiols (RSNOs).[18,53,61-63] The electronic similarity of these two units is demonstrated in thiolate/disulfide interconversion reactions which involve the redox couples, $\{Fe(NO)_2\}^{9/10}$ and Cu^{II}/Cu^{I}.[65,68,80] Furthermore, Cu and $Fe(NO)_2$ in their two redox levels can form structurally analogous coordination complexes as showcased by tetramolecular and cluster compounds wherein the Cu and $Fe(NO)_2$ units occupy analogous sites.[69-71,96]

Glutathione-S transferases represent a family of enzymes that serve as part of the cell detoxification mechanism by binding toxins to activated glutathione and functioning as transport proteins.[13] These enzymes, found predominately in the liver, protect the cell

49

from harmful toxins such as carcinogenic metabolites and metal ions, by catalyzing the nucleophilic attack of glutathione (GSH) on these electrophilic substrates.[73,74] In 2016, Ahmed *et al.* reported the effects of a range of metal ions as chloride salts (NaCl, KCl, $FeCl_2$, $LaCl_2$, $MnCl_2$, $CaCl_2$, $MgCl_2$, $NiCl_2$, $ZnCl_2$, $CdCl_2$, $CoCl_2$, $CuCl_2$, $FeCl_3$, and $AlCl_3$) on camel liver GST.[63] Of all the metals tested, Cu^{II} showed the greatest inhibition of enzyme activity, readily attributed to the strong binding affinity of Cu^{II} for the thiol groups on GST. Studies using GST from rat liver and mouse lung fibroblast cells have further proven the high affinity of Cu^{II} for GST, although no structural evidence for the binding of Cu to GST has been reported to date.[61,97] Interestingly, in 2005, Cesareo *et al.* isolated and structurally characterized human GST P1-1 with the $Fe(NO)_2$ unit bound to the active site via tyrosine.[64] In this study, an exogenously prepared bis-glutathione DNIC, $[(GS)_2Fe(NO)_2]^-$, i.e. the oxidized, $\{Fe(NO)_2\}^9$ form, was introduced to the GST, resulting in replacement of one of the GS ligands with the tyrosine of the GST active site.[64] Although it remains to be seen how the Cu^{II} (and other metals) binds to the GST, we note that the electronic correlation holds, in that the $Fe(NO)_2$ unit is in the oxidized $\{Fe(NO)_2\}^9$ state.

The decomposition of the biological NO carriers S-nitrosothiols (RSNOs), also demonstrates a correlation between Cu and the $Fe(NO)_2$ unit. Copper is known to facilitate the breakdown of RSNOs, yielding NO and disulfide, as shown in Scheme III-1.[53,54,98] A major argument supporting these studies is the attenuation of RSNO decomposition upon the addition of 2,9-dimethyl-1,10-phenanthroline (commonly called neocuproine), known for its high selectivity towards Cu^I. [53,54,98] Although neocuproine

does not as efficiently chelate Fe^{2+}, Vanin, *et al*. reported that in the presence of $NO_{(g)}$, neocuproine does bind to iron, forming stable DNICs.[18,59] The fact that neocuproine binds iron when NO is present (where previously it was assumed that neocuproine selectively bound Cu^I) presents the possibility that copper might not be the sole facilitator of NO release from RSNOs. Indeed, Vanin, *et al.* noted that either Fe^{2+} or Fe^{3+} ions accelerated the degradation of RSNO (where R = cysteine) concomitant with the appearance of a DNIC, where the source of the NO in the DNICs formed was traced to the RSNOs.[18] The DNICs were identified by the appearance of the prototypical signals centered near g = 2.03, and assigned to either cysteine-containing (in the case where L-cysteine was also added) or to phosphate-containing DNICs (when in phosphate buffer).[23] Although not a direct correlation between Cu and $Fe(NO)_2$, the formation of the DNIC in RSNO degradation suggests these two units might be at work in the same process, i.e. the breakdown of RSNO.

The electronic similarities between the $\{Fe(NO)_2\}^{9/10}$ and Cu^{II}/Cu^I redox couples with regards to thiolate/disulfide interconversion are also demonstrated in recent work by the M. Y. Darensbourg laboratories. A DNIC of the form [(sIMes)(SPh)Fe(NO)$_2$], (where sIMes = 1,3- bis(2,4,6- trimethylphenyl)-imidazole and SPh = thiophenol) was found to undergo a reduction in the presence of $CO_{(g)}$ to form disulfide and the reduced, $\{Fe(NO)_2\}^{10}$ [(sIMes)(CO)Fe(NO)$_2$].[65]
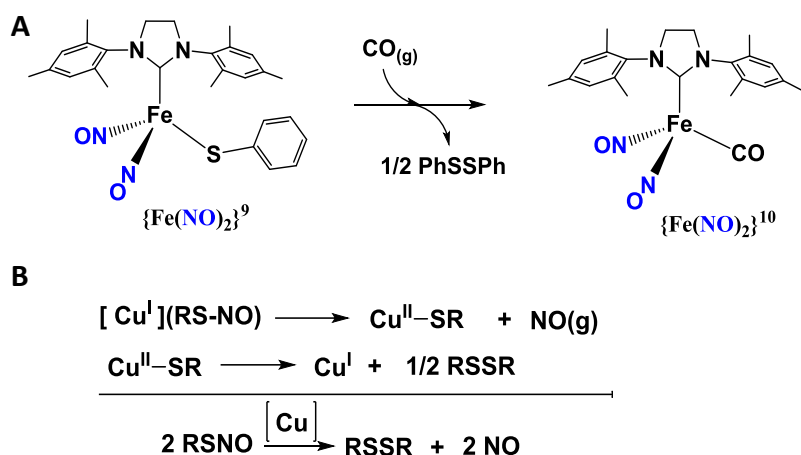
Figure III-1. Electronic similarities between Cu and Fe(NO)$_2$ displayed in the $\{Fe(NO)_2\}^{9/10}$ and Cu^{II}/Cu^{I} redox couples with regards to thiolate/disulfide interconversion.[65]

In a study that parallels the Darensbourg work outlined above (albeit with copper), Henkel *et al.* reported formation of disulfide, concomitant with $Cu^{II/I}$ reduction, induced by addition of chloride ions.[68] In this regard, Cu^{II} is known to be a potent oxidant for disulfide formation in proteins. For example, the metalloprotein responsible for the delivery of Cu to superoxide dismutase 1 (SOD1), is proposed to assemble cysteinyl thiolates resulting in disulfides between itself and the apo-Cu-SOD1, ultimately leading to the translocation of copper into the SOD1.[80]

In addition to the electronic similarities between these two units, there are also examples of structural similarities that have been uncovered in studies of the binding affinities of metal thiolates as S-donor ligands to Cu^{I} and $\{Fe(NO)_2\}^{10}$. Reaction of [Ni(bme-dach)Fe(NO)$_2$(CO)] (where bme-dach = N,N′-bis (2-mercaptoethyl)- 1,4-

diazacycloheptane) with $Fe(CO)_2(NO)_2$ yields a complex containing two six-membered NiS_3Fe_2 cyclohexane-like rings in chair conformations and one eight membered $Ni_2S_4Fe_3$ ring held within an incomplete adamantane-like cluster (highlighted in the structure in Figure III-2).[70]

$M = Ni^{II}, Cu^{II}$
$M' = Cu^{I}Cl, \{Fe(NO)_2\}^{10}$
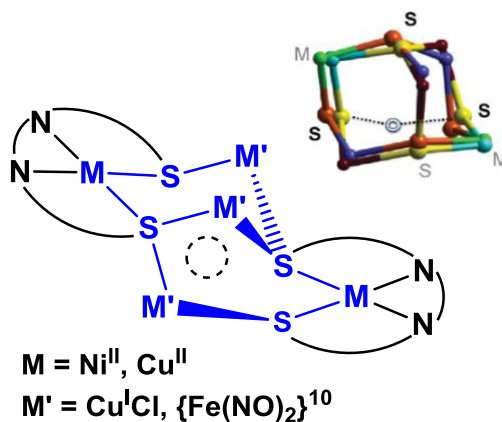
Figure III-2. Simple depiction of the adamantane-like clusters containing a vacant site when $M = Cu^{II}$ and $M' = Cu^{I}Cl$ or when $M = Ni^{II}$ and $M' = Fe(NO)_2$. The two incomplete adamantane cores overlay well, as depicted in the structural overlay.[69,70]

An analogous incomplete adamantane-like cluster is formed from the simple combination of $Cu^{I}Cl$ with $Cu^{II}(N_2S_2)$ ($N_2S_2 =$ bis(N,N'-2-mercapto-2-methylpropyl)-1,5-diazocyclooctane), while the major product in this reaction as well as a similar reaction of $Cu^{I}Cl$ and $Ni(N_2S_2)$ realized the completed adamantane core.[69] An overlay of the two incomplete adamantane-like cores is shown in Figure III-2. As illustrated by the open circle, a vacant site exists wherein a fourth metal would be bound. This possibility

was realized by Cu^I but not by $\{Fe(NO)_2\}^{10}$. Preliminary computations suggested that the reason for this vacant site in the latter case is the steric constraint of the additional $Fe(NO)_2$ unit.[70]
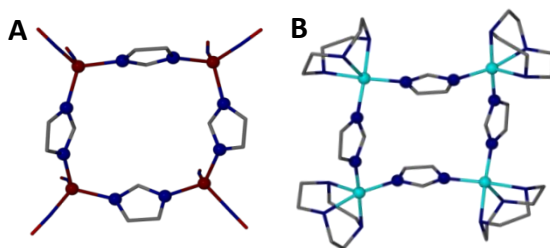
Figure III-3. Tetramolecular squares comprised of imidazole linkers in which either $\{Fe(NO)_2\}$ (A) or CuL (L = 1,4,7-triazacyclononane) (B) occupy the corners.

While Cu^I and $\{Fe(NO)_2\}^{10}$ form cluster compounds with thiolates, the structural analogs of Cu^{II} and $\{Fe(NO)_2\}^9$ reside in a harder donor environment. As shown in Figure III-3, tetrameric molecular squares of Cu^{II} and of $\{Fe(NO)_2\}^9$ bridged by imidazole have also been isolated.[71,96] In both cases, the corner atoms are comprised of either $\{Fe(NO)_2\}^9$ or $Cu^{II}L$, where L = 1,4,7-triazacyclononane).[71,96]

In light of the correlation between Cu and the $Fe(NO)_2$ unit, as well as the high concentration of copper in the cytosol, we have designed an experiment that explores the competition between Cu and $Fe(NO)_2$ for a chelating agent, neocuproine, known to bind both. These reactions show redox changes and NO release, as neocuproine is transferred

54

from the DNIC to the copper. The products of this complex reaction are identified and discussed below.

Results and Discussion

Synthesis and Characterization of the Neutral $\{Fe(NO)_2\}^{10}$ [(neo)Fe(NO)_2] (1) and the Cationic $\{Fe(NO)_2\}^9$ [(neo)Fe(NO)_2]$^+$ (1$^+$)

To explore DNIC reactivity with Cu, we chose the $\{Fe(NO)_2\}^{10}$ DNIC, [(neo)Fe(NO)_2] (**1**), where neo = 2,9-dimethyl-1,10-phenanthroline, a widely used copper chelator. Complex **1** was synthesized in a manner similar to that used by Kim, *et al.* in which neo was added to $Fe(CO)_2(NO)_2$, as shown in Figure III-3.[99]

A color change from orange red to dark red brown was observed, and the resulting solution of the air-sensitive product was characterized by IR and UV-Vis spectroscopies. The IR spectrum of the diatomic ligand region recorded in THF solution (blue spectrum shown in Figure III-4) revealed disappearance of the CO bands of the $Fe(CO)_2(NO)_2$ and a shift of the NO bands from 1761 and 1807 cm^{-1} to 1648 and 1697 cm^{-1} (1628 and 1692 cm^{-1} (KBr) as reported by Kim, *et al.*).[99]
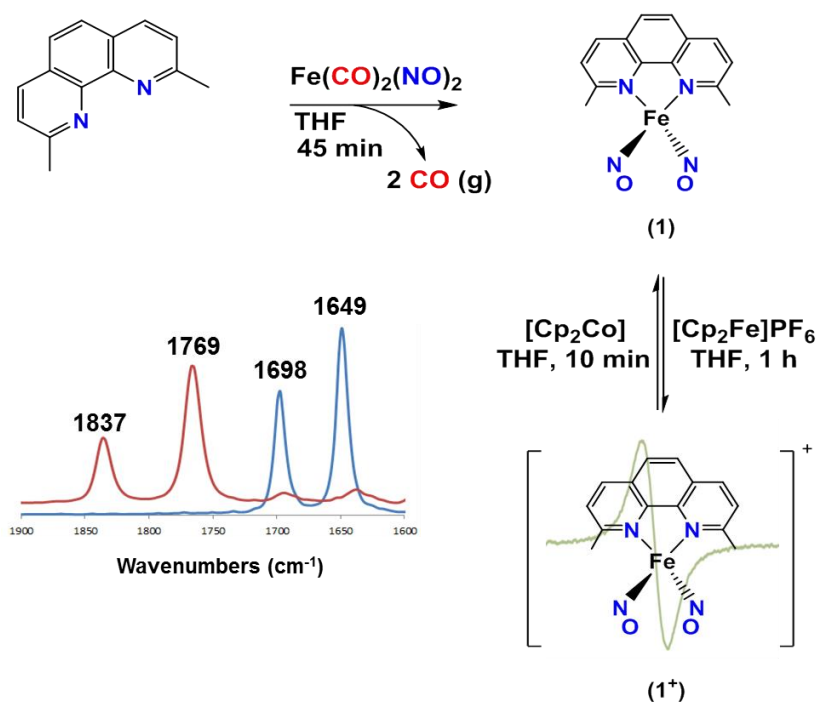
Figure III-4. Reaction scheme for the synthesis of complex **1** and it's oxidation to complex **1**⁺. Also shown is the overlay of the ν(NO) IR spectra of complex **1** (blue) and complex **1**⁺ (red) in THF.

Complex **1** is thermally stable in organic solvents in the absence of oxygen or added reagents, rendering it an ideal candidate to explore NO release. Additionally, we recently reported NO release from **1** in aqueous media in both the presence and absence of endothelial cells, making it one of the only examples of a reduced $\{Fe(NO)_2\}^{10}$ DNICs explored for NO release.[100]
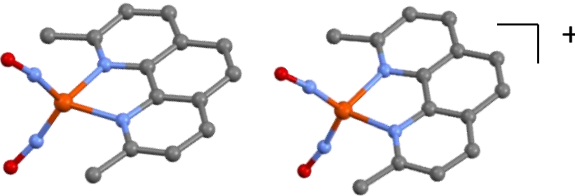
Oxidation of **1** by addition of 1 equiv of FcPF$_6$ at -78°C resulted in a shift in the ν_{NO} bands from 1648, 1697 cm^{-1} to 1769, 1837 cm^{-1}, presumably forming $[(neo)Fe(NO)_2]^+$ (**1**⁺). The large red shift (~130 cm^{-1}, where ~100 cm^{-1} shift is expected

56

for a one electron oxidation) coupled with an increase in the separation between the bands corresponds well to what is observed in similar compounds such as (sparteine)Fe(NO)$_2$, which shows a ν_{NO} shift from 1622, 1679 cm^{-1} to 1746, 1814 cm^{-1} upon oxidation.[101] Although comparison of the IR spectra of **1** and (TMEDA)Fe(NO)$_2$ find the two N-donor ligands are nearly identical in electron-donating ability ((ν(NO): 1648, 1697 cm^{-1} (**1**) and 1648, 1698 cm^{-1} (TMEDA)Fe(NO)$_2$), the (TMEDA)Fe(NO)$_2$$^+$ is only observed as a short-lived intermediate,[45] while **1**$^+$ remains for several hours in solution.

The EPR spectrum of **1**$^+$ (watermark behind chemdraw of **1**$^+$, Figure III-4) exhibits a strong isotropic signal with g = 2.05 at 298 K, very close to that reported for (TMEDA)Fe(NO)$_2$$^+$, albeit slightly higher than what is commonly reported for {Fe(NO)$_2$}^{9} DNICs (g = 2.03).[45] Addition of cobaltocene to a solution of **1**$^+$ cleanly reduces it back to **1**, as confirmed by IR spectroscopy (ν_{NO}: 1648, 1697 cm^{-1}) (Figure III-3). These results align well with the reversible redox couple seen by cyclic voltammetry (E$_{1/2}$ = -0.402 V vs. Fc/Fc$^+$ in CH$_3$CN), which confirms that a cationic [(neo)Fe(NO)$_2$]$^+$ species should be accessible by chemical oxidation.

The oxidized version of **1** (**1**$^+$) was earlier prepared by Lehnert, *et al.* from exposure of a mixture of a ferrous acetonitrile adduct and neocuproine to NO gas. The product **1**$^+$ was isolated and structurally characterized (Figure III-5).[102] Though **1** has been previously synthesized and used in various studies,[99] to our knowledge, it has not been structurally characterized. Slow diffusion of hexanes/ether into a DCM solution of **1** afforded dark red crystals that were analyzed by X-ray diffraction. Complex **1** (as well

57

as its oxidized counterpart **1**$^{+}$) exhibit the pseudotetrahedral geometry typical of these complexes. The slight bend of the NO ligands is toward each other, adopting the well-known "attracto" conformation, which is defined by smaller O-Fe-O angles as compared to the N-Fe-N angles, in the planar FeN_2O_2 unit.

	1.649(1)	1.675(6)
Fe-N$_{(NO)\ (avg)}$ (Å)	1.649(1)	1.675(6)
Fe-N$_{(ligand)\ (avg)}$ (Å)	2.063(2)	2.042(5)
N$_1$-O$_1$ (Å)	1.201(1)	1.177(8)
N$_2$-O$_2$ (Å)	1.199(1)	1.174(8)
∠N$_3$-Fe-N$_4$ (°)	79.7(1)	83.1(2)
∠Fe-N-O $_{(avg)}$ (°)	169.0(3)	169.5(6)

Figure III-5. XRD-derived structures of **1** (left, this work) and **1**$^{+}$ (right)[102] given as ball and stick representations. Key metric parameters of each are given below the structures.

XRD-derived structures of **1** and **1**$^{+}$ along with key metric parameters are given in Figure III-5. Comparison of these parameters trend as expected.

The average Fe-N_{NO} bond lengths are slightly longer for 1^+ than seen in **1** (1.675 (6) Å for 1^+ and 1.649 (1) Å for **1**) while the average N-O bond length is shorter in the case of 1^+ (1.176 (8) Å for 1^+ and 1.200 (1) Å for **1**), both of which are consistent with decreased π backbonding from the NOs in 1^+.[102] The N_{NO}-Fe-N_{NO} angle remains about the same in each at 169°.

The N(3)-Fe-N(4) angle of 79.7(1)° of **1** is slightly smaller than the N(3)-Fe-N(4) angles seen in the other complexes with similar ligand sets (TMEDA)Fe(NO)$_2$ (82.57°) and (sparteine)Fe(NO)$_2$ (84.03°).[101] In all cases, the distorted geometry can be attributed to the strain effect of the chelating ligand.[101] The NO ligands of **1** are slightly bent with an average Fe-N-O angle of 169°, which aligns well with the angles seen in other {Fe(NO)$_2$}[10] DNICs, for example the bis-imidazole (Imid-Me)$_2$Fe(NO)$_2$ (168°)[jen], (TMEDA)Fe(NO)$_2$ (168°), and (sparteine)Fe(NO)$_2$ (164°).[101]
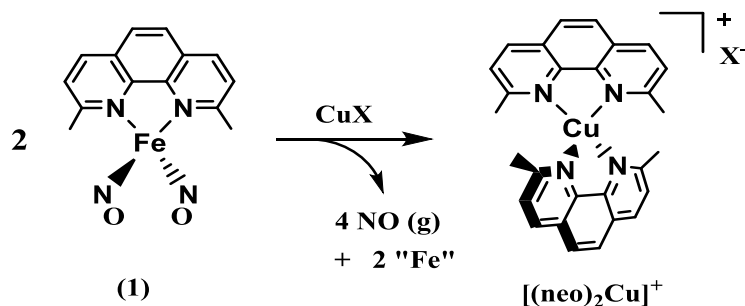
Figure III-6. Reaction of **1** with Cu^{I} salts to form the known complex [Cu(neo)$_2$]$^+$ and NO (g).

Reactivity of 1 with CuX (where X = Br⁻, Cl⁻, PF₆⁻)

To begin investigating how copper might interact with a DNIC *in vivo*, we consider the main environments in which the two might come in contact. Firstly, considering the intracellular environment is reducing, i.e. a high concentration of glutathione, any interaction between copper and $Fe(NO)_2$ within the cell would likely involve Cu^I.[72] Hence, we first explored the reaction between Cu^I salts and **1,** a rather simple yet effective reaction model.

Complex **1** was dissolved in DCM and treated with a DCM solution of CuX (X = Br⁻, Cl⁻, PF₆⁻) (2:1 stoichiometry). Most likely due to the poor solubility of copper salts in DCM, the reaction proceeded slowly. During the course of the reaction, NO gas was released, as confirmed qualitatively by an NO trapping agent, [Fe(bme-daco)]₂, (where bme-daco = N,N′-bis (2-mercaptoethyl)- 1,4-diazacyclooctane) which converts to (bme-daco)Fe(NO) upon reaction with $NO_{(g)}$ (v(NO): 1648 cm⁻¹).[92] In the absence of copper, **1** remains stable and no $NO_{(g)}$ formation is observed, indicating that copper does indeed play a role in NO release. The amount of NO released after 12 h correlated with the solubility of the starting copper salts. Solubility for the copper salts in DCM follows the trend $[Cu(CH_3CN)_4]PF_6 > CuBr > CuCl$, while the percentage of NO released is 97%, 89 % and 40%, respectively, after a 12 h stir.

Although the fate of the Fe remains unknown in these reactions, the copper product was readily identified. After stirring overnight, all reactant NO bands disappeared, and no new IR-active species formed. Additionally, the solution changed color in all cases to a bright orange red, indicating the formation of the well-known tetra-

coordinated copper complex [Cu(neo)$_2$]$^+$; this product was confirmed by both its characteristic UV-vis spectrum and Mass Spectrometry. The ESI mass spectrum showed a single isotopic bundle at 479 m/z, which matches both the calculated and literature reported values for [Cu(neo)$_2$]$^+$. Coppens *et al.* have carried out extensive studies on the solid state structures of [Cu(neo)$_2$]$^+$, finding that it can adopt a variety of conformations with various degrees of rocking or flattening, depending upon the counter anion used.[88] For example, when the counter ion is PF$_6^-$, the X-ray crystal structure shows a distortion by flattening toward a more square planar geometry, while with the BF$_4^-$ counter ion, a rocking distortion is more prominent, leading to a trigonal pyramidal geometry. However, the idealized ground state geometry of all the [Cu(neo)$_2$]$^+$ complexes is comprised of a pseudotetrahedral, D$_2$d-symmetric arrangement of the phenanthroline ligands around the copper center.[88] For this D$_2$d symmetry, four low-energy singlet to singlet transitions are possible,[103] but only one has its dipole moment operator along the 2-fold axis.[88] Thus, there is only one symmetry-allowed transition, which is seen at around 450 nm in the solution absorption spectra.

Overall, the reaction of CuBr with **1** is a ligand exchange reaction in which the neo ligand is transferred to the Cu^I, while the Fe(NO)$_2$ unit most likely falls apart due to the lack of available coordinating ligands. While it is unlikely that the halide would attack the electron rich {Fe(NO)$_2$}^{10} unit, the possibility of such a reaction was nonetheless tested. A reaction similar to that shown in Figure III-6 was carried out as described in the previous paragraph, but with NaBr replacing the CuX. Even after a 24 h stir, **1** remained unreacted (vid IR spectroscopy) and NO release was not observed. We

also note the reaction worked when the copper source was $Cu(CH_3CN)_4PF_6$, demonstrating that the halide is not essential in the reaction mechanism.

Likewise, when $Fe(CO)_2(NO)_2$ (instead of **1**) is reacted with Cu^I, no change in the IR spectrum was observed, even after hours of stirring. Hence, without the neo ligand present, the DNIC appears to be inert (or at least less reactive) toward the Cu^I salts. The reaction of **1** with Cu^I can thus be best described as a ligand exchange reaction, where the driving force appears to be the stability of the product $[Cu(neo)_2]^+$. Changing either of the starting materials in this reaction, i.e. replacing either **1** with $Fe(CO)_2(NO)_2$, or CuX with NaBr, shows no reaction.
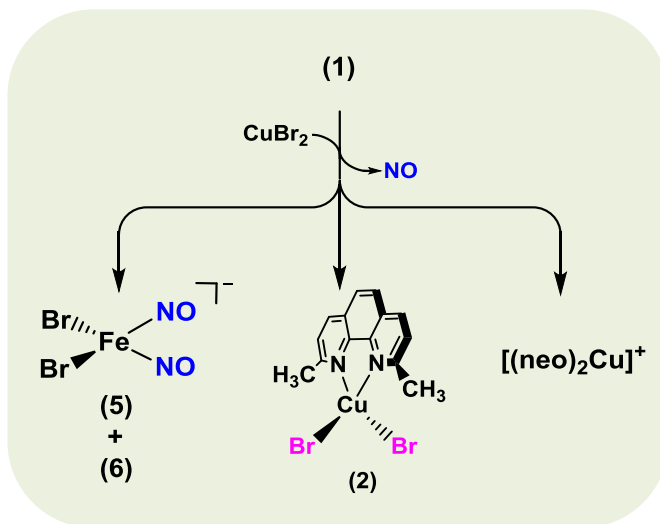
Figure III-7. Reaction of **1** with CuBr₂ exhibits both a redox reaction and ligand transfer, yielding a mixture of products. The products shown are those that have been identified. Complex **6** has been observed spectroscopically and will be discussed in the section on identification of the new DNICs products.

Reactivity of 1 with CuX$_2$ (where X = Br$^-$, Cl$^-$)

Though evidence exists for transport of intact DNICs into the cell,[104] the possibility also remains that DNICs might degrade before entering the cells. Since exogenous addition of DNICs as therapeutics is a translational aspect of these studies both by us and others, developing a clear understanding of interactions at the cell surface, or *en route* to the cell, is of crucial importance. Hence, we employed a similar strategy to that outlined the section on Cu^I reactivity, but this time using CuX$_2$, where X = Cl$^-$, Br$^-$.

Unlike the simple ligand exchange reaction with Cu^I, reaction of **1** with Cu^{II} salts appears to be a one-electron redox process accompanied by ligand exchange. With a much lower redox potential of -0.36 V, **1** is readily oxidized by the CuBr$_2$ (E$_{1/2}$ = 0.18 V, Figure III-8) to yield a mixture of oxidized DNIC products and the Cu^I species [Cu(neo)$_2$]$^+$. The cyclic voltammograms of the two reactants, as well as the copper products are given in Figure III-8 and the redox potentials given assume reversibility, although the event is not rigorously reversible as classically defined.

(2)
$E_{1/2}$ = - 0.21 V

[(neo)₂Cu]⁺
$E_{1/2}$ = 0.43 V

(1)
$E_{1/2}$ = - 0.36 V

CuBr₂
$E_{1/2}$ = 0.18 V

1   0.5   0   -0.5   -1

V vs. Fc/Fc⁺
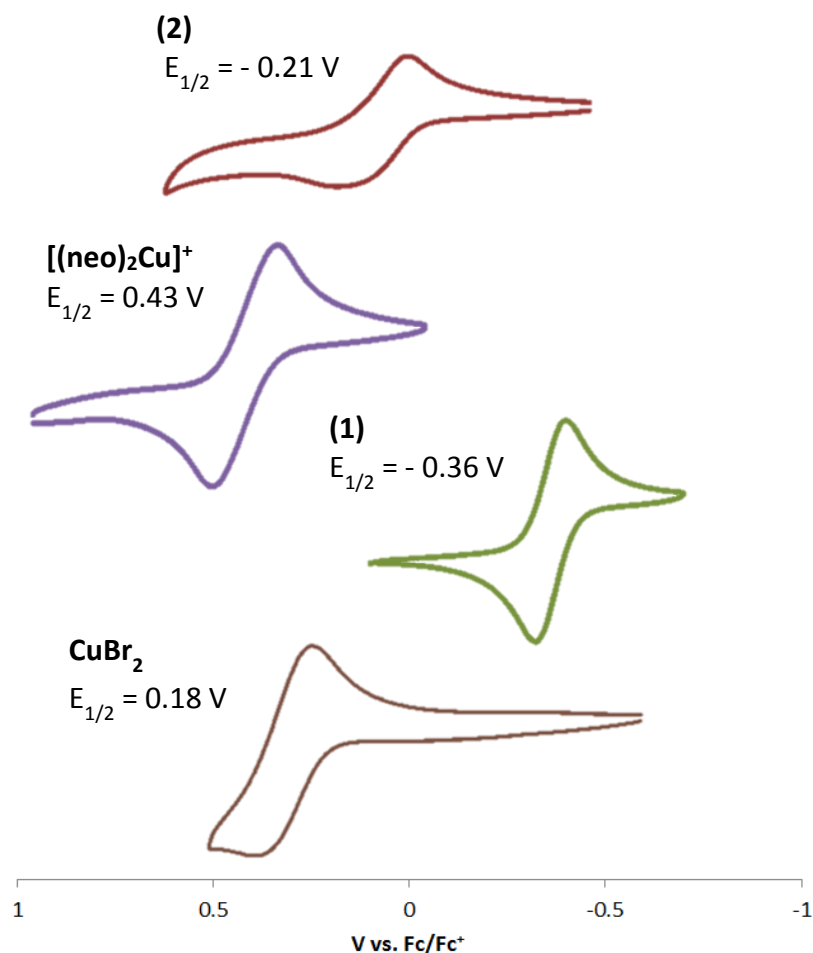
Figure III-8. Cyclic voltammograms of **2** (maroon, top), [Cu(neo)₂]⁺ (purple, second from top), **1** (green, third from top) and CuBr₂ (brown, bottom) all in MeCN.

With a 2:1 ratio of **1**:CuX₂ (X = Cl⁻, Br⁻), the reaction is complete within an hour, forming a dark red-brown solution with CuBr₂ and an orange brown when CuCl₂ is used. The IR spectrum of this solution shows the growth of two new NO bands at 1792 (s), 1765 (sh), 1730 (s), 1705 (sh) cm⁻¹ (when X = Br⁻), concomitant with the disappearance of **1**. Both the pattern and the position of the bands suggest the formation of two

oxidized DNICs, most likely containing bromides. Attempts to separate, isolate and characterize these products were unsuccessful. Hence, we developed alternate synthetic routes (discussed in the next section) to support the presumed identity of the DNIC products. In addition to the formation of new DNICs, the production of NO was also detected (via trapping with [Co(bme-dach)] as described earlier). Both mass spectrometry and UV-vis spectroscopy confirmed that the sole copper product that formed was the $[Cu(neo)_2]^+$(Figure III-9).

When $X = Cl^-$, the IR spectrum of the reaction mixture of **1** and $CuCl_2$ shows the complete disappearance of the $\nu(NO)$ bands of **1** and no new bands appear. The UV-vis spectrum exhibits two distinct absorptions at 353 and 845 nm. X-ray analysis of the green crystalline product formed when $CuCl_2$ is used revealed a trigonal bipyramidal copper complex $[(neo)CuCl_2 \cdot H_2O]$ (**4**). However, we chose the $CuBr_2$ system to study in depth as discussed next.
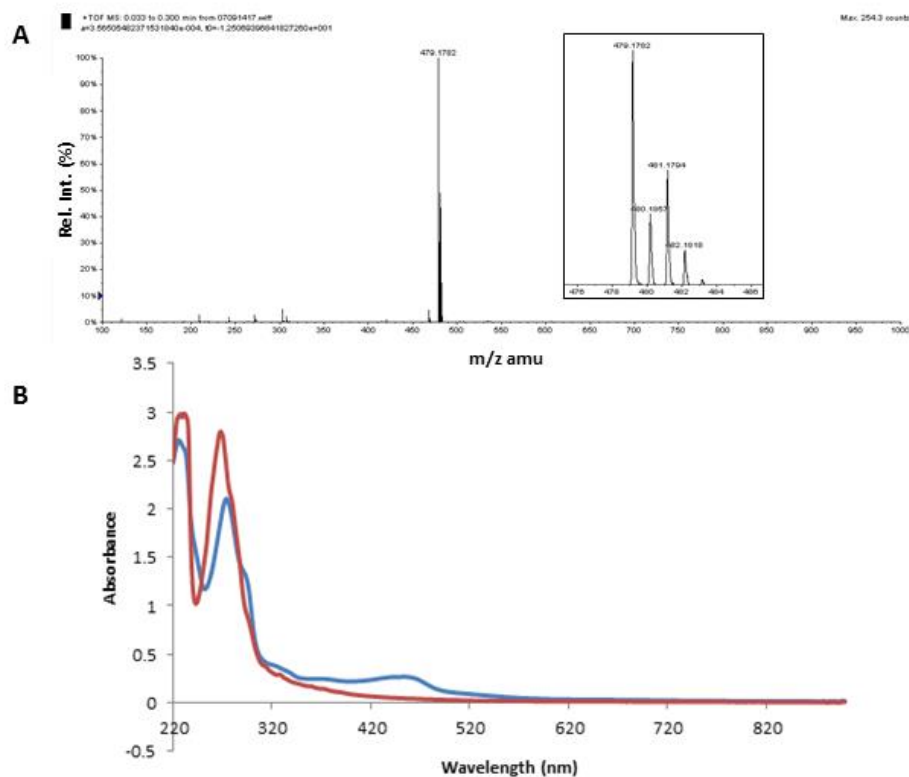
Figure III-9. +ESI-MS of the mixture produced from reaction of **1** with CuPF₆ (reaction stoichiometry 2:1). The isotope bundle for the parent ion [(neo)₂Cu]⁺ is centered at 479 m/z. The top spectrum shows the full range, while the lower spectrum is zoomed in to show the pattern for the parent isotopic bundle. The UV-vis spectrum of **1** (red) with the product mixture from the reaction shown in Figure III-1 (blue) is displayed as an inset and shows the appearance of the absorbance at 454 nm.

When the reactant stoichiometry was changed to a ratio of 1 to 1 (i.e., an excess of CuX₂), an additional Cu product was formed, along with all of the products observed above. In this case, the reaction occurred upon mixing, as evidenced by the immediate color change to a dark red-brown. An IR spectrum of the reaction mixture recorded

66

within 2 min of mixing showed complete disappearance of the NO bands of **1,** and appearance of the new bands at 1792 (s), 1765 (sh), 1730 (s), 1705 (sh) cm^{-1}. An additional copper product, besides the [Cu(neo)$_2$]$^+$, was observed via UV-vis spectroscopy. In the case of X = Br $^-$, there is a distinct absorption band that appears at 567 nm (Figure III-10), which corresponds to the pseudotetrahedral [(neo)CuBr$_2$] (**2**), confirmed by comparison of the UV-vis spectrum obtained from this reaction with that of **2** synthesized via an alternate route.
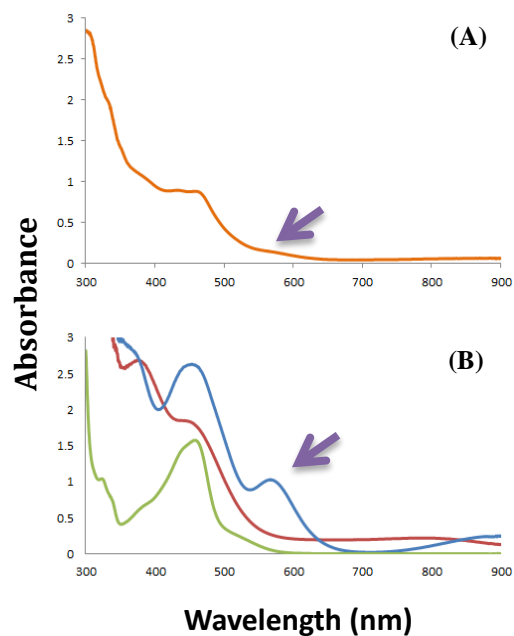
Figure III-**10.** Overlay of the UV-vis spectra of **2** (blue), **1** (red) and [(neo)$_2$Cu]$^+$ (green). The top spectrum is of the reaction mixture of CuBr$_2$ and **1**.

Figure III-10 B shows an overlay of the two copper products, [(neo)$_2$Cu]$^+$ (green) and **2** (blue) , along with that of **1** (red). As can be readily seen, the absorption band at 567 nm that appears in the CuBr$_2$ and **1** product mixture (Figure III-10 A) can be attributed to the formation of **2**. Mass spectrometry further confirmed the formation of both [(neo)$_2$Cu]$^+$ and **2** with two main isotopic bundles centered at 351 m/z (**2** – Br $^-$) and 479 m/z ([(neo)$_2$Cu]$^+$) (Figure III-11).
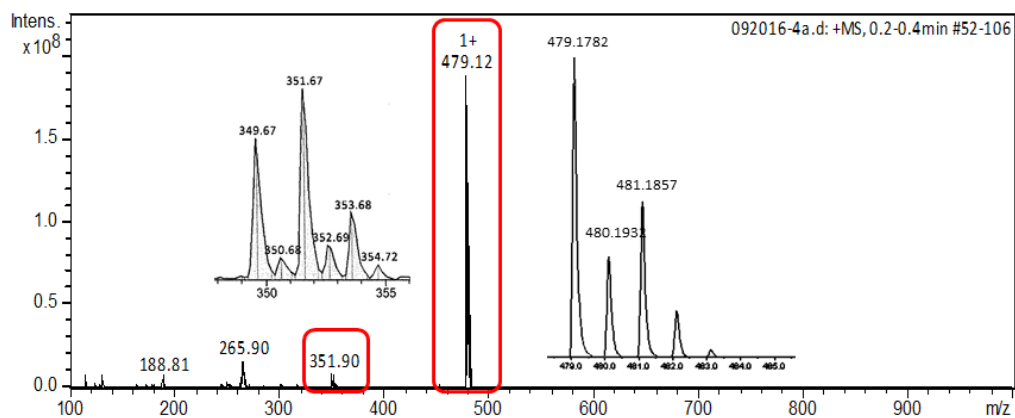
Figure III-11. $^+$ESI-MS of the product mixture from reaction of **1** with CuBr$_2$ (reaction stoichiometry 1:1) (see Figure III-7). Two copper containing products were identified, namely [(neo)$_2$Cu]$^+$ (m/z = 479 m/z) and **2** (m/z = 351, **2** – Cl$^-$).

Ford *et al.* reported the structure of [(neo)$_2$Cu(H$_2$O)]$^{2+}$, which readily converts to the Cu^I analog, [(neo)$_2$Cu]$^+$.[105] This tendency to convert to the reduced species, [(neo)$_2$Cu]$^+$, along with the stability of the [(neo)$_2$Cu]$^+$, might account for the high

intensity of $[(neo)_2Cu]^+$ compared to that of **2** in the mass spectrum. Detailed analysis of each of the products formed in this reaction are given in the sections that follow.

Structural Analysis of the Complexes 2-5

Complexes 2 and 3

In addition to being formed in the reaction shown in Figure III-7, Complex **2** was synthesized directly from addition of the neocuproine ligand to $CuBr_2$. XRD analysis of the dark red needles obtained from this reaction revealed a pseudotetrahedral copper center coordinated by two bromides and the nitrogens of the neocuproine (Figure III-12 A). An identical structure was obtained from the reaction of $CuBr_2$ and **1**.
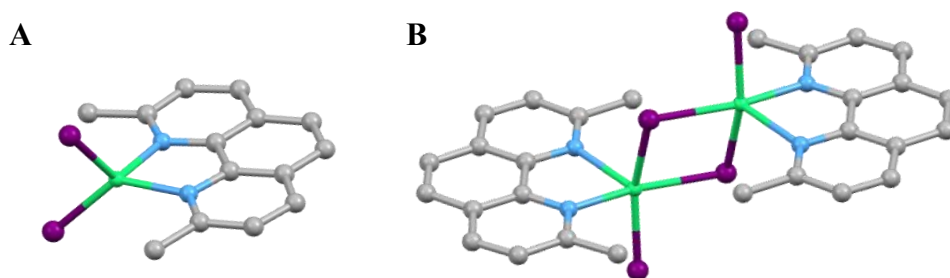
Figure III-12. The ball and stick representation of **2** (A) and its dimeric form, **3** (B). Hydrogens have been omitted for clarity.

The geometry about the Cu^{II} center of **2** is pseudotetrahedral whose dihedral angle, defined as the intersection between the CuN_2 and $CuBr_2$ best planes, is 64.93°, indicating a twist of 25.07° from perfect tetrahedral geometry. The N(1)-Cu-N(2) angle

of 83.5° is comparable to the N-Fe-N angle seen in the **1** and **1$^+$**, but slightly larger than the N(1)-Cu-N(2) angle of 81.2° in a similar complex, (phen)CuBr$_2$ (phen = 1,10-phenanthroline).[106] Although the only difference in these two ligands is the methyl groups on the 2 and 9 positions of the *ortho*-phenanthroline, the geometry adopted by (phen)CuBr$_2$ is planar, and forms a polymer with ladder-like bridging geometry.[106] Other N$_2$CuBr$_2$ complexes, such as where N$_2$ = cyclohexane-1,2-diamine, also adopt a square planar geometry for the asymmetric unit and form a coordination polymer.[107] However, the bite angle in the case of N$_2$CuBr$_2$ (N$_2$ = cyclohexane-1,2-diamine) is 83.7°, which is nearly identical to that of **2**.[107] From this, it appears that neocuproine prevents the coordination polymer formation that is commonly seen in other bidentate, N$_2$ ligands. Indeed, the Cl-analog of **2**, synthesized by Wang and Zhong, maintains a distorted tetrahedral coordination, with an N(1)-Cu-N(2) angle of 81.6°, and does not show polymer formation.[108] The Cu-N bond lengths of 2.028 Å and 1.984 Å in **2** correspond well to those seen in the previously mentioned N$_2$CuBr$_2$ compounds, which range from 2.012 Å to 2.048 Å.[106,107] In each case, one Cu-N bond is always shorter than the other.

Complex **3**, which co-crystalizes with **2**, is simply a dimer of two identical units of **2**. Each Cu^{II} center is coordinated by the two nitrogens of the neocuproine ligand, one terminal bromide and one bridging bromide. The average Cu-N distance is 2.109 (2) Å, which is slightly little longer than the average Cu-N bond in **2** (2.007 (2) Å). The terminal Cu-Br bonds are also longer in **3** compared to **2**, 2.4128(5) and 2.3576 (5) Å,

respectively. The N-Cu-N angle of 79.93 (8)° in **3** is also more pinched than it is in **2** (83.44(9)°).

Furthermore, comparison of **3** with two similar halide-bridged copper species, (μ-Br)$_2$[Cu(neo)]$_2$ and (μ-Cl)$_2$[Cu(DPS)Cl]$_2$ (DPS = Di(2-pyridyl)sulfide) shows that all parameters, besides the Cu-Cu distance and the N-Cu-N angles, are nearly identical.[109] The Cu-Cu distance in **3** is 3.6773(6) Å, very close to that found for (μ-Cl)$_2$[Cu(DPS)Cl]$_2$ (3.69 Å). The (μ-Br)$_2$[Cu(neo)]$_2$ derivative of **3**, lacking only the terminal bromides present in **3**, had a much shorter Cu-Cu distance at 3.097 Å. The N-Cu-N angle of 79.93(8) Å in **3** is essentially identical to the (μ-Br)$_2$[Cu(neo)]$_2$ at 80.3 (2)°.

This dimer appears to be a product of crystallization rather than a separate product in solution. The UV-vis spectrum of the crude reaction mixture of neocuproine and CuBr$_2$ is identical to that of the spectrum of the isolated crystals of **2** (blue spectrum in Figure III-7 B). Furthermore, no dimer was observed in mass spectrometry.

Complex 4

Complex **4** exhibits almost perfect trigonal bipyramidal geometry with $\tau = 0.914$. Here the copper center is coordinated by the bidentate-bound neocuproine ligand, two chlorides and a water molecule.
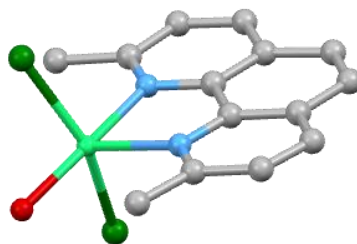
Figure III-13. The ball and stick representation of the trigonal bipyramidal complex **4**. Hydrogens have been omitted for clarity.

Other similar five-coordinate copper complexes of the N_2CuCl_2O-type tend to adopt more square pyramidal geometry, with tau values from 0.03-0.06.[109,110] Complex **4** contains a N(1)-Cu-N(2) bond angle of 79.8°, a 3.7° decrease in bite angle from that of complex **2**, but nearly identical to that seen in complex **1**. The four-coordinate analog of complex **4** (complex **4** without the water), displays a N(1)-Cu-N(2) angle of 81.6°.[108] The Cu-Cl bond distances are 2.303 Å and 2.206 Å, which fit well into the expected range of 2.242-2.560 Å seen in similar compounds.[109,110] The Cu-O bond length of 1.959 Å is slightly lower than the Cu-O bonds of the two analogous N_2CuCl_2O compounds (1.984(2) Å when N_2 = DPS and 1.9864(15) Å when N_2 = bis(tetrazolyl)amine).[109,110]

EPR Analysis of the Complexes 2-5

The EPR spectra of DCM solutions of complexes **2** and **4** were measured at both 77 and 3.6 K, as shown in Figure III-14.
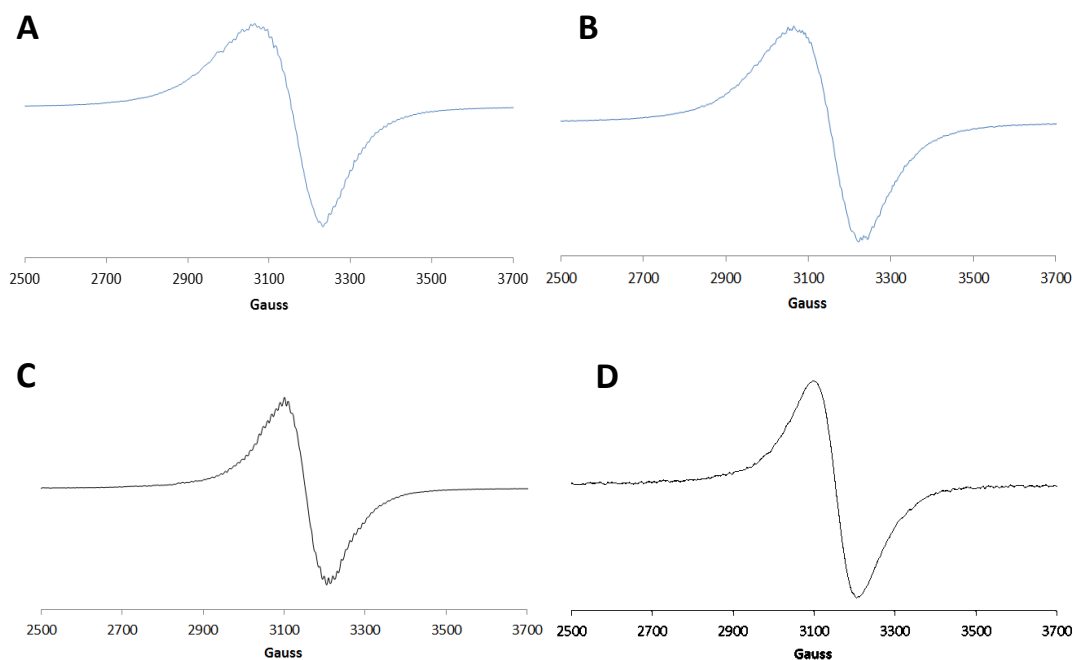
Figure III-14. X-band EPR spectrum of complex **2** in DCM at 3.6 K (A) and 77 K (B) and of complex **4** in DCM at 3.6 K (C) and 77K (D).

Each spectrum displays a broad isotropic signal at g = 2.123 for **2** and g = 2.127 for **4**. The hyperfine splitting is on par with background noise and is hardly distinguishable. With two naturally abundant isotopes of I = 3/2, ^{63}Cu (69.09 %) and ^{65}Cu (30.91 %), each copper isotope could theoretically show four line hyperfine

splitting. Although the majority of four-coordinate Cu(II) complexes show a four line hyperfine splitting, there are several examples described in the literature in which the hyperfine features are not resolved. Particularly pertinent examples include four-coordinate Cu(II) complexes with derivatized phenanthroline ligands, obviously similar to neocuproine.[111] Neither [Cu(TMP)$_2$](ClO$_4$)$_2$ (TMP = 3,4,7,8-tetramethyl-1,10-phenanthroline) or [Cu(DIP)$_2$](ClO$_4$)$_2$ (DIP = 4,7-diphenyl-1,10-phenanthroline) showed copper hyperfine features and both gave broad EPR spectra.[111] The broadening was hypothesized to arise from π stacking and non-covalent interactions between the phenanthroline ligands. Although such interactions are prevalent for phenanthroline ligands, no additional evidence was given to support such a case and no evidence for aggregation was observed in the ESI-MS, UV-vis or HPLC.[111] Complex **2**, however, can dimerize, at least upon crystallization, to form its dimeric counterpart, **3**. The Cu-Cu distance is 3.6773(6) Å in **3**, likely too great for spin coupling. Hence the broadening observed in the spectrum of **2** could be due to some formation of **3**.

In another report, a series of bis-pyrrolate-imine copper(II) complexes showed EPR spectra similar to that obtained for **2** and **4**, i.e., the hyperfine coupling was not well defined and can almost be assumed to be background noise.[112] In this particular study, the copper hyperfine splitting decreased with decreasing ligand-field transition energies.

It is difficult to differentiate the exact number of hyperfine and super-hyperfine features present in the spectra displayed in Figure III-14. In addition to the expected copper hyperfine, **2** and **4** each contain halides, as well as nitrogen ligands, that could theoretically give multiple super-hyperfine features. Both bromine and chlorine have

nuclear spins of I = 3/2, which would each introduce another four line splitting on top of the copper hyperfine. If nitrogen hyperfine splitting is also present, we would expect to see a splitting pattern possibly even in the hundreds. Considering the number paramagnetic centers, magnetic interactions between these centers is also a likely reason for the poor resolution of the hyperfine features.[113]

Identification of the New DNIC Products

The reaction of $CuBr_2$ and **1** yields two different DNIC products, as shown in Figure III-7. Amongst the many possibilities for the identity of these products, two likely products come to mind, namely $(\mu\text{-}Br)_2[Fe(NO)_2]_2$ and a monomeric anion, $[Fe(NO)_2Br_2]^-$. Although all attempts to isolate the DNIC products from this reaction mixture have proven unsuccessful, we developed several alternate synthetic routes to directly synthesize the hypothesized DNICs and spectroscopically prove their identity. The following section outlines our analysis in this regard.

Synthesis of $(\mu\text{-}Br)_2[Fe(NO)_2]_2$

Addition of bromine to a freshly prepared THF solution of $Fe(CO)_2(NO)_2$ resulted in a color change from orange red to dark brown (reaction shown in Figure III-15). The IR spectrum revealed disappearance of the CO bands of the $Fe(CO)_2(NO)_2$ at 2090, 2035 cm^{-1}, and a shift of the NO bands from 1808 and 1763 cm^{-1} to 1816 and 1769 cm^{-1} (Figure III-16).
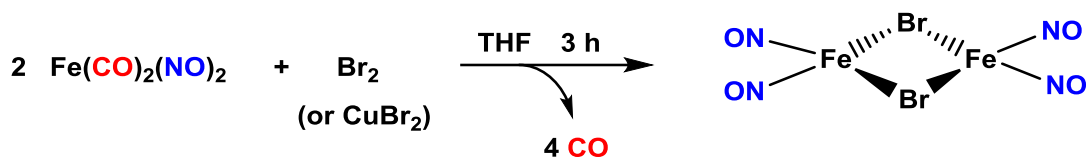
Figure III-15. The synthesis of $(\mu\text{-Br})_2[Fe(NO)_2]_2$ can be achieved by oxidative addition of Br^- (from either Br_2 or $CuBr_2$) to $Fe(CO)_2(NO)_2$.
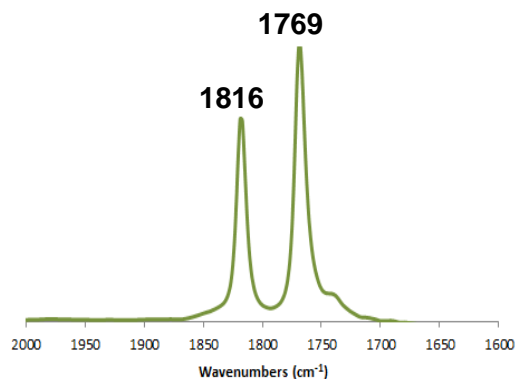
Figure III-16. IR spectrum, $\nu(NO)$ region, of $(\mu\text{-Br})_2[Fe(NO)_2]_2$ in hexanes.

Although a dimeric species is expected, the band separation of 47 cm^{-1} falls into the range of the typical monomeric DNICs (~40-60 cm^{-1}) and above the expected range for dimeric DNICs (15-38 cm^{-1}). Attempts at crystallization proved unsuccessful, however we conclude that the species formed in this reaction is not one of the DNICs formed in the $CuBr_2$ reactions, as the $\nu(NO)$ stretches do not overlay. Additionally, this

product was soluble in hexanes while the DNIC products formed in the $CuBr_2$ reaction are not.

Synthesis of [Fe(NO)₂Br₂]⁻(5)

The monomeric anion $[Fe(NO)_2Br_2]^-$ (**5**) was prepared from NaBr as shown in Figure III-17. Under an argon atmosphere, [Na-18-crown-6-ether][Fe(CO)₃(NO)] and 2 equivalents of $NOBF_4$ were stirred with NaBr for 120 min in THF. The reactant NO bands disappeared with concomitant appearance of new NO bands at 1780, 1712 cm^{-1}.

Figure III-17. Reaction scheme of the synthesis of $[Fe(NO)_2Br_2]^-$ from NaBr. The same reaction was carried out with CuBr replacing the NaBr, although the ν(NO) stretches did not match those of $[Fe(NO)_2Br_2]^-$. The product of the CuBr reaction has yet to be positively identified.

Complex **5** was isolated as a sodium crown ether salt from slow diffusion of hexanes into a THF solution. The structure is discussed below. As displayed by the blue spectrum in Figure III-18, the ν(NO) bands of **5** perfectly overlay the shoulders seen in the IR spectrum from the reaction of **1** and $CuBr_2$.

Figure III-18. Overlay of the IR spectrum of **5** (blue) with that of the new DNICs formed in the reaction of **1** with $CuBr_2$.

Hence, we assign one of the DNIC products formed in the reaction of **1** and $CuBr_2$ to be **5**. Furthermore, UV-vis analysis of **5** showed two main absorption bands at 690 and 520 nm, both of which appear in the spectrum of the reaction mixture of **1** and $CuBr_2$. X-ray analysis of the dark brown crystals of **5** confirmed the formation of the pseudo-tetrahedral DNIC, $[Fe(NO)_2Br_2]^-$ as its sodium 18-crown-6 ether salt.
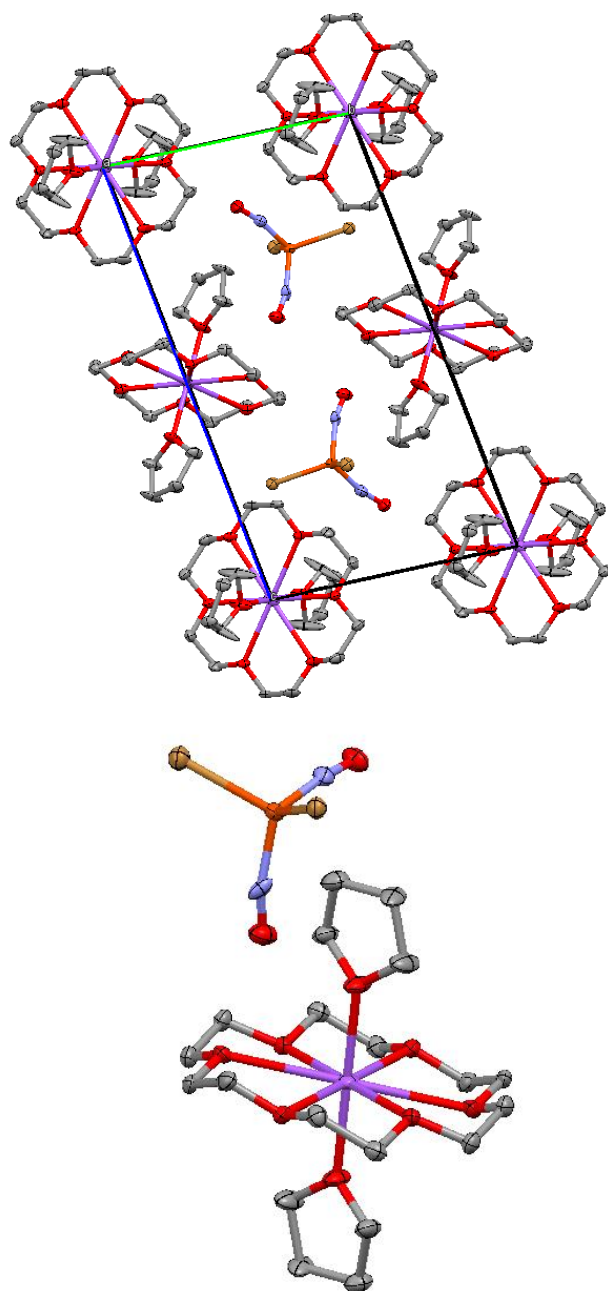
Figure III-19. The crystal packing diagram of **5** showing two of the DNIC units per unit cell (top). The ORTEP of **5** (bottom) with thermal ellipsoids drawn at 50% probability. Hydrogens have been omitted for clarity.

Complex **5** contains a tetrahedral iron center coordinated by two bromides and two nitrosyls (Figure III-19). Each unit cell houses two of the DNIC units, as shown at the top of Figure III-19. To our knowledge, the only other halide DNIC that has been structurally characterized is the iodide-containing DNIC $[I_2Fe(NO)_2]^-$.[114] The Fe-X bonds in **5** are ca. 0.2 Å shorter that those in the iodide case, as expected, while the Fe-N bond distances are about the same (avg. 1.73 Å for each). The N-Fe-N angles are almost exactly the same for each (114.3(3)° for **5** and 114.03(13)° for $[I_2Fe(NO)_2]^-$).[114] The average Fe-N-O angle is 165.9(6)° for **5** and 164.9(3)° for $[I_2Fe(NO)_2]^-$.[114]

Synthesis of Complex 6

Having confirmed the identity of one of the DNIC products formed in the reaction of **1** and CuBr$_2$, we are left with one unidentified product, observed via IR spectroscopy with ν(NO) bands at 1792 and 1730 cm^{-1}. Speculating that this product might be similar to **5** but with perhaps a Cu$^+$ counterion (or even a Cu-DNIC product), we carried out the reaction shown in Figure III-17 but with CuBr instead of NaBr. The resulting IR spectrum is shown as an overlay with the IR spectrum of the reaction mixture of CuBr$_2$ and **1** (Figure III-20).
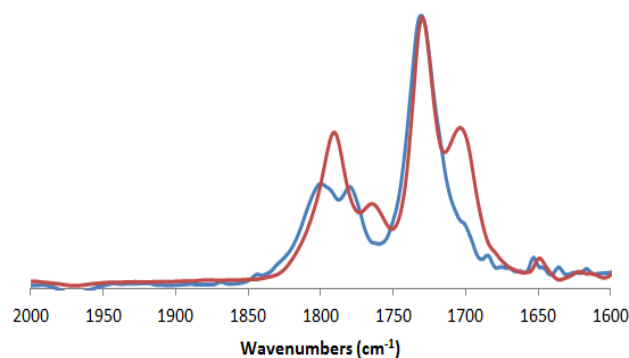
Figure III-20. Overlay of the IR spectrum of **6** (blue) with that of the new DNICs formed in the reaction of **1** with CuBr$_2$.

The NO band at 1730 cm^{-1} perfectly overlays with that of the CuBr$_2$ and **1** product mixture, while the second band at 1792 cm-1 shows an interesting split. We propose that this product might be a Cu-bridged DNIC species, although efforts to structurally characterize the product have thus far been unsuccessful.

Conclusions and Closing Comments

Building on the premise that copper and the Fe(NO)$_2$ unit can both occupy structurally equivalent sites, we designed a study that explored the competition of the copper and Fe(NO)$_2$ for neocuproine. Consistent with the strong affinity of neocuproine for Cu(I), reaction of Cu^I sources with [(neo)Fe(NO)$_2$] resulted in near quantitative formation of the well-known bis-neocuproine cation, [(neo)$_2$Cu^I]X, where X = Cl$^-$, Br$^-$, PF$_6^-$, and release of gaseous NO. For the reaction of [(neo)Fe(NO)$_2$] and Cu(II), specifically CuBr$_2$, redox processes were also involved and resulted in a mixture of copper and DNIC products and NO gas. A portion of the copper was reduced, yielding

81

the $[(neo)_2Cu^I]^+$ cation, while the remainder of the copper formed the new Cu(II) complexes $[(neo)CuBr_2]$ or $[(neo)CuCl_2H_2O]$. Interestingly, two different oxidized $\{Fe(NO)_2\}^9$ DNIC products were also observed via IR spectroscopy. One of the DNICs was isolated as the sodium 18-crown-6 ether salt of $Br_2Fe(NO)_2^-$. While this study highlights the electronic and structural connections between the $Cu^{II/I}$, $d^{9/10}$, and the $\{Fe(NO)_2\}^{9/10}$ redox couples and electronic configurations, the findings have generated many questions whose answers would greatly enhance our understanding of DNICs. The next several paragraphs will address some of the more obvious questions that have been raised and will offer direction for future studies in this area.

The release of NO in these reactions highlights an important point: the use of copper to promote NO release. To our knowledge, copper has never been explored as a promoter for NO release from DNICs prior to this work. However, considering that it catalyzes the decomposition of RSNOs which results in NO release, it is plausible that copper might be at play in endogenous DNIC decomposition. The reaction pathways for RSNO decomposition involve copper forming an adduct with the RSNO, followed by release of NO and the thiyl radical. Considering that sulfurs in thiolate-containing DNICs have available lone pairs, interaction with copper, resulting in copper thiolate complexes and the decomposition of the DNIC with release of NO (due to the lack of a supporting ligand for the $Fe(NO)_2$ unit) is reasonable.

We note that our ligand choice for this study, namely neocuproine, may skew the results towards ligand exchange due to the high affinity of copper for neocuproine. Such a result brings with it multiple questions to be addressed in the future. Will copper

82

facilitate the release of NO from DNICs containing ligand sets other than neocuproine, for example thiolates, N-heterocyclic carbenes, and/or other N-donor ligands?

Due to solubility issues with the copper salts that were used in our study from Chapter III, no kinetic data could be obtained. However, by using more soluble copper sources, such data could be gathered. Because cellular copper is normally found within a coordination sphere rather than as a salt, a more realistic model would be to use copper complexes of histidine, cysteine or glutathione. Such a system, coupled with biocompatible DNICs, for example those covered in Chapter V, would provide a realistic biomimetic study for the effect of copper on NO release from DNICs.

CHAPTER IV

INTERPLAY BETWEEN THE TWO BIOLOGICAL NO CARRIERS/STORAGE

UNITS: S-NITROSOTHIOLS AND DINITROSYL IRON COMPLEXES

Introduction

As was briefly discussed in chapter I, nitrosylation of iron-sulfur clusters results

in the formation of both protein-bound and low molecular weight DNICs, including

Roussin's red esters (RREs), through degradation of the [2Fe−2S] and [4Fe−4S]

clusters.[15] The nitrosylation of the iron-sulfur clusters is important in the regulation of

intracellular iron levels, for it stimulates the binding of iron responsive proteins.[115]

However, iron-sulfur clusters can also be regenerated from these DNICs and RREs.

Ding *et al*. reported that DNICs formed from NO-modified ferredoxin in *Escherichia*

coli (E. coli) cells can be directly transformed back into the ferredoxin cluster by

cysteine desulfurase (an S-donor) and L-cysteine.[116]

Multiple studies have provided EPR evidence for the formation of DNICs from

the interaction of NO with iron-sulfur clusters in proteins including succinate

dehydrogenase, nitrogenase, succinate-Q reductase, mitochondrial aconitase, cytosolic

aconitase, endonuclease III, SoxR and mammalian ferrochelatase.[104,117-123] However, a

complete understanding of this reaction, specifically within a biological setting, has yet

to be elucidated. One of the more insightful studies regarding this reaction was carried

out by Cowen *et al.* wherein the degradation products of a high potential iron protein

(HiPIP) were analyzed upon exposure to NO.[124] As observed by UV-vis, EPR and NMR

spectroscopies, as well as ESI-mass spectrometry, the protein-bound [4Fe-4S] cluster converted to a protein-bound DNIC with two $Fe(NO)_2$ units per cluster.

Lippard *et al.* developed small molecule protein analogs of the metalloprotein active site to give insight into the interactions of NO with iron-sulfur proteins.[90] When added stoichiometrically (1:1), the trityl-S-nitrosothiol reagent, Ph_3CSNO, mononitrosylated each of the four irons of the cluster. With addition of an excess of Ph_3CSNO, an additional nitrosyl was added to three of the four iron centers, forming dinitrosyl iron units on the cuboidal FeS scaffold.[90] This particular study provided an interesting example of the interaction between the two biological NO carrier/storage agents, namely DNICs and RSNOs. Considering that NO is rarely free *in vivo*, an RSNO is a very plausible choice for a biologically relevant source of NO. Hence, further investigation into the interactions of DNICs and RSNOs is warranted.

The formation of DNICs from RSNOs was observed by Vanin *et al.*, discussed in detail in Chapter I. Therein, DNIC formation was observed upon introduction of RSNOs to iron-containing buffer solutions.[18] Liaw *et al.* have noted the reverse of this process, i.e., formation of RSNOs from DNICs.[42] When a chelating disulfide was added to the $\{Fe(NO)_2\}^9$ DNIC $[(NO)_2Fe(C_{12}H_8N)_2]$, $(C_{12}H_8N$ = carbozolate), a mononitrosyl iron species was formed, along with RSNO.[42]

Apart from the reports reviewed above, the interaction between DNICs and RSNOs has not been thoroughly studied. Hence, we took two simple DNICs, both in the reduced $\{Fe(NO)_2\}^{10}$ form, namely $Fe(CO)_2(NO)_2$ and $[(neo)Fe(NO)_2]$ (neo = 2, 9-dimethyl-1,10-phenanthroline) and studied their reaction with trityl-S-nitrosothiol

(Ph$_3$CSNO). Unique to our study is the use of the reduced $\{Fe(NO)_2\}^{10}$ DNICs. Additionally, Ph$_3$CSNO was judiciously chosen for its stability, as well as its ability to act as a sulfide donor. The Ph$_3$CSNO thus has the potential of serving as a sulfide donor and nitrosylating agent, providing a model, albeit crude, for biological interactions between RSNOs and reduced DNICs in the presence of cysteine desulfurase. This chapter describes our findings.

Synthesis and Characterization

Figure IV-1 presents the synthetic routes used to form complexes **1** and **2**. Each reaction, along with the products formed, will be discussed in this section. Figure IV-1 (b) will be addressed first, followed by (a) and then (c).
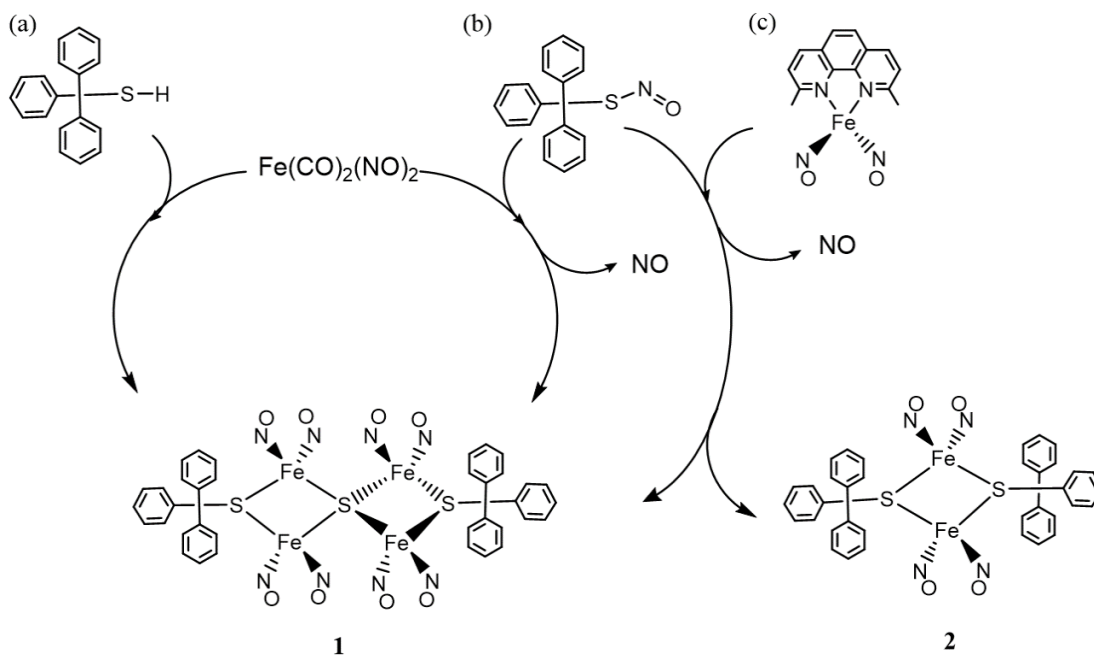
Figure IV-1. Synthesis of complexes **1** and **2**. Only those products that were identified are listed. The NO produced was trapped as [Fe(bme-dach)(NO)] (bme-dach = bis(N,N'-2-mercapto-2-methylpropyl)-1,5-diazocycloheptane).

Room temperature reaction of the orange THF solution of $Fe(CO)_2(NO)_2$ with the green THF solution of Ph_3CSNO in 1:1 stoichiometric ratio results in a dark red solution following a 1 h stir. The disappearance of the CO stretching bands along with a shift in the ν_{NO} IR bands from 1807 and 1761 cm^{-1} to 1786 and 1751 cm^{-1} indicated the complete conversion of $Fe(CO)_2(NO)_2$ to **1** (Figure IV-2 A). Nitric oxide was also released and was detected using the setup shown in Figure IV-2 B, wherein the reaction described above is inititated within the inner tube, while the NO-trapping agent, [Fe(bme-daco)]₂ (bme-daco = N,N′-bis (2-mercaptoethyl)- 1,4-diazacyclooctane) is present in the outer tube. When NO is released, it is taken up by the [Fe(bme-daco)]₂,

resulting in formation of the mononitrosyl species [Fe(bme-daco)NO], as evidenced by a distinct color change from brown to green and the appearance of a single ν_{NO} IR band at 1648 cm^{-1}.[91]
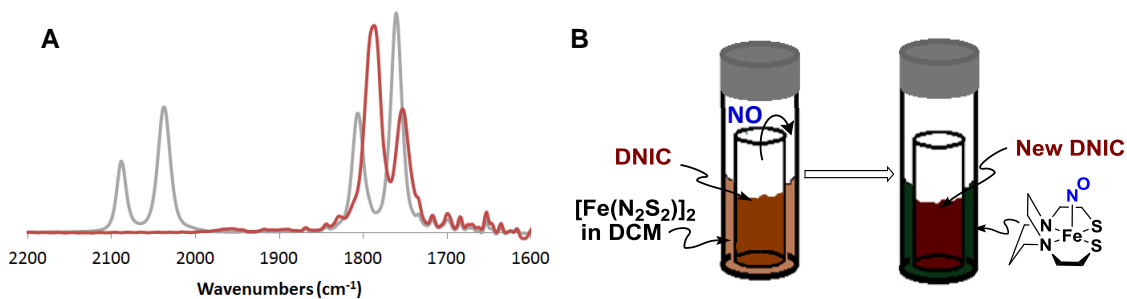
Figure IV-2. IR spectra, ν_{NO} region, of **1** in THF (red) and Fe(CO)$_2$(NO)$_2$ (gray) (A). A diagram of the typical setup used to detect the release of NO during the synthesis of **1** (B).

The ν_{NO} IR bands of **1** show a peak separation ($\Delta\nu_{NO}$) similar to that expected for Roussin's red ester (RRE)-type DNICs. As tabulated by Liaw *et al.*, the separation generally falls within the range of 15-38 cm^{-1}.[21] For **1**, the $\Delta\nu_{NO}$ is 35 cm^{-1}, which is within the expected range for RRE-type DNICs and below that seen in the typical monomeric DNICs ($\Delta\nu_{NO}$: ~ 40-60 cm^{-1}).[21] However, the pattern is rather unusual. For RRE-type DNICs the two NO bands are typically of equal intensity, while the monomeric DNICs show the reverse of the pattern seen for **1**, i.e. the first band has a lower intensity than the second band.

Under an inert atmosphere and at -35˚C, **1** is stable in the solid phase for several weeks. However, stability in the solution phase and towards oxygen was not tested. As would be expected from the presence of the trityl groups, **1** is soluble even in non-polar solvents such as hexanes.

X-ray quality dark red crystals of **1** were grown by slow evaporation of a concentrated hexane solution under an inert atmosphere. The molecular structure that was obtained from XRD analysis is shown in Figure IV-3 A.
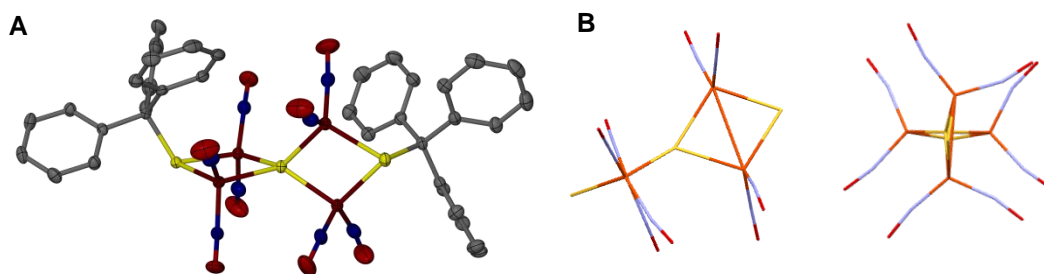
Figure IV-3. XRD structure of complex **1** with thermal ellipsoids drawn at 50% probability (H atoms omitted) (A). Two different views of the FeS-NO core (omitting the trityl groups) showcase the D_2d symmetry of the core (B).

This cluster contains a $S_3[Fe(NO)_2]_4$ core, where the two end sulfurs are μ_2-binding Ph_3CS thiolates, while the inner sulfur is a bridging sulfide. The three S alignment is roughly linear with an S-S-S angle of 170.96(2)˚. Thus, the Fe_4S_3 core shows D_2d symmetry, as displayed in the two renderings of the core given in Figure IV-

3 B. However, the bulky trityl groups introduce some slight distortion from perfect D_2d symmetry.

The D_2d symmetry represents a departure from the overall geometry observed for other sulfur-containing DNIC clusters. As reviewed by Holm and Lo, nitrosylated iron-sulfur clusters adopt rhomic, cuboidal, cubane, prismane, and rhombic dodecahedral geometries.[125] As opposed to being an iron-sulfur cluster derivative, **1** is better described as two RREs joined by an interstitial sulfide. To our knowledge, **1** is structurally unique.

The transformation of a DNIC into an iron-sulfur containing species, **1**, wherein one of the sulfurs is a sulfide, models a reaction and resulting product that could be present in the regeneration of iron-sulfur clusters from DNICs. As observed by Liaw *et al.*, the anionic DNIC $[(NO)_2Fe(SEt)_2]^-$ reacts with Ph_3CSH to yield the sulfide bridged species $[(NO)_2Fe(\mu\text{-}SEt)(\mu\text{-}S)Fe(NO)_2]^-$ along with $HCPh_3$ and half an equivalent of $EtSSEt$.[126] This reaction is rationalized to occur via consecutive reductions of the Ph_3CSH by one of the coordinated ethylthiolates of $[(NO)_2Fe(SEt)_2]^-$ to produce the intermediate $[(NO)_2(SEt)Fe(\mu\text{-}S)Fe(SEt)(NO)_2]^{2-}$. Elimination of an ethylthiolate then yields the isolated product $[(NO)_2Fe(\mu\text{-}SEt)(\mu\text{-}S)Fe(NO)_2]^-$. The same mixed sulfide/ethylthiolate RRE was formed in the reaction of the RRE $[(NO)_2Fe(\mu\text{-}SEt)_2Fe(NO)_2]$ with Ph_3CSH, leading Liaw *et al.* to conclude that the coordinated ethylthiolates initiate sulfide release from Ph_3CSNO.[126]

Based on the studies by Liaw, it is plausible to envision that the reaction of Ph_3CSNO and $Fe(CO)_2(NO)_2$ first forms the RRE (**2**). The tritylthiolates then initiate sulfur release from an additional Ph_3CSNO, forming **1**. However, without NMR data to

90

identify the biproducts, a more convincing mechanism cannot be proposed. In any case, the insertion of a sulfide in this reaction is significant as illustration of a possible intermediate in the regeneration of iron-sulfur clusters from DNICs.

Although not absolutely identical, the two $[(NO)_2Fe(\mu\text{-}SCPh_3)Fe(NO)_2]$ units are very similar. Table IV-1 lists the important metric parameters, reported in each case as an average. For each of the parameters shown, the deviation for the given parameters is very small, with the exception of the N-Fe-N angles.

Table IV-1. Key metric parameters for **1**, given as averages.

	Avg. Distance (Å)		Avg. Angle (˚)
Fe-Fe	2.7835(1)	Fe-N-O	166.5(2)
Fe-S	2.2756(9)	S-Fe-S'	104.05(3)
Fe-S'	2.2720(9)	Fe-S-Fe	75.41(2)
Fe-N	1.679(2)	Fe-S'-Fe	75.55(2)
N-O	1.172(3)	N-Fe-N	113.1(1)
S-S'	3.585(1)	O-Fe-N	102.31(7)
S-C	1.930(2)		

These angles range from 110.5(1)° to 115.3(1)°, although comparison of the two halves show that each half contains one smaller and one larger N-Fe-N angle (110.5(1)° and 114.2(1)° for one half, and 112.5(1)° and 115.3(1)° for the other). The Fe-Fe, Fe-S, and S-S bond lengths are nearly identical to those found in the typical RREs such as SEt-RRE and SPh-RRE. However, the S-C bond length of 1.930(2) Å is appreciably longer than the standard S-C bond length of 1.82 Å. With these rather weak S-C bonds, it is reasonable for this bond to be readily cleaved, leading to the formation of the bridging sulfide.

There are slight differences in the Fe-N-O angles in **1** and those given for Roussin's red esters with ethylthiolate (SEt-RRE) and phenylthiolate (SPh-RRE).[126] The Fe-N-O angle of **1** (166.5(2)°) is slightly smaller than the same angle in SEt-RRE (168.4°) and SPh-RRE (169.95°).[126] Likely, the interstitial sulfide is the influencing factor here. For example, when both bridging sulfurs are sulfides, as in [Fe(μ-S)$_2$(NO)$_2$]$_2$, the Fe-N-O angle is significantly more bent (163.2(6)).[126]

As shown in Figure IV-1 (a), **1** can also be synthesized by addition of a THF solution of trityl thiol to freshly prepared Fe(CO)$_2$(NO)$_2$. The solution color and ν_{NO} IR bands are identical to that seen in the reaction with Ph$_3$CSNO and Fe(CO)$_2$(NO)$_2$. As would be expected in this case however, NO was not a concomitant product.

When the π-accepting CO ligands of the Fe(CO)$_2$(NO)$_2$ are replaced with the better donor ligand neocuproine (neo), and then the resulting DNIC, [(neo)Fe(NO)$_2$], is reacted with Ph$_3$CSNO, a mixture of **1** and the RRE, **2** are obtained, as shown in Figure

IV-1(c). Formation of NO was confirmed by trapping with [Fe(bme-daco)]$_2$ using the same setup as given in Figure IV-2 B.

1 and 2: 1787 (sh), 1780, 1747 cm^{-1}
1: 1787, 1752 cm^{-1}
2: 1779, 1748 cm^{-1}

Wavenumbers (cm^{-1})
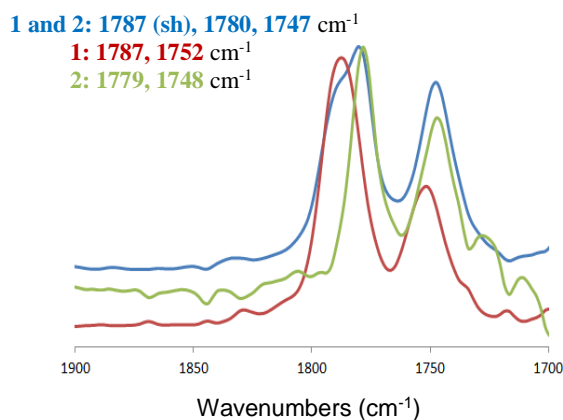
Figure IV-4. Overlay of IR spectra, ν_{NO} region, of the product mixture from the reaction given in Figure IV-1(c) (blue) with **1** (red) and **2** (green), show that a mixture of **1** and **2** are formed in this reaction. All spectra were recorded in DCM.

The ν_{NO} IR bands of the dark red product solution appeared at 1787 (sh), 1780, and 1747 cm^{-1} (blue spectrum, Figure IV-3). The two main bands at 1780 and 1747 cm^{-1} are similar in pattern and separation ($\Delta\nu_{NO}$ = 33 cm^{-1}) to that of a typical RRE.[21] Indeed, product isolation by washing with hexanes to remove **1** resulted in spectroscopically pure **2** (green spectrum, Figure IV-4). Like **1**, **2** is stable for weeks under an inert atmosphere and at -35°C. However, its stability under other conditions has not been tested.

X-ray quality dark red crystals of **2** were obtained by slow evaporation of a concentrated DCM solution of **2** at -35˚C. As expected from the IR spectrum, **2** is composed of two Fe(NO)$_2$ units bridged by two trityl thiolates in the typical RRE arrangement (Figure IV-4).

Avg. Distance (Å)		Avg. Angle (˚)	
Fe-Fe	2.7569(7)	Fe-N-O	165.9(2)
Fe-S	2.2576(7)	S-Fe-S	104.74(2)
Fe-N	1.673(2)	Fe-S-Fe	75.26(2)
N-O	1.171(2)	N-Fe-N	111.87(8)
S-S	3.576(1)		
S-C	1.921(2)		
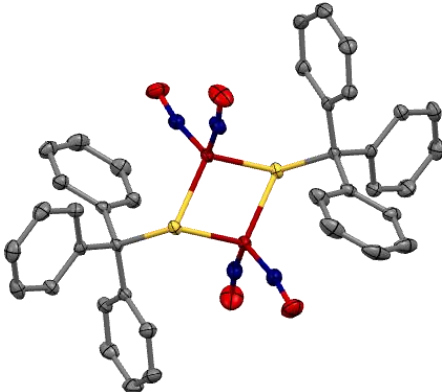
Figure IV-5. Key metric parameters of **2** are given in the table. On the right is the XRD structure of **2** with thermal ellipsoids drawn at 50% probability (H atoms omitted).

The bridging thiolates and the two nitrosyl groups define a slightly distorted tetrahedral geometry for each iron center. All metric parameters listed in the table in Figure IV-5 are nearly identical to those parameters seen in **1** and they align well with what is expected for a typical RRE.[21] The only difference between **1** and **2** significant enough to mention is the N-Fe-N angle whose average differs by ~ 2˚, i.e., 113.1(1)˚ for **1** and 111.87(7)˚ for **2**.

^{14}NO/^{15}NO Exchange

For the reactions discussed above, the NO that is released during the reaction can derive from either the RSNO or the DNIC. In order to confirm the source of the NO, the Ph$_3$CSNO was prepared with the nitrogen labeled as ^{15}N via a synthetic route adopted from Connelly *et al.*[89] The spectra of both **1** and the Fe(bme-daco)NO (within the outer tube in Figure IV-1B) from the reaction with Ph$_3$CS^{15}NO is given in Figure IV-6.[90]

A   B

Wavenumbers (cm^{-1})
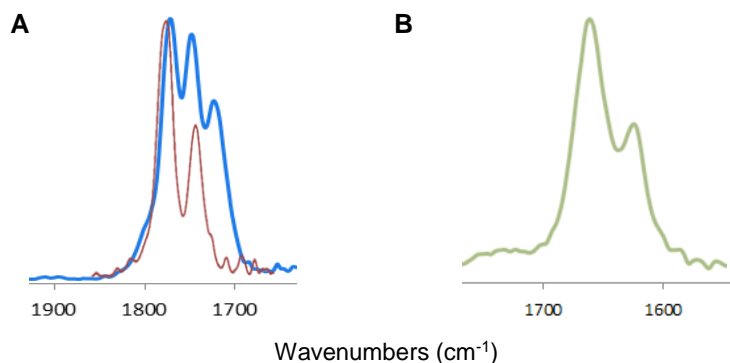
Figure IV-6. Overlay of the IR spectra, ν$_{NO}$ region, of **1** from reaction with trityl-S^{15}NO (blue) and **1** from the unlabeled reaction (red) (A). The spectrum of the [Fe(bme-daco)NO] after the reaction with trityl-S^{15}NO shows the stretch for the unlabeled product (1648 cm^{-1}) and the labeled product (1618 cm^{-1}) (B). Both the DNIC (blue spectrum in A) and the mononitrosyl (spectrum B) show a mixture of labeled and unlabeled NO products.

The IR spectrum of **1** thus prepared from N-15 labeled RSNO showed three distinct stretching frequencies, wherein the two bands at 1787 and 1752 cm^{-1} correspond to the unlabeled **1**. A third band at 1720 cm^{-1} matches very closely to the calculated

value of 1718 cm^{-1} for one of the ^{15}N nitrosyl stretches. The second band, which is expected to appear at 1741 cm^{-1}, is buried beneath the other bands, hence the broad base of the peaks. Some of the ^{15}NO was also incorporated into the [Fe(bme-daco)NO] as shown in Figure IV-5 B. The main stretch at 1648 cm^{-1} arises from the unlabeled [Fe(bme-daco)NO], while the second stretch at 1618 cm^{-1} corresponds exactly to the calculated value for [Fe(bme-daco)^{15}NO]. Thus, we see extensive exchange of the NOs within this system.

Conclusions

We reported the synthesis and structural characterization of two new sulfur-containing DNIC species. Complex **1** was isolated as a unique cluster of D$_2$d symmetry containing an interstitial sulfide. It is tempting to posit that structures of this type might form in the regeneration of iron-sulfur clusters from DNICs. As a hybrid RRE/iron-sulfur cluster of sorts, it is not farfetched to expect such as a possible intermediate in the iron-sulfur cluster repair process. A regular RRE containing tritylthiolates was also isolated and showed great similarity to other RREs. Finally, NO exchange between the nitrosyls of the Ph$_3$CS^{15}NO and the Fe(CO)$_2$(NO)$_2$ was observed in the formation of **1**.

CHAPTER V

TOWARD BIOCOMPATIBLE DINITROSYL IRON COMPLEXES: SUGAR-

APPENDED THIOLATES[*]

Introduction

The discovery of the therapeutic potential of nitric oxide and the existence of

dinitrosyl iron complexes (DNICs) in biological systems have led to extensive

biomimetic synthesis in this area.[21,94] However, only a few studies have focused on the

development of synthetic DNICs that are compatible with cell uptake studies. Notably,

Vanin *et al.* have reported DNICs with natural thiol ligands (cysteine or glutathione),

that display a variety of therapeutic responses including prolonged hypotension,

attenuated platelet and erythrocyte aggregation, and promotion of skin wound healing;

the glutathione DNIC is currently in clinical trials.[48] Liaw *et al.* recently reported a water

soluble neutral $\{Fe(NO)_2\}^9$ DNIC that induced apoptosis in three different cancer cell

lines.[127] Earlier work by Liaw *et al.* described biological activity of dimeric Roussin's

Red Ester (RRE), $[Fe(\mu\text{-}SC_2H_4COOH)(NO)_2]_2$ and monomeric DNIC, $[(PPh_2(Ph\text{-}3\text{-}SO_3Na))_2Fe(NO)_2]$, bearing –COOH and –SO$_3$ functionalities for improved water

solubility.[104] Certain RRE and derivatized RREs also show photochemical NO release,

as investigated by Ford *et al.[128]* Kim *et al.* reported NO release from a

(TMEDA)Fe(NO)$_2$ complex, both within and outside a cellular environment.[45]

We have explored a new class of N-heterocyclic carbene (NHC)-bearing DNICs and trinitrosyl iron complexes, TNICs, and noted the potential of such derivatives to serve as a source of NO to biologically relevant NO-trapping agents such as iron or cobalt porphyrins, albeit in organic solvents and in the absence of air.[22,95] Such limitations highlight the need for strategies to improve the water solubility and air stability of these compounds if meaningful translation into useful pharmaceuticals is to become reality. In the current study, we take advantage of the stability imparted by the lipophilic NHC on the $(L)(X)Fe(NO)_2$ scaffold and employ a thiosugar as the anionic X ligand to improve hydrophilicity and biocompatibility.

There is ample precedent for sugar-bound metal complexes in biomedical applications, ranging from contrast agents to therapeutics.[129,130] Saccharides and their derivatives are naturally involved in many intracellular processes, acting as energy sources and involved in recognition processes.[131] The use of sugars and their derivatives as ligands conjugated to metal complexes therefore presents opportunities to improve targeting properties that utilize the natural mechanisms of the cell for sugar uptake. For example, cellular internalization through lipophilic diffusion or *via* the membrane-bound glucose transporter, GLUT 1, of imaging agents containing [99m]Tc(I), [55]Co(II) and Ga(III) bound to glucose-based ligands has been reported.[130] The tunability of saccharide ligands themselves provides essential control over the lipophilicity and stability of metal-based drugs. Several carbohydrate-metal complexes, including platinum derivatives, have been studied for anticancer properties.[129]

Most notably, the sugar-based, gold-containing drug, Auranofin, [(2,3,4,6-tetra-

O-acetyl-1-thio-β-D-glucopyranosato-*S*)(triethyl-phosphine)]-gold(I), is currently used in the treatment of rheumatoid arthritis.[132] As a monomeric, neutral gold compound, it is lipophilic and administered orally.[132] A number of Auranofin derivatives have also been synthesized, and current work is directed towards testing these compounds for anticancer properties.[133]

Results and Discussion

Inspired by Auranofin, we synthesized and characterized examples of 'sugar appended' monomeric and dimeric DNICs. We have conducted preliminary in situ NO-release studies of these complexes to both NO trapping agents and endothelial cells. Such compounds that combine the therapeutic properties of NO with the cell-attracting properties of a glucose moiety are amongst the few examples, to our knowledge, of DNICs with bio-functionalized ligands.
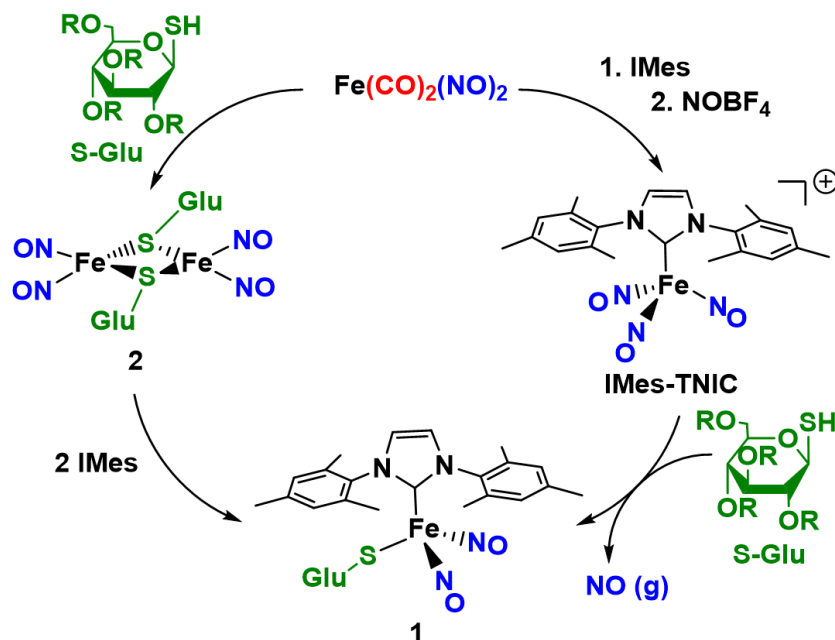
Figure V-1. Synthesis of complexes **1** and **2**; R = (C=O)CH$_3$.

Figure V-1 presents the synthetic routes to the two main compounds of this study, the sugar-appended DNIC **1**, and the sugar-appended RRE, **2**, where R = (C=O)CH$_3$. The NHC-stabilized trinitrosyl iron complex, IMes-TNIC, [(IMes)Fe(NO)$_3$]$^+$,[91] was used as a precursor for the synthesis of the oxidized, {Fe(NO)$_2$}^{9} complex **1**, Figure V-1.
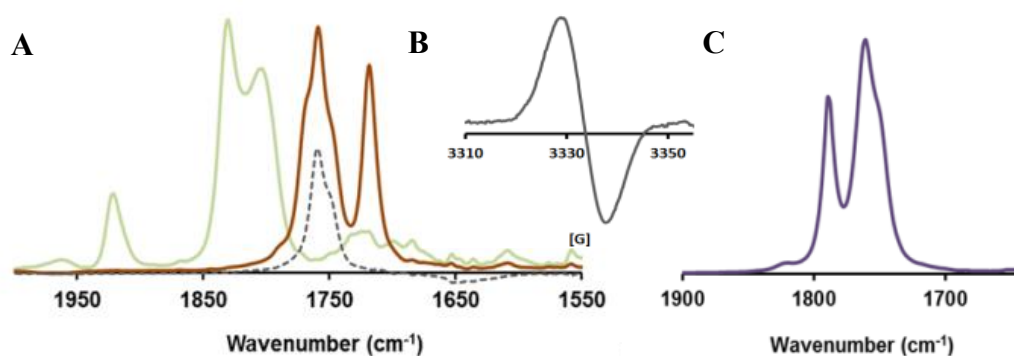
Figure V-2. (A) ν(NO) region IR spectrum overlay of **1** (brown), IMes-TNIC (green) and free 1-thio-β-D-glucosetetraacetate (dashed); (B) EPR spectrum of **1** at R.T.; (C) ν(NO) region IR spectrum of **2**. All spectra recorded in THF.

Reaction of $[(IMes)Fe(NO)_3]^+$ with 1-thio-β-D-glucosetetraacetate in 1:1 stoichiometric ratio (THF solution) results in a color change from green to brown within time of mixing. The shifts in the positions and pattern of the ν_{NO} IR bands accompanying this color change in THF solutions, indicate the conversion of the TNIC to **1**, with concomitant release of NO gas, Figure V-2A.[91] Complex **1** showed the classic isotropic EPR signal for S = ½, oxidized $\{Fe(NO)_2\}^9$ DNICs at g = 2.03, R. T. (Figure V-2B).[21] When exposed to air in the solid state, **1** remained visibly unchanged for ca. 2 h; solid **1** was stable over several weeks under an inert atmosphere. In THF and DMSO solutions, and under N_2, no degradation was obvious over ca. 36 h. On exposure of these solutions to air, however, major changes to the IR spectrum were seen within 1 h, Figure V-3. X-ray quality red colored crystals of **1** were obtained from hexane/THF diffusion under an inert atmosphere. The molecular structure of **1** is shown in Figure V-4, and important metric parameters are listed in supporting information.
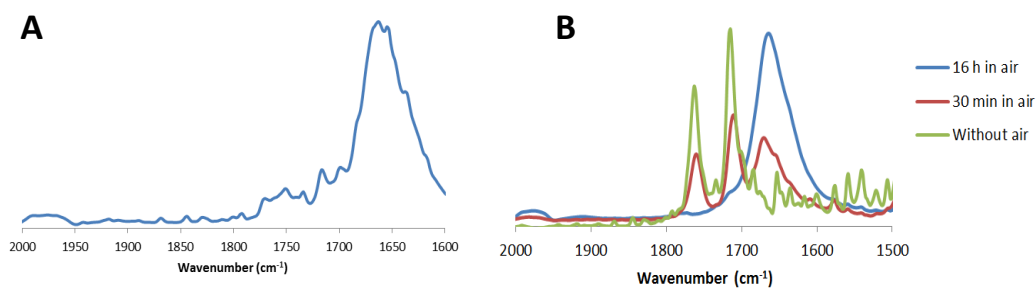
Figure V-3. IR spectra of (A) complex **1** in DMSO upon exposure to air for 3 h: ν(NO) 1663 cm^{-1} and (B) complex **3** in THF (green), after 30 min in DMSO and air (red) and after 16 h DMSO and air (blue). The same species at 1665 cm^{-1} appears here as well.

The molecule maintains the pseudo-tetrahedral geometry seen in all previously reported NHC-DNICs.[21,94] The planes of the mesitylenes are roughly perpendicular to the CN$_2$C$_2$ plane, providing an 'umbrella' to the (RS)Fe(NO)$_2$ trigonal base.
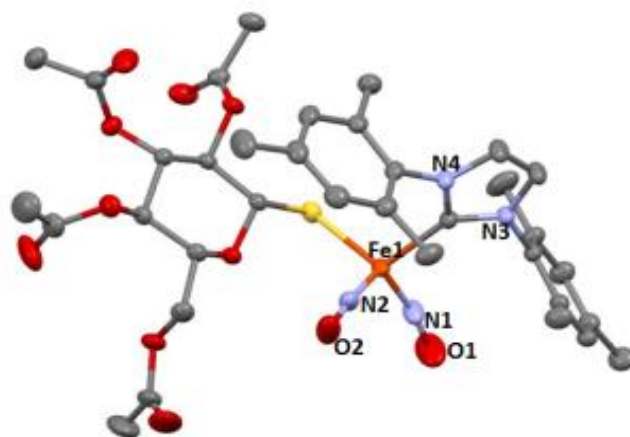
Figure V-4. XRD structure of complex **1** with thermal ellipsoids drawn at 50% probability (H atoms omitted).
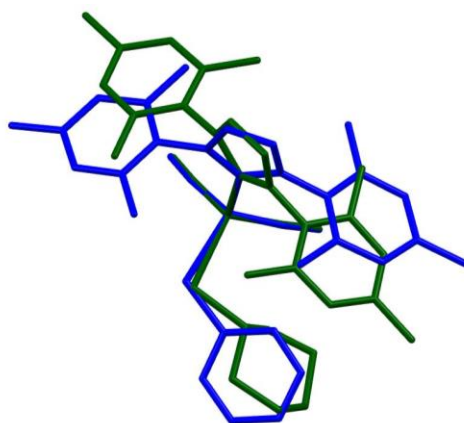
Figure V-5. Overlay of Complex **1** (green) and Complex **3** (blue). The acetyl groups on the thioglucose have been omitted for clarity.

The NO ligands are slightly bent with average $\angle_{\text{Fe-N-O}}$ of 170.8°; they adopt the well-known "attracto" conformation,[134] bending in towards each other as defined by smaller $\angle_{\text{O-Fe-O}}$ compared to $\angle_{\text{N-Fe-N}}$, in the co-planar FeN_2O_2 unit. All other metric parameters are similar to the prototypic analog of this compound, $(\text{IMes})(\text{SPh})\text{Fe}(\text{NO})_2$ (**3**).[91] However, a structural overlay of **1** and **3** along the Fe-C$_{\text{carb}}$ bonds displays a twist of ca. 30° in the orientation of the IMes ligand, which positions the phenyl ring of the IMes in closer proximity to the glucose in **1** than it is to the SPh in **3** (Figure V-5).

Deprotection of the sugar thiol ligand in compound **1** was achieved by reaction with excess NaOMe in MeOH, Figure V-6. The identity of the deprotected product (**1′**) was verified by direct synthesis *via* an alternate route as described in the Chapter II. Complex **1'** was less stable than the protected analogue, with THF solution lifetime of only several hours even under inert atmosphere.
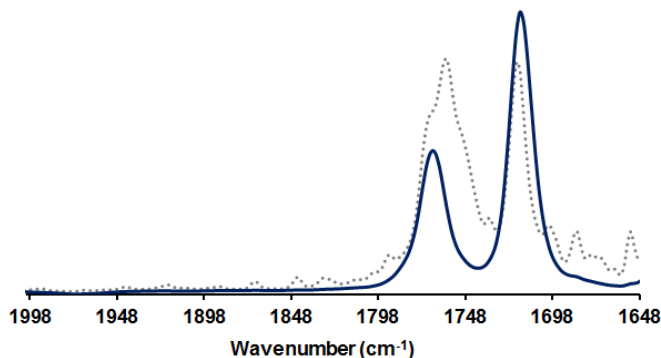
Figure V-6. IR spectrum of complex **1′** in THF: ν(NO) 1768 (sh), 1716 cm^{-1}. Dotted-line inset: IR spectrum of complex **1** (THF).

The dimeric (μ-RS)$_2$[Fe(NO)$_2$]$_2$ form of **1** was synthesized by the known method for other RRE analogues[135] (Figure V-1, counterclockwise reaction); i.e., addition of 1-thio-β-D-glucosetetraacetate to freshly prepared Fe(CO)$_2$(NO)$_2$ (in THF) in 1:1 stoichiometric ratio. The reaction was complete in about 12 h, at 22 °C and the resulting (μ-RS)$_2$[Fe(NO)$_2$]$_2$ complex **2**, bearing acetylated thio-glucose units, could be verified by the corresponding IR shift and pattern shown in Figure V-2C. A brown solid was obtained upon recrystallization of the THF solution of **2** with hexanes and characterized by ESI mass spectrum signals at m/z = 959 [M + H]$^+$ and 980 [M + Na]$^+$. As expected for the dinuclear, spin-paired [{Fe(NO)$_2$}^{9}−{Fe-(NO)$_2$}^{9}] DNICs, this compound was EPR silent in both THF and DCM solutions, but not DMSO, *vide infra*.

In contrast to **1**, **2** showed notably improved stability in air. It was stable in air for 2 days even in solution, increasing to several months under inert atmosphere in the solid state. As with **1**, **2** was also completely soluble in DMSO, a commonly used solvent for administering pro-drugs in cell studies. However, similar to the observation

of Liaw *et al.* for the N-acetyl-D-penicillamine (NAP)-containing dinuclear DNIC, [(μ-S-NAP)$_2$Fe(NO)$_2$]$_2$, upon dissolving **2** in DMSO, a dynamic interconversion occurs between **2** and another {Fe(NO)$_2$}^{9} DNIC.[136] The ν_{NO} and $\nu_{C(O)O}$ IR bands shift slightly from 1786, 1759, and 1749 (sh) cm^{-1} (THF) to 1785, 1754, and 1744 (sh) cm^{-1} (DMSO). Additionally, in DMSO, a rhombic EPR signal (g_x = 2.043, g_y = 2.030, g_z = 2.013) appears, which may be ascribed to the S = ½ species [(S-pGlu)(DMSO)Fe(NO)$_2$] (Figure V-7). Vacuum removal of the DMSO (even after one week of stirring) followed by addition of either THF or DCM recovers diamagnetic **2**.
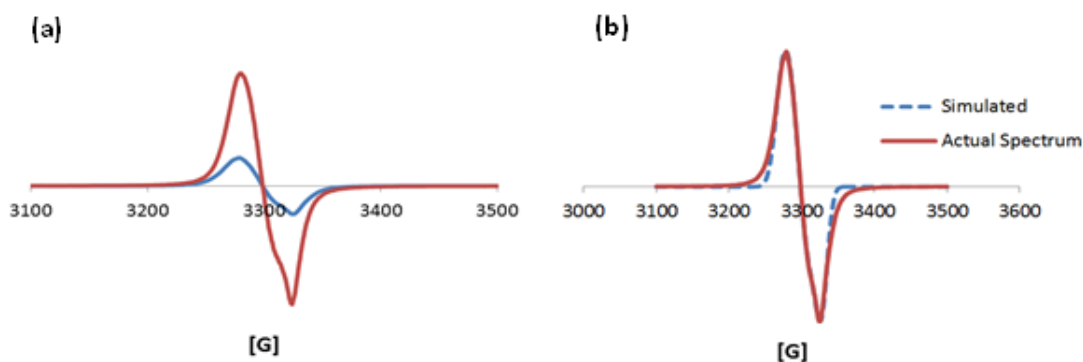
Figure V-7. (a) Overlay of the X-band EPR spectrum of complex **2** in DMSO solution (red) with complex **2** in DMSO and media (blue) at 295 K. (b) Overlay of X-band EPR spectrum of **2** in DMSO and media (red) and that of the simulated spectrum (blue dotted line

Previous studies by Hess *et al.* on the NO release ability of the prototypic NHC-DNICs suggested that oxidized, {Fe(NO)$_2$}^{9} DNICs are better sources of NO in the

presence of NO trapping agents when compared to the reduced $\{Fe(NO)_2\}^{10}$ analogues.[22,128] In fact, these oxidized NHC-DNICs ($[(NHC)_2Fe(NO)_2]^+$) were seen to release NO very rapidly (within minutes) to the cobalt porphyrin-derived NO trapping agent provided *in situ*.[22] To qualitatively probe the ability of the sugar-derivatized DNICs to release or transfer NO, **1** was combined with 2 equiv of the NO-trapping reagent Co(TPP) (Co(TPP) = 5,10,15,20-tetraphenyl-21H,23H-porphine cobalt(II)) in THF solution at 22°C. Over ca. 48 h, a steady decrease in intensity of the ν_{NO} bands of **1** was observed. Poor resolution in this spectrum necessitated product separation. Upon addition of MeOH, the product mixture produced a purple residue; the isolated purple solid showed an IR band at 1683 cm^{-1} in DCM, indicating the formation of (TPP)Co(NO).[38,137] This suggests oxidative nitrosylation of Co(II)TPP by the released NO radical.[38] To augment this study, an alternate NO trapping agent was used.

A host of MN_2S_2 complexes have been well characterized, containing a variety of transition metal ions such as Fe^{II}, Ni^{II}, Pd^{II}, Co^{II}, Cu^{II}, and Zn^{II} with various N_2S_2 ligands.[79] Iron and cobalt N_2S_2 complexes where N_2S_2 = bme-dach (*N*,*N'*-bis(2-mercaptoethyl)-1,4-diazacycloheptane), or bme-daco (*N*,*N'*-bis(2-mercaptoethyl)-1,4-diazacyclooctane), form penta-coordinate, dimeric $[N_2S_2M]_2$ units which are readily cleaved by NO, producing $N_2S_2M(NO)$, M = Fe and Co.[92,138] The $[(bme-dach)Fe]_2$ was successfully used as an NO-trapping agent by Hsieh *et al.* in "double-tube" experiments, where an NHC-TNIC, such as that shown in Scheme V-1 (placed in the inner tube), on addition of PhS$^-$, released NO as free NO radical/gas, trapped as (bme-dach)Fe(NO) in the outer tube.[91] The cobalt analogue is equally efficient as a trapping agent.

Based on such precedents, and the availability of these NO trapping agents, **1** and **2** were separately reacted with excess [(bme-dach)Co]$_2$ in DCM solutions to test for release or transfer of NO, which would subsequently be trapped in the form of the monomeric (bme-dach)Co(NO). For **1**, the ν_{NO} IR bands disappeared over the course of 48 h, indicating loss of NO from **1**. Complex **2** showed loss of NO bands in about 24 h. Upon solvent removal and washing of the brown residue with diethyl ether, the resulting IR spectrum of the residue taken up in DCM (Figure V-8 inset) showed a strong, broad signal at 1601 cm^{-1}, assigned to the ν_{NO} of (bme-dach)Co(NO).[38] A second IR band at 1754 cm^{-1} (1747 (sh)) can be assigned to the (Me-C(O)O) of the acetylated thio-sugar unit. The exact identity of this species is unclear.

To quantify the NO transferred in these reactions, **1** and **2** were again reacted with [(bme-dach)Co]$_2$ in DCM, but both reactions were stopped at 24 h (to correlate with the timescale used in the Griess analysis *vide infra*). Using the intensities of the ν_{NO} of (bme-dach)Co(NO) and a calibration curve (Figure V-8), **1** was found to form 0.5 mols Co(bme-dach)NO per mol **1**, while **2** formed 2.7 mols Co(bme-dach)NO per mol **2**. The poor NO transfer from **1** is most likely due to the robust nature of **1**, as a portion of **1** remains unreacted after 24 h. Although the efficiency of [Co(bme-dach)]$_2$ at NO uptake is not known with certainty, these studies correlate well with the results from the Griess assay described below. Overall, the results provide evidence for the release/transfer of NO from **1** and **2** in the presence of NO trapping agents.
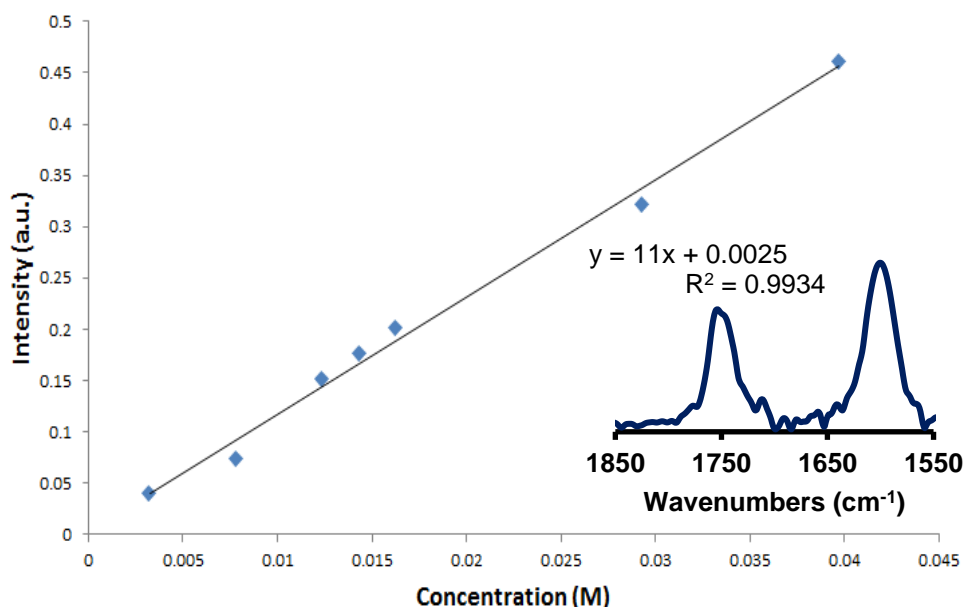
Figure V-8. Plot of the intensity of the ν_{NO} vs. concentration of Co(bme-dach)NO for concentrations ranging from 3-14 mM. This plot was used to calculate the moles of NO transferred from **1** and **2** following a 24-h stir of either **1** or **2** with [Co(bme-dach)]$_2$ in DCM. For **1**, 0.5 moles of the Co(bme-dach)NO were formed per mole of complex, while for **2**, 2.7 moles of the Co(bme-dach)NO were formed per mole of complex. Inset: IR spectrum resulting from complete reaction of **1** or **2** with [(bme-dach)Co]$_2$ in THF: ν(NO) 1601 cm^{-1} indicates the formation of (bme-dach)Co(NO).

The promising results from the NO release chemical studies outlined above, in conjunction with both the considerable air stability and DMSO solubility of these compounds, prompted us to investigate the behavior of these DNICs in a biological environment. It is well established that the tetraacetylthioglucose ligand in Auranofin undergoes a ligand exchange reaction with cysteine-34 in serum albumin.[133] Thus, it is reasonable to postulate that **1** and **2** might undergo a similar exchange, a possibility that gains further credence according to the work by Bello *et al.*[64] Therein, a diglutathionyl

DNIC was shown to bind to human glutathione transferase via exchange of one of the DNIC glutathione ligands for the tyrosine of the active site.[64] Furthermore, the interconversion between **2** and its DMSO adduct (presumably [(S-pGlu)(DMSO)Fe(NO)$_2$]), demonstrates the reactivity of the Fe-S bond. For exploration of the effect of the sugar appendages on the DNIC, we have enlisted two other complexes for comparison with **1** and **2**. Complex **3**, which contains the dinitrosyl iron unit in the oxidized $\{Fe(NO)_2\}^9$ state, is structurally analogous to **1**, differing by X = SPh. Complex **4** is a reduced $\{Fe(NO)_2\}^{10}$ DNIC containing the 2, 9-dimethyl-1,10-phenanthroline ligand, and provides a comparison with a DNIC containing both a very different ligand set and a different redox level. Complex **1'** was not explored in this study due to its instability.

The four compounds under consideration, namely **1**, **2**, **3**, and **4**, were first assessed for their potential cytotoxicity toward endothelial cells. Bovine coronary venular endothelial cells (CVECs) were exposed to various concentrations of each compound (0.01 −100 µM) and screened for % viability using the MTS assay (colorimetric sensitive method for quantification of viable cells). Both **1** and **2** show an increase in cell proliferation prior to a sharp decrease in viability (IC$_{50}$ of 31 µM and 68 µM for **1** and **2**, respectively, Figure V-9 A).
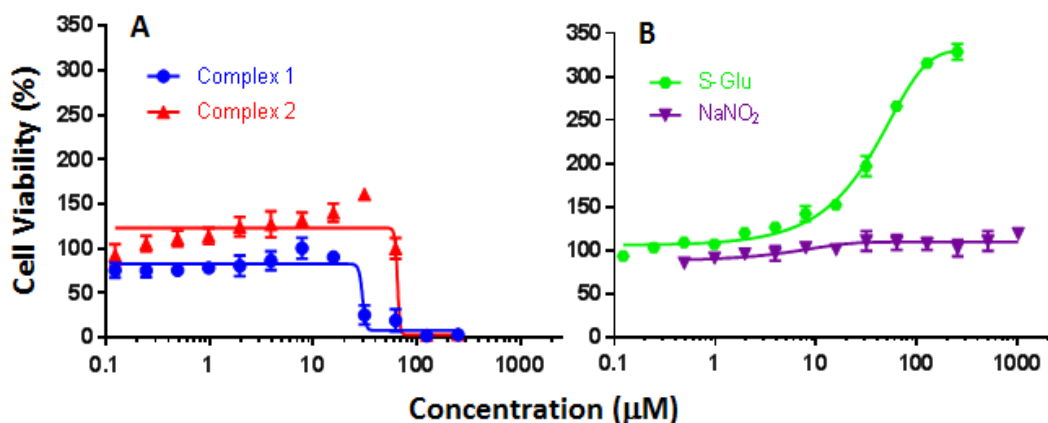
Figure V-9. In vitro cell viability of CVEC cells upon 72 h incubation with **1** and **2** (A) and the thiosugar (green) and sodium nitrite (purple) controls (B) at concentrations between 0.01 and 100 μM.

The IC_{50} values determined for **1** and **2** are similar to those reported by Liaw *et al.* for other DNICs.[104,127] The unusual increase in proliferation may be attributed to the effect of the thiosugar moiety itself, as the control experiment demonstrates a three-fold increase in proliferation over the same concentration range, Figure V-9 B. The sharp decrease in proliferation at higher concentrations of **1** and **2** (>IC_{50}) may thus be attributed to the damage inflicted on the cells by the DNICs, presumably from the generation of free NO, which ultimately results in complete cell death. Data from the second control experiment is also shown in Figure V-9 B in the form of the effect of $NaNO_2$ on cell proliferation; no significant effect is observed. The influence of the glucosylated thiol on the cell viability in **1** is particularly apparent when compared to the viability assay results of the analogous DNIC, **3** (Figure V-10 A). Replacement of the

glucosylated thiol with the thiophenylate causes a dramatic increase in the cytotoxicity, resulting in an IC_{50} of 7.3 μM for **3** compared to 31 μM for **1**.
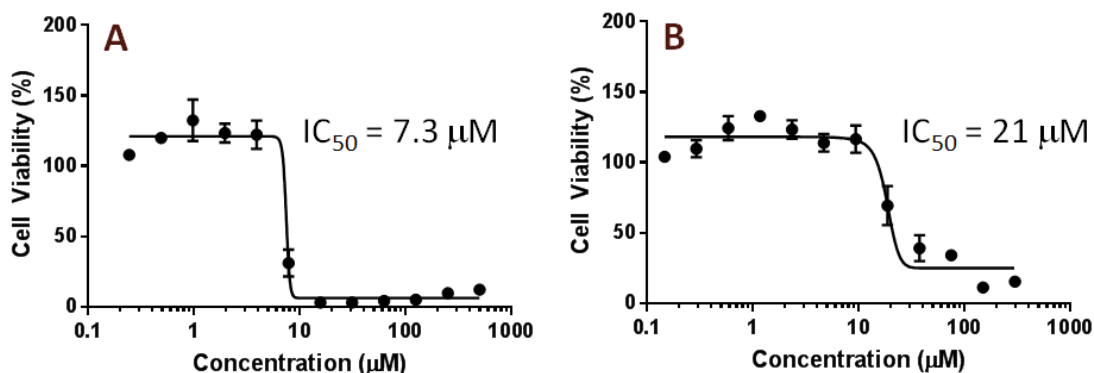
Figure V-10. Cell viability vs. concentration of complex for **3** (A) and **4** (B). Each sample was diluted by a dilution factor of 2. There were ca. 12 ranges of concentrations (high – low) and each concentration was done in a set of triplets. Each dot on the plot represents the average of the three readings at that specific concentration.

Complex **4**, with an IC_{50} of 21 μM (Figure V-10 B), is slightly more toxic than either of the sugar derivatives, but still falls in the range of acceptable toxicity levels for potential pro-drugs. Based on results from similar studies, it is reasonable to conclude that the cell death in each case occurred via apoptosis.[48,104,127]

To quantify the amount of NO produced by **1-4**, the commonly used Griess assay was employed; results are displayed in Figure V-11. In this assay, the conversion of NO to nitrite (NO_2^-) in aqueous solutions is monitored by reaction of the NO_2^- with sulfanilic
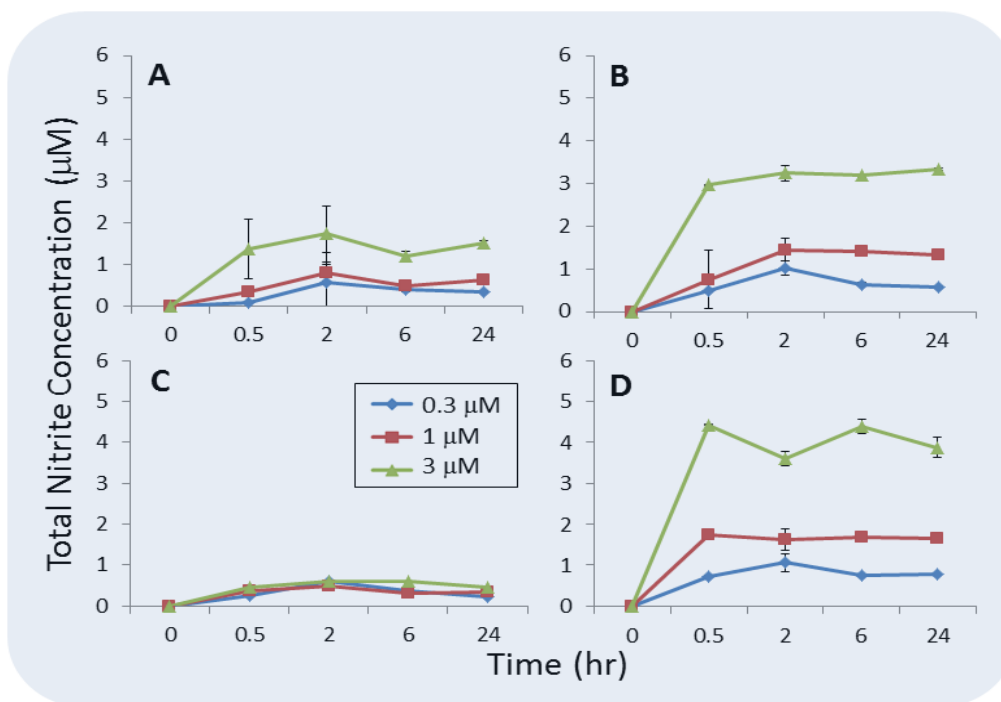
Figure V-11. Griess assay results for addition of **1** (A), **2** (B), **3** (C), and **4** (D) at concentrations of 0.3 μM (blue), 1 μM (red) and 3 μM (green) to the medium without cells. Total nitrite concentration correlates to the NO concentration.

acid to form a diazonium salt, which is then detected by the azo dye, N-(1-naphthyl)ethylenediamine dihydrochloride. In the absence of cells, this assay suggests that **1**, **2**, and **4** released appreciable amounts of NO to the aqueous medium (Figure V-11). Complex **4** exhibited rapid NO release reaching a plateau after 0.5 h. This maximum approaches 2 μM NO for 1 μM of **4**. The NO to **4** stoichiometric ratio of nearly 2:1, was relatively consistent across all three concentrations tested. We conclude that the oxygen sensitivity of **4** (which is in the reduced $\{Fe(NO)_2\}^{10}$ state) activates it towards NO

release.

Complex **2**, being of the RRE-type, can theoretically deliver 4 equiv of NO per molecule. As seen in Figure V-11 B, **2** shows a slight increase in NO release over a 24 h period, reaching a maximum of 3.5 µM NO for 3 µM of **2** at 24 h. The much slower NO-release rate of **2** as compared to **4** highlights the stability of **2** and its potential to serve as a slow-release pro-drug. In a long term study, **2** showed a steady release of NO up to 7 d. Complex **1** proved to be a much poorer NO-release agent, yielding a maximum of 1 equiv of NO per molecule at 2 h (Figure V-11 A). Complex **3** did not show appreciable amounts of NO released over the course of 24 h. The results seen for **1** and **3** reflect their behavior when exposed to oxygen (Figure V-3). As monitored by IR, the ν_{NO} bands of **1** and **3** decrease concomitant with the growth of a new peak at 1664 cm^{-1} in both cases (presumably a mononitrosyl species). We conclude that this contributes to poor results seen from the Griess Assay. When the Griess assay was performed in the presence of cells (Figures V-12), the observed difference in nitrite concentration (Figures V-13) as compared to that in the absence of cells indicated the prospect of NO uptake by the cells, for all four DNICs. However, the margin of error was too great to draw definitive conclusions.
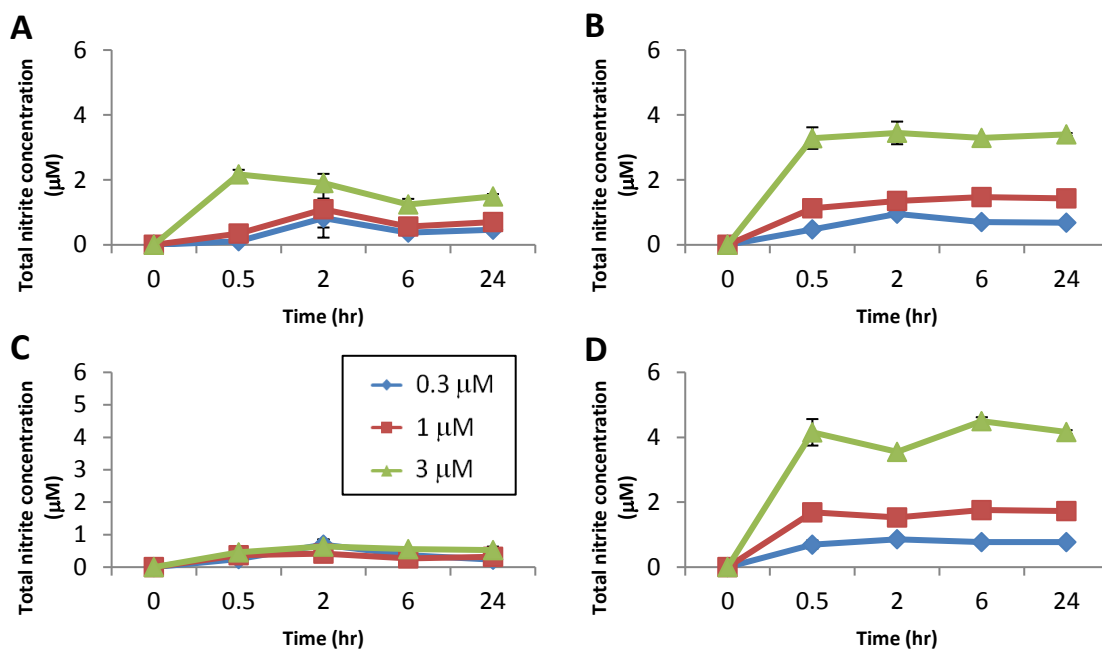
Figure V-12. Griess assay results for addition of **1** (A), **2** (B), **3** (C), and **4** (D) to the medium in presence of cells at concentrations of 0.3 μM (blue), 1 μM (red) and 3 μM (except for **3** (C), where 0.03, 0.1 and 0.3 μM concentrations were used due to high cytotoxicity). Total nitrite concentration correlates to the NO concentration.
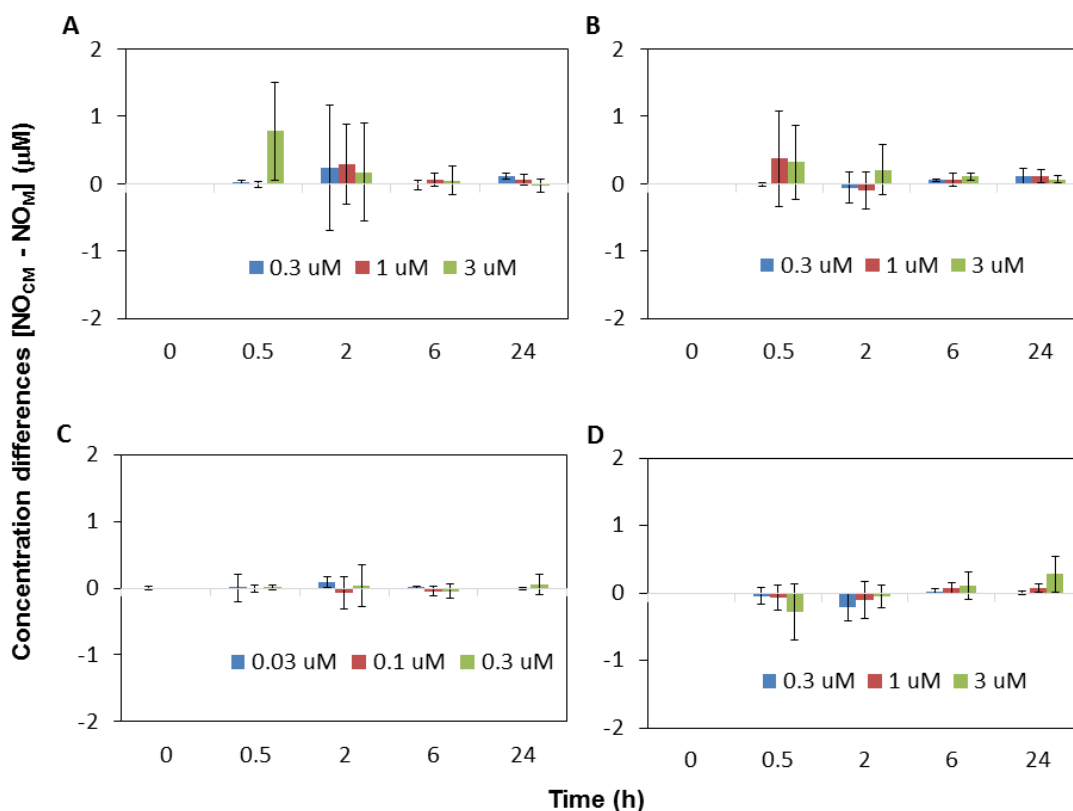
Figure V-13. Differential of NO release to media with and without cells for complexes **1-4**, A-D, respectively. Negative nitrite concentrations are indicative of cellular uptake of NO. The values were calculated by subtracting the amount of nitrite in the media alone (NO_M) from that found in the presence of cells (NO_{CM}).

Conclusions

In conclusion, the first sugar-appended iron dinitrosyl complexes were synthesized and characterized. Qualitative NO release studies in the presence of NO-trapping agents derived from porphyrins or $Co(N_2S_2)$ complexes demonstrated the ability of these compounds to transfer NO and nitrosylate Co(II). Additionally, both **1** and **2** released NO to cell media, both in the presence and absence of cells. In particular,

the long term release of NO displayed by **2** makes it a prime candidate for further exploration as a potential therapeutic agent. The synthetic protocol discussed herein shows that the strategy of glycoconjugation of DNICs holds potential for extension to the attachment of other carbohydrate units already in use as targeting ligands in drug delivery.

CHAPTER VI

STRUCTURAL COMPARISONS OF DNICS INVOLVING MN_2S_2 AND

PHOSPHINE LIGANDS

Introduction

In the preceding chapters, the $Fe(NO)_2$ unit has been explored in its capacity to be stabilized by a variety of C-, N- and S-donor ligands, and for its degradation to release NO under certain conditions. There is also a rather extensive synthetic enterprise developed primarily by the M. Y. Darensbourg laboratory, that examines the binding of the $Fe(NO)_2$ unit to N_2S_2 metalloligands.[79] These cis-dithiolato-metalloligands are inspired by natural Cys-X-Cys tripeptide motifs that utilize the deprotonated amido nitrogens and the cysteinyl sulfurs to form a roughly square planar N_2S_2 binding pocket. Such a motif is realized in the active sites of nitrile and thiocyanate hydratase, binding Fe and Co, although the difference in the hydratases is that in each the sulfurs are oxygenated.[139] The acetyl-CoA synthase active site also contains this binding motif and houses a nickel in the N_2S_2 binding pocket. In this case, the NiN_2S_2 metalloligand binds a second nickel center through the two thiolates of the metalloligand.

The electronic properties of these biomimetic MN_2S_2 metalloligands, where M = Ni, Fe(NO), and Co(NO), have been probed via the formation of stable $W(CO)_4$ adducts.[92] The carbonyls, as well as the nitrosyls for the Fe(NO) and Co(NO) cases, provide spectroscopic handles to rank the electron-donating ability of the metalloligands. The NiN_2S_2 is a slightly better donor than the Fe(NO) and Co(NO) metalloligands; this

result is consistent with the greater electron-withdrawing ability of $\{Co(NO)\}^8$ and $\{Fe(NO)\}^7$ on the bridging thiolate sulfurs.[92] However, discrimination between the electronic properties of the various nickel complexes with different N_2S_2 ligands was not possible using the $W(CO)_4$ reporter; the resulting structures are largely the same, and transfer of electron density towards the tungsten and passed on via π-backbonding to the CO's is not distinguished.[92] Other receiver units have since been utilized, for example the $(\eta^5\text{-}C_5H_5)Fe(L)^+$ unit readily binds the MN_2S_2 metalloligands in the formation of $M(\mu\text{-}SR)_2Fe$ heterobimetallics.[140] As another iron source, the $Fe(NO)_2$ unit binds in its two redox levels and is largely the focus of this dissertation.

Perhaps more intriguing than the electronic properties of these metallo-dithiolates-M' complexes was the host of binding modes and geometries possible and adopted in well-characterized complexes.[79] The dinitrosyliron unit, $Fe(NO)_2$, acts as a Lewis acid fragment to the MN_2S_2 and is isolable in both oxidized, $\{Fe(NO)_2\}^9$, and reduced, $\{Fe(NO)_2\}^{10}$ forms.[79] Pohl *et al.*, have shown that the reduced $\{Fe(NO)_2\}^{10}$ form may be isolated with neutral NiN_2S_2 (N_2S_2 = N,N'-diethyl-3,7-diazanonane-1,9-dithiolate, i.e. an "open chain" ligand) as the stabilizing ligand in which the NiN_2S_2 is bidentate bound to the iron of the $Fe(NO)_2$ forming a butterfly structure analogous to the $W(CO)_4$ derivatives.[141] In contrast, when $(\mu\text{-}I)_2[Fe(NO)_2]_2$, used as a source of $\{Fe(NO)_2\}^9$, reacts with bis-mercaptoethanediazacyclooctane nickel, [(bme-daco)Ni], in a 2:1 ratio, the NiN_2S_2 metalloligand binds two units of $Fe(NO)_2I$ on opposite sides of the NiN_2S_2 plane in a transoid fashion (*vide infra*).[142] The M. Y. Darensbourg group has prepared multiple $(MN_2S_2)Fe(NO)_2$ biomimetic complexes, M = Ni^{II}, $\{Fe(NO)\}^7$,

{Co(NO)}^{8}, and (V≡O)$^{2+}$, some of which are my own; these will be discussed in this chapter.[79]
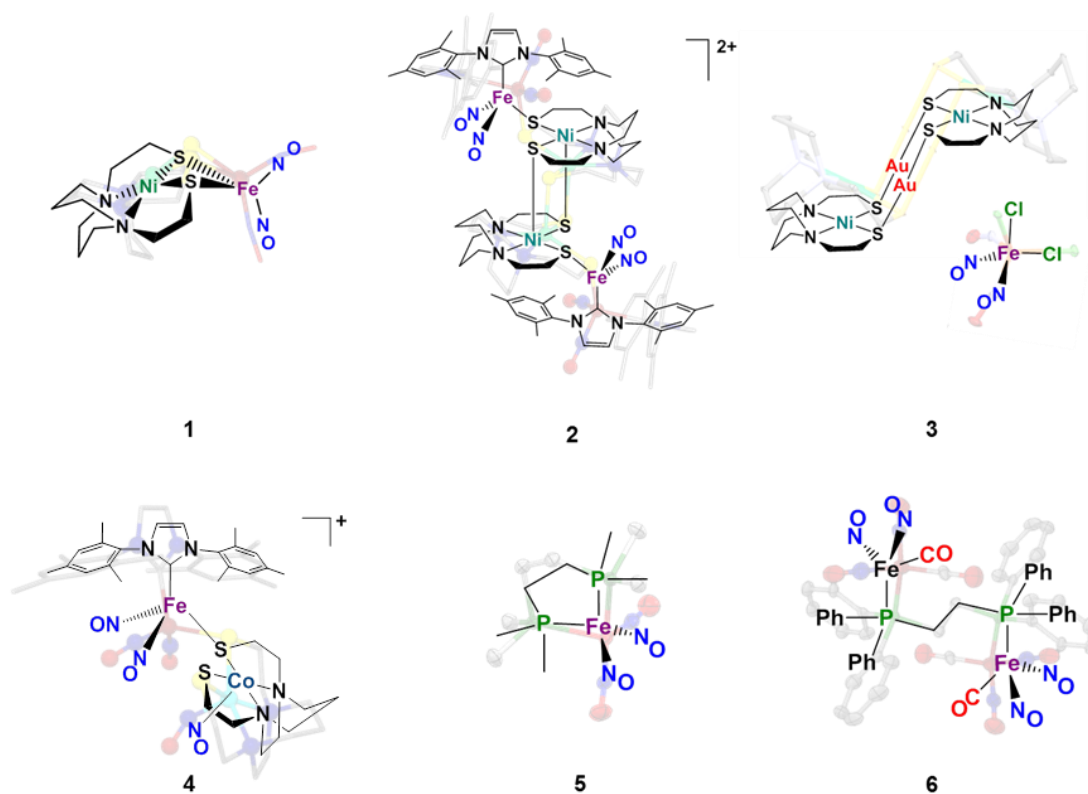
Figure VI-1. Chemdraw representations of complexes **1-6**, each of which will be discussed in this chapter.

We also note the various coordination modes of the metalloligands, i.e. monodentate through one thiolate, bidentate to one metal center, or each thiolate bound

119

to a different metal center, finding similarities and differences with modes seen with phosphine ligands. This chapter will include examples of phosphine-DNICs that exhibit the similar binding arrangements to those of the metallodithiolato ligands. The crystal data and structure refinement information for **1-5** are provided at the end of the chapter.

[Ni (bme-daco)Fe(NO)₂] (1)

Synthesis

$Fe(CO)_2(NO)_2$ was freshly prepared from the reaction of sodium tetrafluoroborate (0.012 g, 0.10 mmol) and [Na-18-crown- 6-ether][Fe(CO)3(NO)] (0.046 g, 0.10 mmol) in THF. Under a nitrogen atmosphere, a THF solution of Ni(bme-daco) (0.029 g, 0.10 mmol) was added to the freshly prepared $Fe(CO)_2(NO)_2$ and the mixture was stirred for 1 h at room temperature. Complete disappearance of the $\nu(CO)$ bands and a red shift of the $\nu(NO)$ IR bands confirmed the formation of **1**. Solvent removal *in vacuo* resulted in the degradation of the unstable product. Dark red crystals suitable for X-ray crystallographic studies were obtained by slow diffusion of a hexanes/diethyl ether mixture into a concentrated THF solution of **1** at -35°C. IR (THF, cm⁻¹): $\nu(NO)$ 1677(s), 1630(vs). The instability of the complex rendered other characterization impossible.
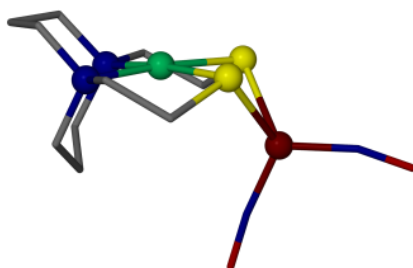
Figure VI-2. Ball and stick representation of complex **1**.

Structural Analysis

Similar to the report of Pohl *et al*.,[141] but incorporating a different N_2S_2 ligand, namely N,N′-bis (2-mercaptoethyl)- 1,4-diazacyclooctane (bme-daco), the author, in collaboration with former group member Chung-Hung Hsieh, synthesized a reduced Ni(bme-daco)Fe(NO)$_2$ (**1**) from addition of a THF solution of Ni(bme-daco) to a freshly prepared THF solution of Fe(CO)$_2$(NO)$_2$. The structure of **1,** which adopts a classic butterfly core, is given in Figure VI-2. An analogous butterfly structure, Ni(bme-dach) (bme-dach = N,N′-bis (2-mercaptoethyl)-1,4-diazacycloheptane) was synthesized in a similar manner and reported by the M. Y. Darensbourg group.[70] Some key parameters of **1** are given in Table VI-1, along with comparative parameters from the Ni(bme-dach)Fe(NO)$_2$ and the Ni(N$_2$S$_2$)Fe(NO)$_2$ open chain complex isolated by Pohl *et al.*[70,141] The Ni-Fe distance of 3.001(2) Å in **1** falls between the other two analogous Ni(N$_2$S$_2$)Fe(NO)$_2$ complexes, as seen in Table VI-1.

Table VI-1. Selected bond lengths (Å) and bond angles (˚) for complex **1** compared to those parameters in the analogous bme-dach and $Ni(N_2S_2)Fe(NO)_2$ (*) "open chain" (synthesized by Pohl *et al*).[70,141]

Complex	Ni-Fe (Å)	Fe-N-O (º)	ν (NO) (cm^{-1})
[Ni(bme-daco) Fe(NO)$_2$] (**1**)	3.001(2)	162.8(2) 172.0(2)	1677, 1630
[Ni(bme-dach) Fe(NO)$_2$]	3.229(3)	172.4(3) 175.8(4)	1732, 1689
Ni(N$_2$S$_2$)Fe(NO)$_2$*	2.797(1)	167.0(5) 174.6(5)	1663, 1624

With the increasing rigidity of the N_2S_2 backbone (i.e. less flexibility), undoubtedly affecting the optimal orientation of the S lone pairs that converge on the second metal, the Ni-Fe bond length increases. The notable elongation of ca. 0.2 Å in going from the open chain ligand to bme-daco to bme-dach in implies a role for carbon linkers between the nitrogens in the N_2S_2 backbone. The Fe-N-O angles in **1** are slightly bent toward each other and are very similar to those seen in other similar complexes. The ν(NO) IR stretches of **1** correlate well with the angles obtained and again fall in the middle between the bme-dach and open chain analogs.

[Ni (bme-daco)Fe(NO)$_2$(IMes)]$_2$[BF$_4$]$_2$ (2)

Synthesis

Under an argon atmosphere, Ni(bme-daco) (0.029 g, 0.10 mmol), a purple solid, and [(IMes)Fe(NO)$_3$][BF$_4$] (0.054 g, 0.10 mmol), a green solid, were loaded into a Schlenk flask and dissolved in CH$_2$Cl$_2$ (20 mL). The resulting dark red solution was stirred for 2 h at room temperature and monitored by IR spectroscopy to insure complete conversion to product. Solvent was then reduced to a minimum *in vacuo*, followed by addition of hexanes to precipitate the dark maroon product. The solid product was then washed with a mixture of hexanes and diethyl ether (3 x 20 mL) to remove impurities and residual volatiles were removed *in vacuo*. After again dissolving in CH$_2$Cl$_2$, the product was filtered through Celite to remove any insoluble solids. Dark maroon crystals, suitable for X-ray crystallographic studies, were obtained by slow diffusion of a hexanes/diethyl ether mixture into a concentrated CH$_2$Cl$_2$ solution of **2** at -35°C. IR (CH$_2$Cl$_2$, cm^{-1}): ν(NO) 1793(s), 1734(vs). Elem. Anal. Calc. for C$_{62}$H$_{88}$B$_2$F$_8$Fe$_2$N$_{12}$Ni$_2$O$_6$S$_4$: C, 45.73; H, 5.45; N, 10.32. Found: C, 46.63; H, 5.59; N, 10.50. +ESI-MS (CH$_2$Cl$_2$) m/z = 710.1942 for [Ni (bme-daco)Fe(NO)$_2$(IMes)]$_2$$^{2+}$.
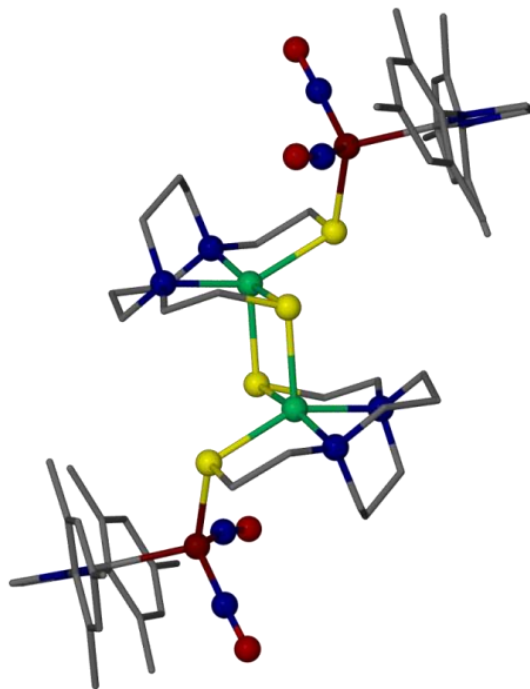
Figure VI-3. Ball and stick representation of complex **2**.

Structural Analysis

      Complex **2** represents a rare example of a pentacoordinate Ni^{2+} that is distorted toward trigonal bipyramidal geometry with τ = 0.31. Each $Fe(NO)_2$ unit is in the oxidized $\{Fe(NO)_2\}^9$ state. The two Ni^{2+} ions are separated by 3.326(1) Å and are each coordinated by the two nitrogens and the two thiolates of the N_2S_2 ring as well as a fifth thiolate that binds to the nickel center from a second N_2S_2 metalloligand (Figure VI-3). The distance between each nickel center and the sulfur of the bridging thiolate is 2.3714 (14) Å. The bridging Ni-S distance is only slightly longer than the Ni-S distances within the N_2S_2 plane (avg. 2.3524(15) Å).

For the $Fe(NO)_2$ units, the Fe-N and N-O bond distances are typical of that seen in other $\{Fe(NO)_2\}^9$ DNICs with similar ligand sets.[79] The average Fe-N and N-O bond lengths, 1.672(5)Å and 1.181(6) Å, respectively, are essentially identical to the average Fe-N and N-O bond distances in the cobalt analog (complex **4**) (1.675(6) Å and 1.171(7) Å) and in $IMesFe(NO)_2SPh$ (1.672(3) Å and 1.184(3) Å).[93] All the other main distances and angles for the $IMesFe(NO)_2$ unit also match nearly perfectly with those of $IMesFe(NO)_2SPh$. Thus the thiolate of the Ni(bme-daco) bound to the Fe in **2** can be considered very similar to the thiolate of phenylthiolate.

The similarities between the structures of this nickel dimer and the corresponding iron and zinc analogs are truly remarkable, as displayed by the overlays in Figure VI-4.[79,143] The M_2S_2 diamond core in complex **2** (defined by Ni(1)-S(2)-Ni(2)-S(3) with Ni-S-Ni angles equal to 89.95°) is a nearly precise match to that of analogous iron (Figure VI-4 (a)) and zinc cores (Figure VI-4 (b)).[79,143]
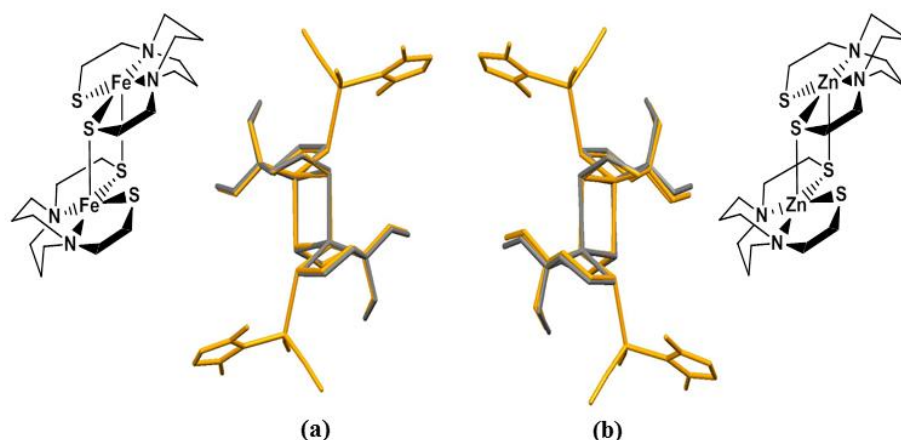
Figure VI-4. Overlay of **1** (gold) with [Fe(bme-daco)]$_2$ (a) and [Zn(bme-daco)]$_2$ (b). The Fe and Zn dimers are shown in Chemdraw form next to each overlay.[79,143]

Thus, it appears that the two DNIC units present in complex **2** act as sufficiently strong electron withdrawing groups to result in the electron density at each nickel becoming more like that of iron or zinc. This decrease in the electron density is then compensated by the binding of a third sulfur to each nickel. Hence, the nickel deviates from its preferred square planar geometry and becomes pentacoordinate to gain extra stability via electron donation from the sulfur.

Cyclic Voltammetry (CV)

The cyclic voltammogram of **2** (Figure VI-5 A) shows one main quasi-reversible event at $E_{1/2} = -1.03$ V, assigned to the $\{Fe(NO)_2\}^{9/10}$ redox couple. The assignment is made based on comparison with other similar complexes.[144] While the reduced analogs, such as **1**, show an electrochemical response to added acid, addition of HBF$_4$ to **2**

caused a distinct shift in the redox event at $E_{1/2} = -1.03$ V to $E_{1/2} = -0.77$ V indicative of the formation of a new species.
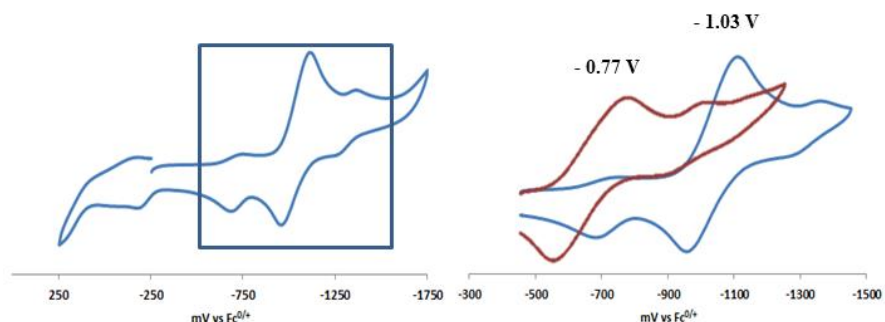
Figure VI-5. Cyclic voltammogram of **2** shown as a full scan at 200 mV/s (A). Overlay of the CV scan of **2** in DCM (blue) and of **2** after addition of 1 equiv. of HBF$_4$ (red).

IR analysis of the solution from the electrochemical cell following acid addition is shown in green in Figure VI-6, overlaid with the IR spectrum of **2** (blue). We propose that the acid protonates one of the thiolate sulfurs, which weakens the Ni-S bonds and causes the cleavage of the dimer (reaction scheme in Figure VI-6). The resulting species is then a monomeric derivative of Ni(bme-daco) in which one of the thiolates is protonated while the other remains bound to the Fe(NO)$_2$ unit.
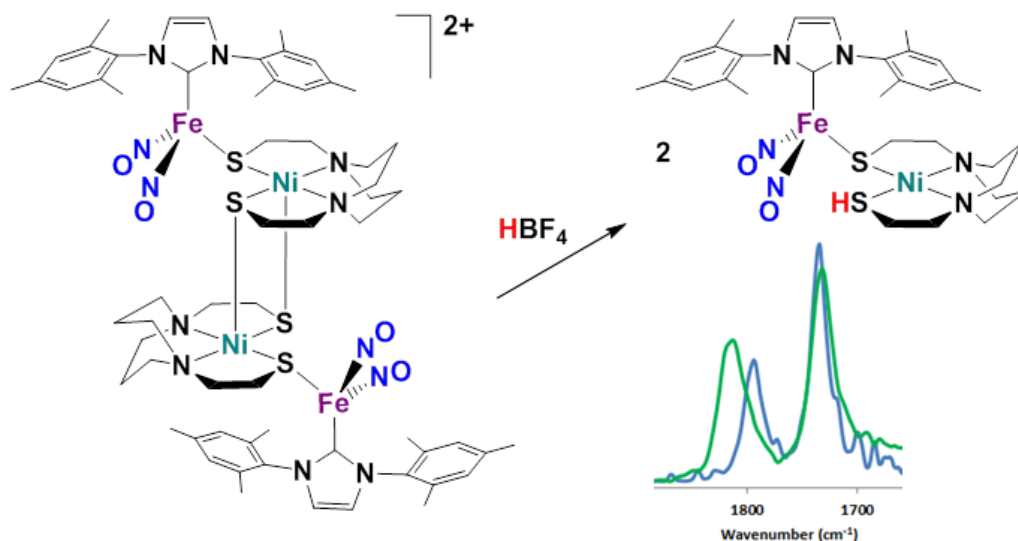
Figure VI-6. IR spectrum, ν(NO) region, of **2** in DCM (blue) (ν(NO): 1793, 1733 cm^{-1}) and the DCM solution of **2** from the electrochemical studies following addition of ca. 3 equiv. of HBF$_4$ (green) (ν(NO): 1817, 1732 cm^{-1}).

In summary, complex **2** is a unique example not only structurally, in that it adopts a rare penta-coordinate geometry about each nickel center, but also in its reactivity toward acids. Both the shift in the IR spectrum and in the CV indicate the formation of a new species, which we assign as a monomer. Studies are ongoing to identify this presumed monomeric species. One method that can be imployed to identify this product structurally is to use triphenylphosphine gold(I) as a surrogate for the proton. Thus far, we have not been able to obtain our proposed monomer with one of the thiolates bound to gold and the other to the Fe(NO)$_2$. Rather, the Ni(bme-daco) typically falls out and binds the gold, forming a stair-step structure where two Ni(bme-daco) units are bridged by two Au^I ions, similar to that described in the next section.

[{Ni(bme-daco)}₂Au₂]²⁺(Cl₂Fe(NO)₂)²⁻ (3)

Synthesis

Complex **1** was prepared using a 0.10 mmol scale as described earlier in this chapter. To the freshly prepared THF solution of **1** was added a THF solution of AuPPh₃Cl (0.049 g, 0.10 mmol). Following a 1 h stir, the IR spectrum revealed complete conversion to the product. The solvent was removed *in vacuo* and the resulting dark red solid was washed with hexanes (3 x 5 mL). The product solid was then redissolved in DCM, filtered through Celite to remove any insoluble solids, and solution volume was reduced to a minimum. X-ray quality crystals were obtained by slow diffusion of a hexanes/diethyl ether mixture into such a concentrated CH_2Cl_2 solution of **3** at -35°C. IR (CH_2Cl_2, cm⁻¹): ν(NO) 1673(s), 1625(s).

Structural Analysis

The cationic species $[(Ni(bme-daco))_2Au_2]^{2+}$ has been reported by the M. Y. Darensbourg group, albeit with chlorides as the counterions.[142] The metric parameters of the $[(Ni(bme-daco))_2Au_2]^{2+}$ isolated with the DNIC counteranion (**3**) are nearly identical to those reported previously.[142] A significant difference here is the formation of a rare $[Cl_2Fe(NO)_2]^{2-}$ species as the counteranion.
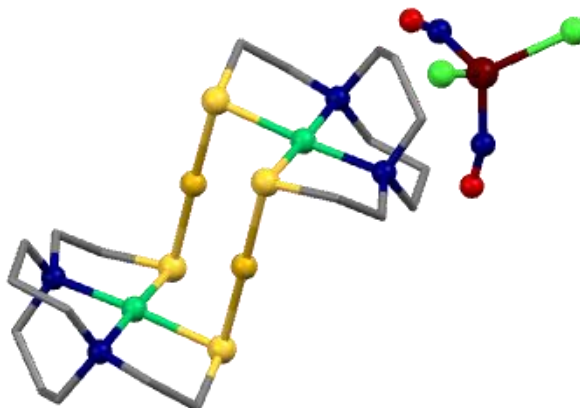
Fe(1)-N(4)	1.697(4)	Fe(1)-N(4)-O(2)	160.9(4)
Fe(1)-N(3)	1.719(6)	Fe(1)-N(3)-O(1)	158.3(4)
Fe(1)-Cl(4)	2.255(1)	Cl(4)-Fe(1)-Cl(3)	106.47(6)
Fe(1)-Cl(3)	2.281(1)	N(3)-Fe(1)-N(4)	106.6(2)
N(3)-O(1)	1.136(7)	O(2)-Fe(1)-O(1)	90.4(1)
N(4)-O(2)	1.163(6)		

Figure VI-7. Ball and stick representation of complex **3.** Bond lengths (Å) and bond angles (°) for the counteranion, $[Cl_2Fe(NO)_2]^{2-}$ are given in the table.

The structure of **3** is given in Figure VI-7 and key metric parameters of $[Cl_2Fe(NO)_2]^{2-}$ are listed in the table below the structure. Halide-containing DNICs, $[Br_2Fe(NO)_2]^-$ (reported and discussed in Chapter III) and $[I_2Fe(NO)_2]^-$ [114] in which the countercations are sodium 18-crown-6 ethers, were obtained as monoanions. The monoanionic $[Cl_2Fe(NO)_2]^-$ has been utilized in many DNIC reactions, but has never been structurally characterized. To our knowledge, no dianionic DNIC of this type has been reported. Interestingly, the Fe-N and N-O distances of **3** are nearly identical to

those of other halide DNICs.[114] The Fe-Cl bonds are ca. 0.2 Å shorter than the average Fe-I bonds in $[I_2Fe(NO)_2]^-$ but are nearly identical to the Fe-Br bond lengths in $[Br_2Fe(NO)_2]^-$.

The notable difference comes in the Fe-N-O angles. The average Fe-N-O angle is 165.9(6)° for $[Br_2Fe(NO)_2]^-$ and 164.9(3)° for $[I_2Fe(NO)_2]^-$; for **3**, the average is 159.6(4)°.[114] The significantly more bent Fe-N-O angles coupled with the lack of any additional anionic species in the crystal structure, supports the assignment of $[Cl_2Fe(NO)_2]^{2-}$ as a dianionic species. Liaw *et al.*, reported the only other dianionic, four-coordinate $\{Fe(NO)_2\}^{10}$ DNIC: $[(EtS)_2Fe(NO)_2]^{2-}$, which contains two potassium 18-crown-6 ethers as countercations.[26] Each of the thiolates of $[(EtS)_2Fe(NO)_2]^{2-}$ sits 3.328 Å away from a potassium, close enough for S⋯K interaction that is likely necessary to stabilize the dianionic species. In a similar manner, one of the chlorides in **3** is positioned at 3.333(1) Å from one of the gold centers, allowing for Cl⁻⋯Au[I] interaction and stabilization of the dianion.

[(NO)Co(bme-dach)(IMes)Fe(NO)₂](BF₄) (4)[*]

Synthesis

The trinitrosyl iron complex [(IMes)Fe(NO)₃][BF₄] (0.11 g, 0.20 mmol) (where IMes = the N-heterocyclic carbene of 1,3-bis(2,4,6-trimethylphenyl)imidazole) and [Co(bme-dach)]₂ (0.056 g, 0.10 mmol) were loaded in a degassed 50 mL Schlenk flask, septum sealed, and 10 mL CH_2Cl_2 solvent were added by syringe. The reaction mixture

was stirred for 1 h; its IR spectrum (CH_2Cl_2 solution) indicated complete conversion to product. The solution was filtered through Celite to remove insoluble solid. Addition of pentane to the CH_2Cl_2 solution yielded a dark brown precipitate, which was washed by diethyl ether (3 x 20 mL) to remove impurities (Yield: 0.099 g, 61%). Recrystallization in CH_2Cl_2/pentane-diethyl ether at 35°C afforded crystals of complex **4** suitable for X-ray crystallographic study. IR (CH_2Cl_2), cm^{-1}: v(NO): 1794 (s), 1735 (vs), 1622(m). Elem. Anal. Calc. for $C_{30}H_{42}CoFeN_7O_3S_2BF_4$: C, 44.24; H, 5.20; N, 12.04. Found: C, 44.37; H, 5.08; N, 12.69%. + ESI-MS (CH_2Cl_2) m/z = 727.1138 for [(NO)Co(bme-dach)(IMes)Fe(NO)$_2$] $^+$.
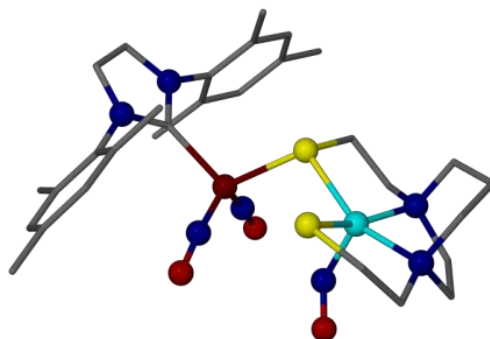
Figure VI-8. Ball and stick representation of complex **4**.

Structural Analysis

      Crystals of complex **4** as its BF$_4$ salt were obtained as described above. Selected distances and angles are in Table VI-2. The structure of complex **4** (see Figure VI-7),

shows the (bme-dach)Co(NO) unit bound to the $Fe(NO)_2$ unit through a single bridging thiolate. This positions the Fe at 3.697 Å from the Co, with the Co–Fe–S angle at 108.6(2)°. The nitrogen and sulfur donors define a square plane about the cobalt with deviation from best N_2S_2 plane in the range of 0.011–0.014 Å.

Table VI-2. Selected bond lengths (Å) and bond angles (°) for complex **4**.

Fe(1)–N(2)	1.673(6)	Co(2)–N(3)	1.778(6)
Fe(1)–N(1)	1.676(6)	Co(2)–N(4)	1.944(5)
Fe(1)–C(1)	2.009(7)	Co(2)–N(5)	1.974(6)
Fe(1)–S(1)	2.299(2)	Co(2)–S(2)	2.196(2)
N(1)–O(1)	1.171(7)	Co(2)–S(1)	2.277(2)
N(2)–O(2)	1.171(7)	N(3)–O(3)	1.163(7)
C(1)–Fe(1)–S(1)	108.65(19)	O(2)–N(2)–Fe(1)	172.6(6)
O(1)–N(1)–Fe(1)	168.2(5)	O(3)–N(3)–Co(2)	128.5(5)
Fe(1)–S(1)–Co(2)	107.74(9)	N(1)–Fe(1)–N(2)	119.6(3)

The cobalt is displaced from the N_2S_2 best plane by 0.38 Å, which is an increase of 0.074 Å from the 0.306 Å displacement seen in the free (bme-dach)Co(NO) ligand. The Co–N–O angle of 128.5° is 5° larger than that found in (bme-dach)Fe(NO), 123.8° [8]. Thus the coordination geometry about cobalt is little changed from that of the free metallodithiolate ligand. The Fe center in complex **4** retains its tetrahedral environment with the carbene, bridging thiolate, and two nitrosyls, both bound in a slightly bent fashion, as shown by the bond angles given in Table VI-2. The N–Fe–N angle is 119.6(3)° and the Fe–N–O bond angles are 168.2(5)° and 172.6(6)°. There are no other

significant differences between the appropriate portions of the precursors to the heterobimetallic and the adduct itself.

[(Dmpe)Fe(NO)₂] (5) (Dmpe = 1,2-Bis(Dimethylphosphino)Ethane)

Synthesis

Under an argon atmosphere, dmpe (33 mL, 0.20 mmol) was added to a THF solution of (IMes)(SPh)Fe(NO)₂ (prepared according to published procedure).[91] Following a 2 h stir, the solution turned from the deep purple starting material to a red brown. IR spectroscopy confirmed complete conversion to complex **5**. Solvent was removed *in vacuo* and the solid product washed with hexanes (2 x 10 mL). Solid **5** was redissolved in ether and filtered through Celite to remove any insoluble impurities. X-ray quality crystals were obtained by slow evaporation of a concentrated ether solution of **5** at -35°C. IR (THF, cm⁻¹): ν(NO): 1699 (s), 1658 (vs).
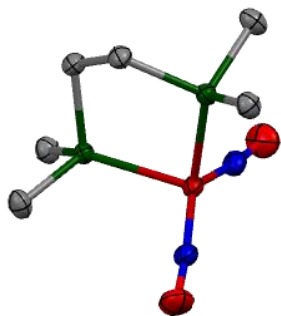
Fe-P	2.2044(6)
Fe-N	1.6536(17)
N-O	1.200(2)
Fe-N-O	174.46(14)
P-Fe-P	87.10(3)
N-Fe-N	139.16(11)

Figure VI-9. ORTEP drawing of complex **5** with thermal ellipsoids at 50 % probability level. Selected bond lengths (Å) and bond angles (°) for **5** are given in the table.

Structural Analysis

The crystals of **5** were grown by Randara Pulukkody and the solved structure was given to the author for analysis and further investigation. The structure contains a pseudotetrahedral iron center coordinated by the phosphorous atoms of a single dmpe ligand and the two nitrosyl nitrogens (Figure VI-9). The Fe-N, N-O and Fe-P bond lengths align well with values reported for other phosphorous-containing DNICs.[145] Although the Fe-N-O angle for **5** is on the high end (Fe-N-O angle range for neutral, $\{Fe(NO)_2\}^{10}$ ca. 166-178°, considering S-, N-, O- and C-donar ligands) the bis(phosphine) DNICs generally have larger Fe-N-O angles.[21,145]

Unlike the majority of DNICs isolated to date, the nitrosyls are oriented away from each other in the rare "repulso" conformation. The "repulso" conformation is defined by an O-Fe-O angle that is greater than the N-Fe-N angle. In **5**, the O-Fe-O angle is 143.76° while the N-Fe-N angle is 139.16°. This conformation is more typical of second and third row transition metal nitrosyls, for example the neutral $M(NO)_2(PPh_3)_2$, where M = Ru, Os, and the cationic species $[M(NO)_2(PPh_3)_2]^+$, where M = Ir, Rh.[145-151] To our knowledge, the only DNICs with the "repulse" conformation reported were two bisphosphine DNICs, where the bisphosphine was either 1,2-bis(diphenylphosphino)benzene or cis-1,2-bis(diphenyllphosphino)ethylene.[145] The authors attributed the rare conformation of the nitrosyls to electronic effects due to the C=C π bonds within the ligand.[145] Although **5** does not contain any C=C bonds, the dmpe ligand is strongly donating into the N-O bonds as seen from extremely low ν(NO) IR stretching frequencies 1699, 1658 cm^{-1}.

{μ-(Dppe)[Fe(NO)₂]₂} (6) (Dppe = 1,2-Bis(Diphenylphosphino)Ethane)

Synthesis

Under a nitrogen atmosphere, a THF solution of dppe (0.040 g, 0.10 mmol) was added to a THF solution of $Fe(CO)_2(NO)_2$ (freshly prepared from the reaction of sodium tetrafluoroborate (0.012 g, 0.10 mmol) and [Na-18-crown- 6-ether][$Fe(CO)_3(NO)$] (0.046 g, 0.10 mmol)). The mixture was stirred for 1 h at room temperature. Complete disappearance of one of the ν(CO) bands, and a red shift in both the ν(NO) bands and the remaining ν(CO) band confirmed the formation of **6**. Solvent was removed *in vacuo* and the dark brown product residue was redissolved in hexanes and filtered through Celite. X-ray quality crystals were obtained from slow evaporation of the concentrated hexanes solution of **6** at -35˚C. IR (THF, cm⁻¹): ν(NO): 1764 (s), 1723 (vs); ν(CO): 2008 (s).

Structural Analysis

Crystals of complex **6** were obtained as described above. Though the crystals were not of sufficient quality to obtain publishable data, a structure was obtained and is given in Figure VI-10. We highlight this structure to illustrate the ability of the phophine ligand to serve as a spanning ligand. Complex **5** demonstrated the well-known ability of the bis-phosphine to serve as a bidentate ligand to the $Fe(NO)_2$ unit, paralleling the binding seen in complex **1** in which the Ni(bme-daco) is bound in a bidentate fashion to the $Fe(NO)_2$.[152,153,157]

136
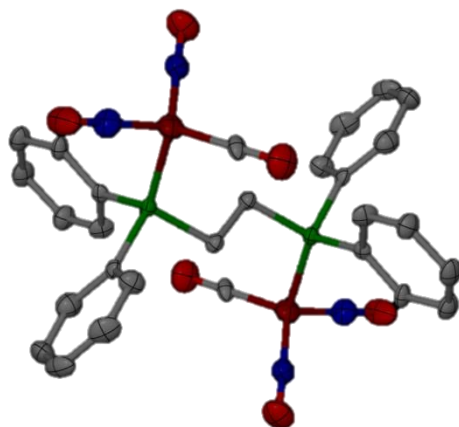
Figure VI-10. ORTEP drawing of complex **6** with thermal ellipsoids at 50 % probability level.

In a similar manner, the MN_2S_2 ligands can also serve as spanning ligands in which the metallodithiolate binds two different metal centers, one through each thiolate sulfur. Two examples are shown in Figure VI-11. The $[Ni(bme\text{-}dach)\cdot(W(CO)_5)_2]$ structure (Figure VI-11 A) was obtained by group member Pokhraj Ghosh (unpublished) and the $[Ni(bme\text{-}daco)\cdot(Fe(NO)_2I)_2]$ (Figure VI-11 B) was reported by the M. Y. Darensbourg laboratory in 2014.[142]
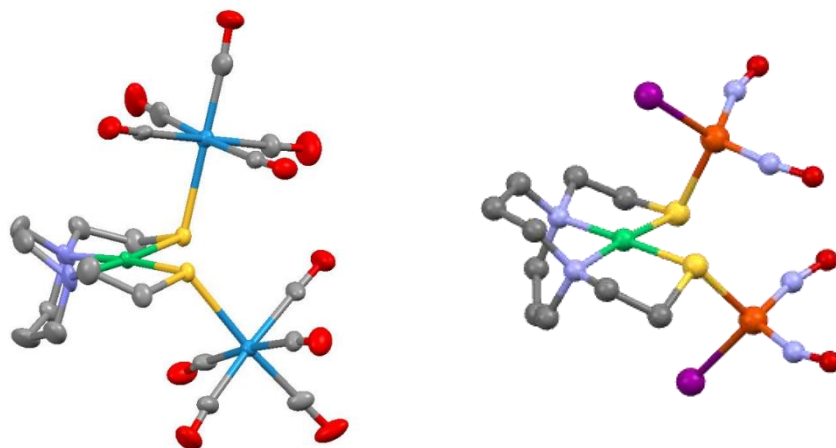
Figure VI-11. Ball and stick representation of [Ni(bme-dach)·(W(CO)$_5$)$_2$] (left) and [Ni(bme-daco)·(Fe(NO)$_2$I)$_2$] (right) each of which display the NiN$_2$S$_2$ acting as a spanning ligand, similar to what is seen with the posphines.

Summary and Conclusions

Although some of the structures presented are similar to others reported in the literature, there are also some presented herein that contain rarely seen and rather unique structural properties. Complex **2** is one of only a handful of five-coordinate nickel complexes.[154-156] Additionally, with one of the thiolates of the bme-daco binding the iron of the DNIC unit and the other thiolate binding the nickel center of a separate Ni(bme-daco), **2** becomes nearly geometrically identical to the [Fe(bme-daco)]$_2$ and the [Zn(bme-daco)]$_2$, suggesting that the nickel center in this coordination environment behaves more like Fe or Zn.[79,143]

The counteranion in **3**, being the dianionic species [Cl$_2$Fe(NO)$_2$]$^{2-}$ is the lone example of a dianionic halide-containing DNIC. As was shown, the Fe-N-O angles are significantly more bent, indicative of increased electron density on the nitrosyls. The

only other dianionic, four-coordinate, monomeric $\{Fe(NO)_2\}^{10}$ DNIC reported to date is $[(EtS)_2Fe(NO)_2]^{2-}$, which is stabilized by two potassium 18-crown-6 ether cations.[26]

Both of the phospine DNICs presented in this chapter are also worth highlighting. Complex **5** houses the nitrosyls in the rather rare "repulso" configuration, only reported in a couple of other phosphine DNICs, as well as second and third row transition metal nitrosyls.[145-151] Though there are many examples of bisphosphines acting as spanning ligands,[152,153,157] complex **6** represents the only example of a bisphosphine spanning two different $Fe(NO)_2$ units.

Finally, comparison of the $M(N_2S_2)$ and phosphine structures presented within this chapter showcase the similarities between the two ligands in regards to binding modes towards the $Fe(NO)_2$ unit. For example, both **1** (containing the Ni(bme-daco)) and **5** (with dmpe) present bidentate binding of the ligand to a single $Fe(NO)_2$ unit. In both **2** and **3**, the Ni(bme-daco) spans two different metal centers, in a manner similar to dppe in **6**, which spans between two different $Fe(NO)_2$ units. However, while each phosporous has only one lone pair, each thiolate sulfur contains two lone pairs. Because each of these lone pairs is oriented in a different direction, an array of binding orientations is possible between the metallodithiolate ligands and the $Fe(NO)_2$ unit. The contrast in binding modes displayed in **1** and **3** illustrates this point well. In **1**, the convergent lone pairs are utilized, resulting in bidentate binding of the $Fe(NO)_2$ while the divergent lone pairs remaining on each sulfur create the butterfly structure. In **3**, the divergent lone pairs are involved, each binding a separate Au^I ion to yield the stairstep structure.

139

Crystallographic Data

Table VI-3. Crystal data and structure refinement for [Ni (bme-daco)Fe(NO)$_2$] **(1)**.

Identification code	feni
Empirical formula	C10.50 H21 Cl Fe N4 Ni O2 S2
Formula weight	449.44
Temperature	110(2) K
Wavelength	0.71073 Å
Crystal system	Monoclinic
Space group	C 2/c
Unit cell dimensions	a = 12.318(8) Å α= 90°.
	b = 11.116(7) Å β= 90.062(7)°.
	c = 24.241(15) Å γ = 90°.
Volume	3319(4) Å^3
Z	8
Density (calculated)	1.799 Mg/m^3
Absorption coefficient	2.429 mm^{-1}
F(000)	1848
Crystal size	0.400 x 0.200 x 0.050 mm^3
Theta range for data collection	2.468 to 29.638°.
Index ranges	-16<=h<=16, -15<=k<=15, -33<=l<=33
Reflections collected	20288
Independent reflections	4376 [R(int) = 0.0487]
Completeness to theta = 25.242°	99.9 %
Absorption correction	Semi-empirical from equivalents
Max. and min. transmission	0.7459 and 0.6617
Refinement method	Full-matrix least-squares on F^2
Data / restraints / parameters	4376 / 0 / 195
Goodness-of-fit on F^2	1.085
Final R indices [I>2sigma(I)]	R1 = 0.0314, wR2 = 0.0671
R indices (all data)	R1 = 0.0437, wR2 = 0.0708
Extinction coefficient	n/a
Largest diff. peak and hole	0.809 and -0.733 e.Å^{-3}

Table VI-4. Crystal data and structure refinement for Ni(daco)Fe(NO)$_2$IMes (**2**).

Identification code	Ni(daco)Fe(NO)$_2$IMes
Empirical formula	C62 H88 B2 F8 Fe2 N12 Ni2 O4 S4
Formula weight	1596.42
Temperature	150(2) K
Wavelength	0.71073 Å
Crystal system	Monoclinic
Space group	P2(1)/c
Unit cell dimensions	a = 18.764(2) Å α= 90°.
	b = 19.612(3) Å β= 90.044(2)°.
	c = 19.820(3) Å γ = 90°.
Volume	7294.0(16) Å^3
Z	4
Density (calculated)	1.454 Mg/m^3
Absorption coefficient	1.086 mm^{-1}
F(000)	3320
Crystal size	0.16 x 0.11 x 0.06 mm^3
Theta range for data collection	1.09 to 22.96°.
Index ranges	-20<=h<=20, -21<=k<=21, -21<=l<=21
Reflections collected	73449
Independent reflections	8396 [R(int) = 0.1235]
Completeness to theta = 22.96°	83.0 %
Absorption correction	None
Max. and min. transmission	0.9377 and 0.8454
Refinement method	Full-matrix least-squares on F^2
Data / restraints / parameters	8396 / 0 / 877
Goodness-of-fit on F^2	0.940
Final R indices [I >2sigma(I)]	R1 = 0.0410, wR2 = 0.0957
R indices (all data)	R1 = 0.0744, wR2 = 0.1143
Largest diff. peak and hole	0.539 and -0.434 e.Å^{-3}

Table VI-5. Crystal data and structure refinement for [{Ni(bme-daco)}$_2$Au$_2$]$^{2+}$(Cl$_2$Fe(NO)$_2$)$^{2-}$ (**3**).

Identification code	[{Ni(bme-daco)}$_2$Au$_2$]$^{2+}$(Cl$_2$Fe(NO)$_2$)$^{2-}$
Empirical formula	C11 H22 Au Cl4 Fe N4 Ni O2 S2
Formula weight	759.77
Temperature	100(2) K
Wavelength	1.54178 Å
Crystal system	Monoclinic
Space group	P2$_1$/n
Unit cell dimensions	a = 11.0317(3) Å $\quad$ α= 90°.
	b = 14.2453(4) Å $\quad$ β= 104.5580(10)°.
	c = 14.0475(3) Å $\quad$ γ = 90°.
Volume	2136.69(10) Å^3
Z	4
Density (calculated)	2.362 Mg/m^3
Absorption coefficient	25.622 mm^{-1}
F(000)	1460
Crystal size	0.200 x 0.050 x 0.020 mm^3
Theta range for data collection	4.495 to 65.147°.
Index ranges	-12<=h<=12, -16<=k<=16, -16<=l<=16
Reflections collected	23192
Independent reflections	3642 [R(int) = 0.0553]
Completeness to theta = 65.147°	100.0 %
Absorption correction	None
Refinement method	Full-matrix least-squares on F^2
Data / restraints / parameters	3642 / 60 / 230
Goodness-of-fit on F^2	1.054
Final R indices [I>2sigma(I)]	R1 = 0.0274, wR2 = 0.0611
R indices (all data)	R1 = 0.0318, wR2 = 0.0629
Extinction coefficient	0.00036(2)
Largest diff. peak and hole	1.918 and -1.760 e.Å^{-3}

Table VI-6. Crystal data and structure refinement for [(NO)Co(bme-dach)(IMes)Fe(NO)$_2$][BF$_4$] (**4**).

Identification code	datax
Empirical formula	C31 H44 B Cl2 Co F4 Fe N7 O3 S2
Formula weight	899.34
Temperature	110(2) K
Wavelength	0.71073 Å
Crystal system	Monoclinic
Space group	P21/n
Unit cell dimensions	a = 20.372(9) Å α= 90°.
	b = 7.966(4) Å β= 94.387(18)°.
	c = 24.785(10) Å γ = 90°.
Volume	4010(3) Å^3
Z	4
Density (calculated)	1.490 Mg/m^3
Absorption coefficient	1.072 mm^{-1}
F(000)	1852
Crystal size	0.10 x 0.08 x 0.02 mm^3
Theta range for data collection	1.25 to 25.00°.
Index ranges	-24<=h<=24, -6<=k<=9, -29<=l<=20
Reflections collected	19398
Independent reflections	7039 [R(int) = 0.1060]
Completeness to theta = 25.00°	99.6 %
Absorption correction	Semi-empirical from equivalents
Max. and min. transmission	0.9789 and 0.9003
Refinement method	Full-matrix least-squares on F^2
Data / restraints / parameters	7039 / 0 / 475
Goodness-of-fit on F^2	1.010
Final R indices [I>2sigma(I)]	R1 = 0.0685, wR2 = 0.1674
R indices (all data)	R1 = 0.1359, wR2 = 0.2094
Largest diff. peak and hole	2.001 and -0.668 e.Å^{-3}

Table VI-7. Crystal data and structure refinement for [(dmpe)Fe(NO)$_2$] (**5**).

Identification code	dmpe
Empirical formula	C6 H16 Fe N2 O2 P2
Formula weight	266.00
Temperature	150.15 K
Wavelength	0.71073 Å
Crystal system	Monoclinic
Space group	C 1 2/c 1
Unit cell dimensions	a = 9.460(3) Å α= 90°.
	b = 10.947(3) Å β= 111.478(3)°.
	c = 12.118(3) Å γ = 90°.
Volume	1167.7(5) Å^3
Z	4
Density (calculated)	1.513 Mg/m^3
Absorption coefficient	1.539 mm^{-1}
F(000)	552
Crystal size	0.08 x 0.05 x 0.02 mm^3
Theta range for data collection	2.969 to 27.523°.
Index ranges	-12<=h<=12, -14<=k<=14, -15<=l<=15
Reflections collected	6496
Independent reflections	1342 [R(int) = 0.0426]
Completeness to theta = 25.242°	99.9 %
Absorption correction	Semi-empirical from equivalents
Max. and min. transmission	0.7456 and 0.6336
Refinement method	Full-matrix least-squares on F^2
Data / restraints / parameters	1342 / 0 / 62
Goodness-of-fit on F^2	1.038
Final R indices [I>2sigma(I)]	R1 = 0.0257, wR2 = 0.0574
R indices (all data)	R1 = 0.0352, wR2 = 0.0605
Extinction coefficient	n/a
Largest diff. peak and hole	0.472 and -0.247 e.Å^{-3}

CHAPTER VII

CONCLUSIONS AND FUTURE DIRECTIONS

Through advances in synthetic and spectroscopic methodologies and the combined efforts of inorganic and biochemists, the fundamental chemistry of the biologically recognized nitric oxide storage and transport agents, dinitrosyl iron complexes (DNICs), has been firmly established.[21,94,95] With such advances in this field, the development of DNICs into meaningful pharmaceuticals can finally be realized. Inspired by such a potential, the work reported in this dissertation was focused on addressing the little explored area of DNIC reactivity with components of cellular environments. The reactivity studies recognized the DNIC/Copper/RSNO connections and their interwoven chemistry regarding NO release, and explored structural studies of aggregates of DNICs with metallodithiolates. Design strategies for NO-release therapeutic development of DNICs were also presented.

As discussed in Chapter I, very few studies within the field of DNIC chemistry have been devoted to understanding NO release from DNICs. Most simply assess the ability of the DNIC to transfer NO in the presence of an NO acceptor, such as an iron or cobalt porphyrins.[22,41,45] Such studies however, fail to address other plausible modes of NO release, specifically what effect other components of the cellular environment would have on DNICs. Work by Liaw *et al.*represents a single example of exploring such interactions, and demonstrated that addition of various chelating agents to a carbazolate DNIC resulted in release of NO as NO^+, $NO^·$, or NO^-, depending upon the incoming

145

ligand.[42] Considering that the other biological NO carrier, S-nitrosothiol (RSNO), requires copper to catalyze the release of NO,[52-55] we were surprised that copper had not been considered as a player in NO release from DNICs. Chapter III described our investigation of copper promoted NO release from DNICs. Addition of Cu^I and Cu^{II} salts to solutions of the reduced, $\{Fe(NO)_2\}^{10}$ DNIC $[(neo)Fe(NO)_2]$, where neo = 2,9-dimethyl-1,10-phenanthroline (neocuproine), resulted in the transfer of the neocuproine ligand to Cu and concomitant release of NO. Such results open the door to many possibilities, most important of which is triggered NO release.

One of the challenges in the development of DNICs as pharmaceuticals is control of the delivery of NO. As pioneered by Ford *et al*., one of the strategies for solving this issue is through light-activated NO release.[36,37] Photo-activation, while attractive, is limited to more topical applications. More promising strategies would involve working with the natural cellular components and mechanisms. Our study with copper provides one such approach. Considering that copper is an important cofactor in many cellular metalloenzymes and thus prevalent within the cell, it is reasonable to suggest that cellular copper species might play a role in NO release from DNICs.[158] As Chapter III has only laid the basic foundation for copper-promoted NO release from DNICs, future studies should build on these results by employing more biologically relevant DNICs and copper sources. Possible copper sources could include copper complexes of histidine, cysteine or glutathione, all of which have been previously reported and mimic endogenous copper sources.[159-162] Such copper complexes, coupled with DNICs such as the thiosugar-DNICs discussed in Chapter V, would provide a realistic biomimetic study

for the effect of copper on NO release from DNICs. Although both the thiosugar-DNICs presented in Chapter V did release NO in the aqueous media, neither released its full nitrosyl payload, even after 24 h. If copper proves to be effective in promoting full NO release from these DNICs or if it enhances the rate of NO release, a two component drug formulation could be created wherein the copper and DNIC are only allowed to mix at the target site. We note that copper in any significant concentrations would be cytotoxic. Hence a detailed analysis of the concentration ranges of copper that would be effective in promoting NO release should be performed.

In collaboration with Dr. Soon-Mi Lim at Texas A&M University, we are currently investigating the effect of copper on these sugar DNICs through live imaging of smooth muscle cells. Smooth muscle cells do not produce NO, but rather respond to added NO by relaxing. The efficacy of the DNIC both with and without Cu can then be assessed through confocal microscopy by visualizing the cellular relaxation.

The idea of using components of the cell to yield pharmacologically active species is not a new one. The activity of the anti-cancer agent cis-platin also relies upon the differences in intra- and extracellular chloride concentration.[46] Since the intracellular chloride ion concentration is significantly lower than the extracellular concentration, cisplatin loses both chloride ions upon entering the cell, at which point it becomes active.[46] Kim *et al.* also utilized such a method with a five-coordinate, iodide-containing DNIC, which was discussed in Chapter I.[45] Upon loss of the iodide, a metastable, four-coordinate DNIC is formed, which spontaneously decomposes to release NO. Hence, it

147

was proposed that the labile iodide would dissociate upon entering the cell, thus forming the NO-releasing four-coordinate DNIC only after entering the cell.[45]

Another finding presented in Chapter III that merits further study is the correlation between the redox levels of both the DNIC and the copper regarding NO release, i.e. does Cu^{II} work better for the reduced $\{Fe(NO)_2\}^{10}$ DNICs while Cu^{I} is more effective for the oxidized $\{Fe(NO)_2\}^{9}$ DNICs? For the reduced DNIC $[(neo)Fe(NO)_2]$ employed in our study, this was the case. Although addition of both Cu^{I} and Cu^{II} resulted in NO release from $[(neo)Fe(NO)_2]$, the Cu^{II} reaction occurred within minutes, while the Cu^{I} reaction time was on the order of hours. Ideally, a DNIC that is stable in both redox levels should be used to test this hypothesis. One such possibility is $[(Ar-nacnac)Fe(NO)_2]$ (Ar-nacnac = anion of $[(2,6-diisopropylphenyl)NC(Me)]_2CH)$, which was developed by Lippard *et al.* and isolated in both redox levels.[41] All four combinations, namely $Cu(I)/\{Fe(NO)_2\}^{10}$, $Cu(II)/\{Fe(NO)_2\}^{10}$, $Cu(I)/\{Fe(NO)_2\}^{9}$ and $Cu(II)/\{Fe(NO)_2\}^{9}$ could then be analyzed using the same ligand set.

The interconnection between copper and DNICs, discussed in both Chapters I and III, was also demonstrated in the interaction of DNICs with another cellular component, S-nitrosothiols (RSNOs). Drawing inspiration from the work of Vanin *et al.*,[18,59] that claims DNICs, as well as Cu, can promote NO release from RSNOs, Chapter IV described the reactivity of the trityl-S-nitrosothiol with two reduced $\{Fe(NO)_2\}^{10}$ DNICs of the form $[(L)_2Fe(NO)_2]$ (L = CO or neo). In both cases, NO was released, which agreed with the findings of Vanin *et al.* that DNICs promote NO release from RSNOs.[18,59] However, labeling studies showed complete scrambling of the nitrosyls.

148

A more interesting result presented in Chapter IV was the formation of a unique $(\mu\text{-}S)(SR)_2[Fe(NO)_2]_4$ cluster. This cluster is particularly intriguing in that it contains an interstitial sulfide. Although tritylthiol is a known sulfide donor,[126] the formation of a sulfide-containing species from reaction of the two biological NO carries might point to an additional role for RSNOs, namely as possible sulfide donors in the repair mechanism of iron sulfur clusters. Although many FeS(NO) clusters have been isolated,[125] the cluster reported here is structurally unique. Such a species can be viewed as a possible intermediate within the pathway of iron sulfur cluster repair.

Further studies in this area could again be aimed at making a more biologically relevant system. Would the cluster still form if a different RSNO was used (where R = glutathione or cysteine)? Also, investigating this reaction using oxidized DNICs would be of interest, as such species are confirmed to exist endogenously (vid EPR spectroscopy).[10-14]

Even with the impressive advances that have been made in DNIC chemistry, there is surprising lack of biologically viable DNICs available for development into pharmaceuticals. The main roadblock in this area is selecting ligands that are both biocompatible and provide sufficient stability to the $Fe(NO)_2$ unit. Beyond these basic guidelines, ligands tagged with specific cell receptors for targeted delivery or improved cellular uptake, is an attractive possibility. The approach outlined in Chapter V employed glucose-based ligands in the form of acetylated thioglucose. The use of the thioglucose not only incorporates needed stability and enhanced biocompatibility, but it allows the potential to exploit the natural mechanisms of the cell for sugar uptake.[130,131]

The two thioglucose DNICs reported, one of the dimeric Roussin's red ester form and the other a monomeric species containing both an N-heterocyclic carbene and the thioglucose, showed remarkable air stability and low cytotoxicity towards endothelial cells. Although neither DNIC released more than 50% of its NO payload, cellular uptake was observed.

The release of NO from the thioglucose DNICs was measured indirectly using the Griess Assay, which measures the amount of nitrite produced via the formation of an azo dye. Furthermore, the measurements of the amount of NO taken up by the endothelial cells was calculated based on a difference measurement between the concentration of NO released in the presence of cells vs the NO concentration in the absence of cells. Such limitations leave one vital question unanswered: how does the NO release occur. Is the DNIC transported intact into the cell prior to NO release or is the NO released outside the cell and carried in via passive diffusion? Liaw, Vanin and others have probed cellular DNICs using EPR spectroscopy.[44,47,104] The drawback to this technique is the extreme similarity of many of the signals produced by DNICs. Even if a signal is observed within the cell, such a signal could arise from the formation of a new DNIC upon entry of NO into the cell. A better method for tracking the fate of the DNIC would be through fluorescent tagging.

Perhaps one of the most intriguing contributions to dinitrosyl iron chemistry in the past two decades has been the isolation of glutathione S-transferase (GST) with a dinitrosyl iron unit bound in the active site.[64] Although none of the work presented in this dissertation involved GST, the important role it plays in DNIC chemistry merits

mention. Not only is this the first, and to date, the only protein-bound DNIC that has been structurally characterized, it is also another example of the correlation between copper and the $Fe(NO)_2$ unit.

As discussed in Chapter I, GST is an important part of cell detoxification. The GST accomplishes this detoxification by catalyzing the conjugation of glutathione to xenobiotic substrates, which include metal ions.[73,74] Considering this mode of action coupled with the successful binding of the glutathione DNIC to the GST active site, the question arises as to whether non-glutathione DNICs (such as the thiosugar DNICs, for example) would still be taken up by GST. Such a study that would test GST uptake of DNICs containing various ligand sets, would inform on the fate of exogenously added, non-glutathione DNICs. It is also surprising that although copper strongly inhibits GST activity,[60-63] no Cu-bound GST has been isolated to date. Such a structure would allow for further comparison between the electronically similar $Cu^{II/I}$ and $\{Fe(NO)_2\}^{9/10}$ species and add to the already strong correlation between copper and DNICs.

Chapter VI represents a departure from the much more biological focus of the other chapters. This structurally focused chapter, however, demonstrated a few of the diverse complexes that incorporate the $Fe(NO)_2$ unit. Additionally, the metallodithiolate ligands, which mimic Cys-X-Cys tripeptide motifs, showcase the types of interactions such species might have the $Fe(NO)_2$ unit.

Overall, dinitrosyl iron chemistry is a fascinating field with great potential both chemically and medicinally. From the extensive possibilities for improved ligand design to further probing DNIC reactivity within a biological environment to better

understanding the mechanism of NO release much remains to be explored. The strides that have been made in this area position DNICs on the road to answering the need for safe NO-releasing pharmaceuticals.

REFERENCES

1. Furchgott, R. F.; Ignarro, L. J.; Murad, F. *Biosci. Rep.* **1999***, 19*, 235-251.

2. Riccio, D. A.; Schoenfisch, M. H. Nitric oxide release: Part I. Macromolecular scaffolds. *Chem. Soc. Rev.* **2012***, 41*, 3731-3741.

3. Calabrese, V.; Mancuso, C.; Calvani, M.; Rizzarelli, E.; Butterfield, D. A.; Stella, A. M. G. Nitric oxide in the central nervous system: neuroprotection versus neurotoxicity. *Nature reviews.Neuroscience* **2007***, 8*, 766.

4. Santolini, J. The molecular mechanism of mammalian NO-synthases: a story of electrons and protons. *J. Inorg. Biochem.* **2011***, 105*, 127-141.

5. Miller, M.; Megson, I. Recent developments in nitric oxide donor drugs. *Br. J. Pharmacol.* **2007***, 151*, 305-321.

6. AnonymousScience of Nitric Oxide- What Nitric Oxide does for the health and wellness of our cardiovascular system, according to Dr. Rainer Böger, M.D. *Arginine Cardio* **2017**.

7. Toledo Jr, J. C.; Augusto, O. Connecting the chemical and biological properties of nitric oxide. *Chem. Res. Toxicol.* **2012***, 25*, 975-989.

8. Tennyson, A. G.; Lippard, S. J. Generation, translocation, and action of nitric oxide in living systems. *Chem. Biol.* **2011***, 18*, 1211-1220.

9. Maron, B. A.; Tang, S.; Loscalzo, J. S-nitrosothiols and the S-nitrosoproteome of the cardiovascular system. *Antioxidants & redox signaling* **2013***, 18*, 270-287.

10. Woolum, J. C.; Commoner, B. Isolation and identification of a paramagnetic complex from the livers of carcinogen-treated rats. *Biochimica et Biophysica Acta (BBA)-General Subjects* **1970***, 201*, 131-140.

11. Tonzetich, Z. J.; Wang, H.; Mitra, D.; Tinberg, C. E.; Do, L. H.; Jenney Jr, F. E.; Adams, M. W.; Cramer, S. P.; Lippard, S. J. Identification of protein-bound dinitrosyl iron complexes by nuclear resonance vibrational spectroscopy. *J. Am. Chem. Soc.* **2010***, 132*, 6914-6916.

12. Mülsch, A.; Mordvintcev, P.; Vanin, A. F.; Busse, R. The potent vasodilating and guanylyl cyclase activating dinitrosyl-iron (II) complex is stored in a protein-bound form in vascular tissue and is released by thiols. *FEBS Lett.* **1991**, *294*, 252-256.

13. Crack, J. C.; Smith, L. J.; Stapleton, M. R.; Peck, J.; Watmough, N. J.; Buttner, M. J.; Buxton, R. S.; Green, J.; Oganesyan, V. S.; Thomson, A. J. Mechanistic Insight into the Nitrosylation of the [4Fe− 4S] Cluster of WhiB-like Proteins. *J. Am. Chem. Soc.* **2011**, *133*, 1112-1121.

14. Tinberg, C. E.; Tonzetich, Z. J.; Wang, H.; Do, L. H.; Yoda, Y.; Cramer, S. P.; Lippard, S. J. Characterization of iron dinitrosyl species formed in the reaction of nitric oxide with a biological Rieske center. *J. Am. Chem. Soc.* **2010**, *132*, 18168-18176.

15. Harrop, T. C.; Tonzetich, Z. J.; Reisner, E.; Lippard, S. J. Reactions of synthetic [2Fe-2S] and [4Fe-4S] clusters with nitric oxide and nitrosothiols. *J. Am. Chem. Soc.* **2008**, *130*, 15602-15610.

16. Toledo, J. C.,Jr; Bosworth, C. A.; Hennon, S. W.; Mahtani, H. A.; Bergonia, H. A.; Lancaster, J. R.,Jr Nitric oxide-induced conversion of cellular chelatable iron into macromolecule-bound paramagnetic dinitrosyliron complexes. *J. Biol. Chem.* **2008**, *283*, 28926-28933.

17. Hickok, J. R.; Sahni, S.; Shen, H.; Arvind, A.; Antoniou, C.; Fung, L. W.; Thomas, D. D. Dinitrosyliron complexes are the most abundant nitric oxide-derived cellular adduct: biological parameters of assembly and disappearance. *Free Radical Biology and Medicine* **2011**, *51*, 1558-1566.

18. Vanin, A. F.; Muller, B.; Alencar, J. L.; Lobysheva, I. I.; Nepveu, F.; Stoclet, J. Evidence that intrinsic iron but not intrinsic copper determines S-nitrosocysteine decomposition in buffer solution. *Nitric Oxide* **2002**, *7*, 194-209.

19. Ye, S.; Neese, F. The unusual electronic structure of dinitrosyl iron complexes. *J. Am. Chem. Soc.* **2010**, *132*, 3646-3647.

20. Enemark, J.; Feltham, R. Principles of structure, bonding, and reactivity for metal nitrosyl complexes. *Coord. Chem. Rev.* **1974**, *13*, 339-406.

21. Tsai, M.; Tsou, C.; Liaw, W. Dinitrosyl iron complexes (DNICs): from biomimetic synthesis and spectroscopic characterization toward unveiling the biological and catalytic roles of DNICs. *Acc. Chem. Res.* **2015**, *48*, 1184-1193.

22. Hess, J. L.; Hsieh, C.; Reibenspies, J. H.; Darensbourg, M. Y. N-Heterocyclic Carbene Ligands as Mimics of Imidazoles/Histidine for the Stabilization of Di-and Trinitrosyl Iron Complexes. *Inorg. Chem.* **2011***, 50*, 8541-8552.

23. Mazak, R.; Collins, R. Mössbauer Studies of Iron Organometallic Complexes. VII. The Iron (− II) Tetrahedral Compounds. *J. Chem. Phys.* **1969***, 51*, 3220-3225.

24. Sanina, N. A.; Rakova, O. A.; Aldoshin, S. M.; Shilov, G. V.; Shulga, Y. M.; Kulikov, A. V.; Ovanesyan, N. S. Structure of the neutral mononuclear dinitrosyl iron complex with 1, 2, 4-triazole-3-thione [Fe (SC2H3N3)(SC2H2N3)(NO) 2]· 0.5 H2O. *Mendeleev Communications* **2004***, 14*, 7-8.

25. Tsai, M.; Tsai, F.; Lu, T.; Tsai, M.; Wei, Y.; Hsu, I.; Lee, J.; Liaw, W. Relative binding affinity of thiolate, imidazolate, phenoxide, and nitrite toward the {Fe (NO) 2} motif of dinitrosyl iron complexes (DNICS): the characteristic pre-edge energy of {Fe (NO) 2} 9 DNICS. *Inorg. Chem.* **2009***, 48*, 9579-9591.

26. Yeh, S.; Lin, C.; Liu, B.; Tsou, C.; Tsai, M.; Liaw, W. Chelate-Thiolate-Coordinate Ligands Modulating the Configuration and Electrochemical Property of Dinitrosyliron Complexes (DNICs). *Chemistry-A European Journal* **2015***, 21*, 16035-16046.

27. Shih, W.; Lu, T.; Yang, L.; Tsai, F.; Chiang, M.; Lee, J.; Chiang, Y.; Liaw, W. New members of a class of dinitrosyliron complexes (DNICs): The characteristic EPR signal of the six-coordinate and five-coordinate {Fe (NO) 2} 9 DNICs. *J. Inorg. Biochem.* **2012***, 113*, 83-93.

28. Tsai, M.; Hsieh, C.; Liaw, W. Dinitrosyl Iron Complexes (DNICs) Containing S/N/O Ligation: Transformation of Roussin's Red Ester into the Neutral {Fe (NO) 2} 10 DNICs. *Inorg. Chem.* **2007***, 46*, 5110-5117.

29. Tsou, C.; Lu, T.; Liaw, W. EPR, UV− Vis, IR, and X-ray Demonstration of the Anionic Dimeric Dinitrosyl Iron Complex [(NO) 2Fe (μ-StBu) 2Fe (NO) 2]-: Relevance to the Products of Nitrosylation of Cytosolic and Mitochondrial Aconitases, and High-Potential Iron Proteins. *J. Am. Chem. Soc.* **2007***, 129*, 12626-12627.

30. Yeh, S.; Lin, C.; Li, Y.; Hsu, I.; Chen, C.; Jang, L.; Lee, J.; Liaw, W. Insight into the dinuclear {Fe (NO) 2} 10 {Fe (NO) 2} 10 and mononuclear {Fe (NO) 2} 10 dinitrosyliron complexes. *Inorg. Chem.* **2012***, 51*, 4076-4087.

31. Lu, T.; Lai, S.; Li, Y.; Hsu, I.; Jang, L.; Lee, J.; Chen, I.; Liaw, W. Discrimination of mononuclear and dinuclear dinitrosyl iron complexes (DNICs) by S K-edge X-ray

absorption spectroscopy: insight into the electronic structure and reactivity of DNICs. *Inorg. Chem.* **2011***, 50*, 5396-5406.

32. Lancaster, K. M.; Roemelt, M.; Ettenhuber, P.; Hu, Y.; Ribbe, M. W.; Neese, F.; Bergmann, U.; DeBeer, S. X-ray emission spectroscopy evidences a central carbon in the nitrogenase iron-molybdenum cofactor. *Science* **2011***, 334*, 974-977.

33. Lu, T.; Weng, T.; Liaw, W. X-Ray Emission Spectroscopy: A Spectroscopic Measure for the Determination of NO Oxidation States in Fe–NO Complexes. *Angewandte Chemie International Edition* **2014***, 53*, 11562-11566.

34. Berto, T. C.; Speelman, A. L.; Zheng, S.; Lehnert, N. Mono-and dinuclear non-heme iron–nitrosyl complexes: Models for key intermediates in bacterial nitric oxide reductases. *Coord. Chem. Rev.* **2013***, 257*, 244-259.

35. Tsai, F.; Kuo, T.; Liaw, W. Dinitrosyl Iron Complexes (DNICs) Bearing O-Bound Nitrito Ligand: Reversible Transformation between the Six-Coordinate {Fe (NO) 2} 9 [(1-MeIm) 2 (η2-ONO) Fe (NO) 2](g= 2.013) and Four-Coordinate {Fe (NO) 2} 9 [(1-MeIm)(ONO) Fe (NO) 2](g= 2.03). *J. Am. Chem. Soc.* **2009***, 131*, 3426-3427.

36. Wecksler, S. R.; Mikhailovsky, A.; Korystov, D.; Ford, P. C. A two-photon antenna for photochemical delivery of nitric oxide from a water-soluble, dye-derivatized iron nitrosyl complex using NIR light. *J. Am. Chem. Soc.* **2006***, 128*, 3831-3837.

37. Wecksler, S. R.; Hutchinson, J.; Ford, P. C. Toward development of water soluble dye derivatized nitrosyl compounds for photochemical delivery of NO. *Inorg. Chem.* **2006***, 45*, 1192-1200.

38. Chiang, C.; Darensbourg, M. Y. Iron nitrosyl complexes as models for biological nitric oxide transfer reagents. *JBIC Journal of Biological Inorganic Chemistry* **2006***, 11*, 359-370.

39. Vanin, A. F. Endothelium-derived relaxing factor is a nitrosyl iron complex with thiol ligands. *FEBS Lett.* **1991***, 289*, 1-3.

40. Jenkins, R. M.; Singleton, M. L.; Leamer, L. A.; Reibenspies, J. H.; Darensbourg, M. Y. Orientation and Stereodynamic Paths of Planar Monodentate Ligands in Square Planar Nickel N2S Complexes. *Inorg. Chem.* **2010***, 49*, 5503-5514.

41. Tonzetich, Z. J.; Héroguel, F.; Do, L. H.; Lippard, S. J. Chemistry of Nitrosyliron Complexes Supported by a β-Diketiminate Ligand. *Inorg. Chem.* **2011***, 50*, 1570-1579.

42. Lu, T.; Chen, C.; Liaw, W. Formation of the Distinct Redox-Interrelated Forms of Nitric Oxide from Reaction of Dinitrosyl Iron Complexes (DNICs) and Substitution Ligands. *Chemistry-A European Journal* **2010**, *16*, 8088-8095.

43. Feelisch, M.; Stamler, J. S. Donors of nitrogen oxides. *Methods in nitric oxide research* **1996**, *71*, 107-108.

44. Burgova, E. N.; Tkachev, N. A; Adamyan, L. V.; Mikoyan, V. D.; Paklina, O. V.; Stepanyan, A. A.; Vanin, A. F. Dinitrosyl iron complexes with glutathione suppress experimental endometriosis in rats. *Eur. J. Pharmacol.* **2014**, *727*, 140-147.

45. Skodje, K. M.; Kwon, M.; Chung, S. W.; Kim, E. Coordination-triggered NO release from a dinitrosyl iron complex leads to anti-inflammatory activity. *Chem. Sci.* **2014**, *5*, 2374-2378.

46. Kelland, L. The resurgence of platinum-based cancer chemotherapy. *Nature reviews.Cancer* **2007**, *7*, 573-584.

47. Vanin, A. F.; Burbaev, D. S. Electronic and Spatial Structures of Water-Soluble Dinitrosyl Iron Complexes with Thiol-Containing Ligands Underlying Their Ability to Act as Nitric Oxide and Nitrosonium Ion Donors. *Journal of Biophysics* **2011**, *2011*, 878236.

48. Vanin, A. F. Dinitrosyl iron complexes with thiol-containing ligands as a "working form" of endogenous nitric oxide. *Nitric Oxide* **2016**, *54*, 15-29.

49. Shamova, E. V.; Shishlo, L. M.; Gorudko, I. V.; Aleksandrova, E. N.; Cherenkevich, S. N.; Shumaev, K. B. Effect of Dinitrosyl Iron Complexes on Platelet Aggregation Induced by HeLa Cervical Carcinoma Cells. *Bull. Exp. Biol. Med.* **2011**, *150*, 372-374.

50. Gaston, B.; Reilly, J.; Drazen, J. M.; Fackler, J.; Ramdev, P.; Arnelle, D.; Mullins, M. E.; Sugarbaker, D. J.; Chee, C.; Singel, D. J. Endogenous nitrogen oxides and bronchodilator S-nitrosothiols in human airways. *Proc. Natl. Acad. Sci. U. S. A.* **1993**, *90*, 10957-10961.

51. Feelisch, M.; Te Poel, M.; Zamora, R.; Deussen, A.; Moncada, S. Understanding the controversy over the identity of EDRF. *Nature* **1994**, *368*, 62-65.

52. McAninly, J.; Williams, D. L.; Askew, S. C.; Butler, A. R.; Russell, C. Metal ion catalysis in nitrosothiol (RSNO) decomposition. *J. Chem. Soc. , Chem. Commun.* **1993**, 1758-1759.

53. Williams, D. L. The mechanism of nitric oxide formation from S-nitrosothiols (thionitrites). *Chem. Commun.* **1996**, 1085-1091.

54. Dicks, A. P.; Swift, H. R.; Williams, D. L.; Butler, A. R.; Al-Sa'doni, H. H.; Cox, B. G. Identification of Cu+ as the effective reagent in nitric oxide formation from S-nitrosothiols (RSNO). *J. Chem. Soc. , Perkin Trans. 2* **1996**, 481-487.

55. Williams, D. L. H. The chemistry of S-nitrosothiols. *Acc. Chem. Res.* **1999**, *32*, 869-876.

56. Szaciłowski, K.; Stasicka, Z. S-nitrosothiols: materials, reactivity and mechanisms. *Progress in Reaction Kinetics and Mechanism* **2001**, *26*, 1-58.

57. Richter-Addo, G. B. Binding of organic nitroso compounds to metalloporphyrins. *Acc. Chem. Res.* **1999**, *32*, 529-536.

58. Zhang, S.; Melzer, M. M.; Sen, S. N.; Çelebi-Ölçüm, N.; Warren, T. H. A motif for reversible nitric oxide interactions in metalloenzymes. *Nature chemistry* **2016**, *8*, 663-669.

59. Vanin, A. F.; Serezhenkov, V. A.; Malenkova, I. V. Nitric oxide initiates iron binding to neocuproine. *Nitric Oxide* **2001**, *5*, 166-175.

60. Yoshinaga, M.; Ueki, T.; Michibata, H. Metal binding ability of glutathione transferases conserved between two animal species, the vanadium-rich ascidian Ascidia sydneiensis samea and the schistosome Schistosoma japonicum. *Biochimica et Biophysica Acta (BBA)-General Subjects* **2007**, *1770*, 1413-1418.

61. Letelier, M. E.; Martinez, M.; Gonzalez-Lira, V.; Faúndez, M.; Aracena-Parks, P. Inhibition of cytosolic glutathione S-transferase activity from rat liver by copper. *Chem. Biol. Interact.* **2006**, *164*, 39-48.

62. Salazar-Medina, A. J.; García-Rico, L.; García-Orozco, K. D.; Valenzuela-Soto, E.; Contreras-Vergara, C. A.; Arreola, R.; Arvizu-Flores, A.; Sotelo-Mundo, R. R. Inhibition by Cu2 and Cd2 of a mu-class glutathione S-transferase from shrimp Litopenaeus vannamei. *J. Biochem. Mol. Toxicol.* **2010**, *24*, 218-222.

63. Ahmed, A.; Malik, A.; Jagirdar, H.; Rabbani, N.; Khan, M. S.; Al-Senaidy, A. M.; Ismael, M. A. Copper-Induced Inactivation of Camel Liver Glutathione S-Transferase. *Biol. Trace Elem. Res.* **2016**, *169*, 69-76.

64. Cesareo, E.; Parker, L. J.; Pedersen, J. Z.; Nuccetelli, M.; Mazzetti, A. P.; Pastore, A.; Federici, G.; Caccuri, A. M.; Ricci, G.; Adams, J. J.; Parker, M. W.; Lo Bello,

M. Nitrosylation of human glutathione transferase P1-1 with dinitrosyl diglutathionyl iron complex in vitro and in vivo. *J. Biol. Chem.* **2005***, 280*, 42172-42180.

65. Pulukkody, R.; Kyran, S. J.; Bethel, R. D.; Hsieh, C.; Hall, M. B.; Darensbourg, D. J.; Darensbourg, M. Y. Carbon monoxide induced reductive elimination of disulfide in an N-heterocyclic carbene (NHC)/thiolate dinitrosyl iron complex (DNIC). *J. Am. Chem. Soc.* **2013***, 135*, 8423-8430.

66. Ording-Wenker, E. C.; van der Plas, M.; Siegler, M. A.; Bonnet, S.; Bickelhaupt, F. M.; Fonseca Guerra, C.; Bouwman, E. Thermodynamics of the CuII μ-Thiolate and CuI Disulfide Equilibrium: A Combined Experimental and Theoretical Study. *Inorg. Chem.* **2014***, 53*, 8494-8504.

67. Lappin, A. G.; McAuley, A. Reactions between copper(II) and 2-mercaptosuccinic acid in aqueous perchlorate solution. *J. Chem. Soc. , Dalton Trans.* **1978**, 1606-1609.

68. Neuba, A.; Haase, R.; Meyer-Klaucke, W.; Flörke, U.; Henkel, G. A Halide-Induced Copper (I) Disulfide/Copper (II) Thiolate Interconversion. *Angewandte Chemie International Edition* **2012***, 51*, 1714-1718.

69. Miller, M. L.; Ibrahim, S. A.; Golden, M. L.; Darensbourg, M. Y. Adamantane-like Cluster Complexes of Mixed-Valent Copper− Copper and Nickel− Copper Thiolates. *Inorg. Chem.* **2003***, 42*, 2999-3007.

70. Hsieh, C.; Chupik, R. B.; Brothers, S. M.; Hall, M. B.; Darensbourg, M. Y. cis-Dithiolatonickel as metalloligand to dinitrosyl iron units: the di-metallic structure of Ni (μ-SR)[Fe (NO) 2] and an unexpected, abbreviated metalloadamantyl cluster, Ni 2 (μ-SR) 4 [Fe (NO) 2] 3. *Dalton Transactions* **2011***, 40*, 6047-6053.

71. Chaudhuri, P.; Karpenstein, I.; Winter, M.; Lengen, M.; Butzlaff, C.; Bill, E.; Trautwein, A. X.; Floerke, U.; Haupt, H. J. An imidazolate-bridged tetranuclear copper (II) complex: synthesis, magnetic and EPR studies, and crystal structure of [L4Cu4 (Im) 4](ClO4) 4.2 H2O (L= 1, 4, 7-triazacyclononane, Im= imidazolate anion). *Inorg. Chem.* **1993***, 32*, 888-894.

72. Montero, D.; Tachibana, C.; Winther, J. R.; Appenzeller-Herzog, C. Intracellular glutathione pools are heterogeneously concentrated. *Redox biology* **2013***, 1*, 508-513.

73. Sheehan, D.; Meade, G.; Foley, V. M.; Dowd, C. A. Structure, function and evolution of glutathione transferases: implications for classification of non-

mammalian members of an ancient enzyme superfamily. *Biochem. J.* **2001**, *360*, 1-16.

74. Morgenstern, R.; Zhang, J.; Johansson, K. Microsomal glutathione transferase 1: mechanism and functional roles. *Drug Metab. Rev.* **2011**, *43*, 300-306.

75. Tamás, M. J.; Sharma, S. K.; Ibstedt, S.; Jacobson, T.; Christen, P. Heavy metals and metalloids as a cause for protein misfolding and aggregation. *Biomolecules* **2014**, *4*, 252-267.

76. Almar, M. M.; Dierickx, P. J. In vitro interaction of mercury, copper (II) and cadmium with human glutathione transferase pi. *Res. Commun. Chem. Pathol. Pharmacol.* **1990**, *69*, 99-102.

77. Settivari, R.; VanDuyn, N.; LeVora, J.; Nass, R. The Nrf2/SKN-1-dependent glutathione S-transferase π homologue GST-1 inhibits dopamine neuron degeneration in a Caenorhabditis elegans model of manganism. *Neurotoxicology* **2013**, *38*, 51-60.

78. Neuefeind, T.; Huber, R.; Reinemer, P.; Knäblein, J.; Prade, L.; Mann, K.; Bieseler, B. Cloning, sequencing, crystallization and X-ray structure of glutathione S-transferase-III from Zea mays var. mutin: a leading enzyme in detoxification of maize herbicides. *J. Mol. Biol.* **1997**, *274*, 577-587.

79. Denny, J. A.; Darensbourg, M. Y. Metallodithiolates as ligands in coordination, bioinorganic, and organometallic chemistry. *Chem. Rev.* **2015**, *115*, 5248-5273.

80. Furukawa, Y.; Torres, A. S.; O'Halloran, T.,V. Oxygen-induced maturation of SOD1: a key role for disulfide formation by the copper chaperone CCS

    . *EMBO J.* **2004**, *23*, 2872-2881.

81. Bruker, S. APEX2 and SAINT. *Bruker AXS Inc., Madison, Wisconsin, USA* **2007**.

82. SADABS, B. 1; Bruker AXS Inc. *Madison, Wisconsin, USA* **2001**.

83. Sheldrick, G. M. A short history of SHELX. *Acta Crystallographica Section A: Foundations of Crystallography* **2008**, *64*, 112-122.

84. Macrae, C. F.; Edgington, P. R.; McCabe, P.; Pidcock, E.; Shields, G. P.; Taylor, R.; Towler, M.; Streek, J. v. d. Mercury: visualization and analysis of crystal structures. *Journal of Applied Crystallography* **2006**, *39*, 453-457.

85. Farrugia, L. J. WinGX suite for small-molecule single-crystal crystallography. *Journal of Applied Crystallography* **1999**, *32*, 837-838.

86. McBride, D.; Stafford, S.; Stone, F. Chemistry of the Metal Carbonyls. XVI. Synthesis of Dicarbonyldinitrosyliron (0). *Inorg. Chem.* **1962**, *1*, 386-388.

87. Connelly, N. G.; Gardner, C. Simple halogenonitrosyl anions of iron. *J. Chem. Soc. , Dalton Trans.* **1976**, 1525-1527.

88. Kovalevsky, A. Y.; Gembicky, M.; Novozhilova, I. V.; Coppens, P. Solid-state structure dependence of the molecular distortion and spectroscopic properties of the Cu (I) bis (2, 9-dimethyl-1, 10-phenanthroline) ion. *Inorg. Chem.* **2003**, *42*, 8794-8802.

89. Connelly, N. G.; Draggett, P. T.; Green, M.; Kuc, T. A. Synthesis and reactivity of the tetrakis (acetonitrile) nitrosylrhodium dication. *Journal of the Chemical Society, Dalton Transactions* **1977**, 70-73.

90. Victor, E.; Lippard, S. J. A Tetranitrosyl [4Fe–4S] Cluster Forms En Route to Roussin's Black Anion: Nitric Oxide Reactivity of [Fe4S4 (LS3) L′] 2–. *Inorg. Chem.* **2014**, *53*, 5311-5320.

91. Hsieh, C.; Darensbourg, M. Y. A {Fe (NO) 3} 10 trinitrosyliron complex stabilized by an N-heterocyclic carbene and the cationic and neutral {Fe (NO) 2} 9/10 products of its NO release. *J. Am. Chem. Soc.* **2010**, *132*, 14118-14125.

92. Hess, J. L.; Conder, H. L.; Green, K. N.; Darensbourg, M. Y. Electronic effects of (N2S2) M (NO) complexes (M= Fe, Co) as metallodithiolate ligands. *Inorg. Chem.* **2008**, *47*, 2056-2063.

93. Hsieh, C.; Chupik, R. B.; Pinder, T. A.; Darensbourg, M. Y. Dinitrosyl iron adducts of (N 2 S 2) M (NO) complexes (M= Fe, Co) as metallodithiolate ligands. *Polyhedron* **2013**, *58*, 151-155.

94. Tran, C. T.; Skodje, K. M.; Kim, E. Monomeric dinitrosyl iron complexes: synthesis and reactivity. *Progress in Inorganic Chemistry: Volume 59* **2014**, 339-380.

95. Pulukkody, R.; Darensbourg, M. Y. Synthetic advances inspired by the bioactive dinitrosyl iron unit. *Acc. Chem. Res.* **2015**, *48*, 2049-2058.

96. Hess, J. L.; Hsieh, C.; Brothers, S. M.; Hall, M. B.; Darensbourg, M. Y. Self-assembly of dinitrosyl iron units into imidazolate-edge-bridged molecular squares:

characterization including Mossbauer spectroscopy. *J. Am. Chem. Soc.* **2011***, 133*, 20426-20434.

97. Jiang, J.; St. Croix, C. M.; Sussman, N.; Zhao, Q.; Pitt, B. R.; Kagan, V. E. Contribution of glutathione and metallothioneins to protection against copper toxicity and redox cycling: quantitative analysis using MT / and MT−/− mouse lung fibroblast cells. *Chem. Res. Toxicol.* **2002***, 15*, 1080-1087.

98. Gordge, M.; Meyer, D.; Hothersall, J.; Neild, G.; Payne, N.; Noronha-Dutra, A. Copper chelation-induced reduction of the biological activity of S-nitrosothiols. *Br. J. Pharmacol.* **1995***, 114*, 1083-1089.

99. Skodje, K. M.; Williard, P. G.; Kim, E. Conversion of {Fe (NO) 2} 10 dinitrosyl iron to nitrato iron (III) species by molecular oxygen. *Dalton Transactions* **2012***, 41*, 7849-7851.

100. Pulukkody, R.; Chupik, R. B.; Montalvo, S. K.; Khan, S.; Bhuvanesh, N.; Lim, S.; Darensbourg, M. Y. Toward biocompatible dinitrosyl iron complexes: sugar-appended thiolates. *Chemical Communications* **2017***, 53*, 1180-1183.

101. Hung, M.; Tsai, M.; Lee, G.; Liaw, W. Transformation and structural discrimination between the neutral {Fe (NO) 2} 10 dinitrosyliron complexes (DNICs) and the anionic/cationic {Fe (NO) 2} 9 DNICs. *Inorg. Chem.* **2006***, 45*, 6041-6047.

102. Speelman, A. L.; Zhang, B.; Silakov, A.; Skodje, K. M.; Alp, E. E.; Zhao, J.; Hu, M. Y.; Kim, E.; Krebs, C.; Lehnert, N. Unusual Synthetic Pathway for an {Fe (NO) 2} 9 Dinitrosyl Iron Complex (DNIC) and Insight into DNIC Electronic Structure via Nuclear Resonance Vibrational Spectroscopy. *Inorg. Chem.* **2016***, 55*, 5485-5501.

103. Parker, W.; Crosby, G. Assignment of the charge-transfer excited states of bis (N-heterocyclic) complexes of copper (I). *J. Phys. Chem.* **1989***, 93*, 5692-5696.

104. Chen, Y.; Ku, W.; Feng, L.; Tsai, M.; Hsieh, C.; Hsu, W.; Liaw, W.; Hung, C.; Chen, Y. Nitric oxide physiological responses and delivery mechanisms probed by water-soluble Roussin's red ester and {Fe (NO) 2} 10 DNIC. *J. Am. Chem. Soc.* **2008***, 130*, 10929-10938.

105. Tran, D.; Skelton, B. W.; White, A. H.; Laverman, L. E.; Ford, P. C. Investigation of the Nitric Oxide Reduction of the Bis (2, 9-Dimethyl-1, 10-phenanthroline) Complex of Copper (II) and the Structure of [Cu (dmp) 2 (H2O)](CF3SO3) 2. *Inorg. Chem.* **1998***, 37*, 2505-2511.

162

106. Garland, M. T.; Grandjean, D.; Spodine, E.; Atria, A. M.; Manzur, J. Structure of dibromo (1, 10-phenanthroline) copper (II). *Acta Crystallographica Section C: Crystal Structure Communications* **1988***, 44*, 1547-1549.

107. Rademeyer, M.; Turnbull, M. M.; Landee, C. P.; Kunene, M.; Liles, D. C. Crystal structure and magnetic properties of catena-poly [bromido [trans (1S, 2S)/(1R, 2R)-cyclohexane-1, 2-diamine copper (II)]-µ 3-bromido]. *Solid State Sciences* **2012***, 14*, 1106-1110.

108. Wang, B.; Zhong, H. Dichlorido (2, 9-dimethyl-1, 10-phenanthroline-κ2N, N′) copper (II). *Acta Crystallographica Section E: Structure Reports Online* **2009***, 65*, m1156-m1156.

109. Teles, W. M.; Marinho, M. V.; Yoshida, M. I.; Speziali, N. L.; Krambrock, K.; Pinheiro, C. B.; Pinhal, N. M.; Leitão, A. A.; Machado, F. C. Mono-and binuclear copper (II) complexes containing di (2-pyridyl) sulfide (DPS) as chelating ligand: Spectroscopic characterization and crystal structures of [Cu (DPS)(H 2 O) Cl 2]· H 2 O and [{Cu (DPS) Cl} 2 µ-(Cl) 2]. *Inorg. Chim. Acta* **2006***, 359*, 4613-4618.

110. Li, N.; Chen, W.; Guan, Y.; OuYang, Z.; Dong, W. Chlorine anion–π and π−−π− interactions in two tetrazolyl derivative based Cu 2 complexes and quantum chemical calculations. *Inorg. Chim. Acta* **2014***, 409*, 349-352.

111. Ng, N. S.; Wu, M. J.; Jones, C. E.; Aldrich-Wright, J. R. The antimicrobial efficacy and DNA binding activity of the copper (II) complexes of 3, 4, 7, 8-tetramethyl-1, 10-phenanthroline, 4, 7-diphenyl-1, 10-phenanthroline and 1, 2-diaminocyclohexane. *J. Inorg. Biochem.* **2016***, 162*, 62-72.

112. Wansapura, C. M.; Juyoung, C.; Simpson, J. L.; Szymanski, D.; Eaton, G. R.; Eaton, S. S.; Fox, S. From Planar Toward Tetrahedral Copper (Il) Complexes: Structural and Electron Paramagnetic Resonance Studies of Substituent Steric Effects in an Extended Class of Pyrrolate-Imine Ligands. *Journal of Coordination Chemistry* **2003***, 56*, 975-993.

113. Zabel, A.; Winter, A.; Kelling, A.; Schilde, U.; Strauch, P. Tetrabromidocuprates (II)—Synthesis, Structure and EPR. *International journal of molecular sciences* **2016***, 17*, 596.

114. Bryar, T. R.; Eaton, D. R. Electronic configuration and structure of paramagnetic iron dinitrosyl complexes. *Canadian Journal of Chemistry* **1992***, 70*, 1917-1926.

115. Stys, A.; Galy, B.; Starzynski, R. R.; Smuda, E.; Drapier, J. C.; Lipinski, P.; Bouton, C. Iron regulatory protein 1 outcompetes iron regulatory protein 2 in

regulating cellular iron homeostasis in response to nitric oxide. *J. Biol. Chem.* **2011**, *286*, 22846-22854.

116. Yang, W.; Rogers, P. A.; Ding, H. Repair of nitric oxide-modified ferredoxin [2Fe-2S] cluster by cysteine desulfurase (IscS). *J. Biol. Chem.* **2002**, *277*, 12868-12873.

117. Kennedy, M. C.; Antholine, W. E.; Beinert, H. An EPR investigation of the products of the reaction of cytosolic and mitochondrial aconitases with nitric oxide. *J. Biol. Chem.* **1997**, *272*, 20340-20347.

118. Salerno, J. C.; Ohnishi, T.; Lim, J.; King, T. E. Tetranuclear and binuclear iron-sulfur clusters in succinate dehydrogenase: a method of iron quantitation by formation of paramagnetic complexes. *Biochem. Biophys. Res. Commun.* **1976**, *73*, 833-840.

119. Meyer, J. Comparison of carbon monoxide, nitric oxide, and nitrite as inhibitors of the nitrogenase from Clostridium pasteurianum. *Arch. Biochem. Biophys.* **1981**, *210*, 246-256.

120. Welter, R.; Yu, L.; Yu, C. The effects of nitric oxide on electron transport complexes. *Arch. Biochem. Biophys.* **1996**, *331*, 9-14.

121. Rogers, P. A.; Eide, L.; Klungland, A.; Ding, H. Reversible inactivation of E. coli endonuclease III via modification of its [4Fe-4S] cluster by nitric oxide. *DNA repair* **2003**, *2*, 809-817.

122. Sellers, V. M.; Johnson, M. K.; Dailey, H. A. Function of the [2Fe− 2S] Cluster in Mammalian Ferrochelatase: A Possible Role as a Nitric Oxide Sensor. *Biochemistry (N. Y.)* **1996**, *35*, 2699-2704.

123. Ding, H.; Demple, B. Direct nitric oxide signal transduction via nitrosylation of iron-sulfur centers in the SoxR transcription activator. *Proc. Natl. Acad. Sci. U. S. A.* **2000**, *97*, 5146-5150.

124. Foster, M. W.; Cowan, J. Chemistry of nitric oxide with protein-bound iron sulfur centers. Insights on physiological reactivity. *J. Am. Chem. Soc.* **1999**, *121*, 4093-4100.

125. Holm, R.; Lo, W. Structural Conversions of Synthetic and Protein-Bound Iron–Sulfur Clusters. *Chem. Rev.* **2016**, *116*, 13685-13713.

126. Lu, T.; Huang, H.; Liaw, W. Anionic Mixed Thiolate− Sulfide-Bridged Roussin's Red Esters [(NO) 2Fe (μ-SR)(μ-S) Fe (NO) 2]−(R= Et, Me, Ph): A Key

Intermediate for Transformation of Dinitrosyl Iron Complexes (DNICs) to [2Fe-2S] Clusters. *Inorg. Chem.* **2009**, *48*, 9027-9035.

127. Wu, S.; Lu, C.; Chen, Y.; Lo, F.; Wang, T.; Chen, Y.; Yuan, S.; Liaw, W.; Wang, Y. Water-Soluble Dinitrosyl Iron Complex (DNIC): a Nitric Oxide Vehicle Triggering Cancer Cell Death via Apoptosis. *Inorg. Chem.* **2016**, *55*, 9383-9392.

128. Ford, P. C. Polychromophoric metal complexes for generating the bioregulatory agent nitric oxide by single-and two-photon excitation. *Acc. Chem. Res.* **2008**, *41*, 190-200.

129. Hartinger, C. G.; Nazarov, A. A.; Ashraf, S. M.; Dyson, P. J.; Keppler, B. K. Carbohydrate-metal complexes and their potential as anticancer agents. *Curr. Med. Chem.* **2008**, *15*, 2574-2591.

130. Gottschaldt, M.; Schubert, U. S. Prospects of metal complexes peripherally substituted with sugars in biomedicinal applications. *Chemistry-A European Journal* **2009**, *15*, 1548-1557.

131. Sharon, N.; Lis, H. Carbohydrates in cell recognition. *Sci. Am.* **1993**, *268*, 82-89.

132. Mjos, K. D.; Orvig, C. Metallodrugs in medicinal inorganic chemistry. *Chem. Rev.* **2014**, *114*, 4540-4563.

133. Nobili, S.; Mini, E.; Landini, I.; Gabbiani, C.; Casini, A.; Messori, L. Gold compounds as anticancer agents: chemistry, cellular pharmacology, and preclinical studies. *Med. Res. Rev.* **2010**, *30*, 550-580.

134. Reginato, N.; McCrory, C. T.; Pervitsky, D.; Li, L. Synthesis, X-ray crystal structure, and solution behavior of Fe (NO) 2 (1-MeIm) 2: implications for nitrosyl non-heme-iron complexes with g= 2.03. *J. Am. Chem. Soc.* **1999**, *121*, 10217-10218.

135. Rauchfuss, T. B.; Weatherill, T. D. Roussin's Red Salt revisited: reactivity of Fe2 (.mu.-E) 2 (NO) 42-(E= S, Se, Te) and related compounds. *Inorg. Chem.* **1982**, *21*, 827-830.

136. Tsou, C.; Liaw, W. Transformation of the {Fe (NO) 2} 9 Dinitrosyl Iron Complexes (DNICs) into S-Nitrosothiols (RSNOs) Triggered by Acid–Base Pairs. *Chemistry-A European Journal* **2011**, *17*, 13358-13366.

137. Richter-Addo, G. B.; Hodge, S. J.; Yi, G.; Khan, M. A.; Ma, T.; Van Caemelbecke, E.; Guo, N.; Kadish, K. M. Synthesis, characterization, and spectroelectrochemistry

of cobalt porphyrins containing axially bound nitric oxide. *Inorg. Chem.* **1996**, *35*, 6530-6538.

138. Chiang, C.; Lee, J.; Dalrymple, C.; Sarahan, M. C.; Reibenspies, J. H.; Darensbourg, M. Y. Synthesis and molecular structures of mononitrosyl (N2S2) M (NO) complexes (M= Fe, Co). *Inorg. Chem.* **2005**, *44*, 9007-9016.

139. Nagashima, S.; Nakasako, M.; Dohmae, N.; Tsujimura, M.; Takio, K.; Odaka, M.; Yohda, M.; Kamiya, N.; Endo, I. Novel non-heme iron center of nitrile hydratase with a claw setting of oxygen atoms. *Nature structural & molecular biology* **1998**, *5*, 347-351.

140. Ghosh, P.; Quiroz, M.; Wang, N.; Bhuvanesh, N.; Darensbourg, M. Y. Complexes of MN 2 S 2· Fe (η 5-C 5 R 5)(CO) as platform for exploring cooperative heterobimetallic effects in HER electrocatalysis. *Dalton Transactions* **2017**, *46*, 5617-5624.

141. Osterloh, F.; Saak, W.; Haase, D.; Pohl, S. Synthesis, X-ray structure and electrochemical characterisation ofa binuclear thiolate bridged Ni–Fe–nitrosyl complex, relatedto the active site of NiFe hydrogenase. *Chemical Communications* **1997**, 979-980.

142. Pinder, T. A.; Montalvo, S. K.; Hsieh, C.; Lunsford, A. M.; Bethel, R. D.; Pierce, B. S.; Darensbourg, M. Y. Metallodithiolates as Ligands to Dinitrosyl Iron Complexes: Toward the Understanding of Structures, Equilibria, and Spin Coupling. *Inorg. Chem.* **2014**, *53*, 9095-9105.

143. Almaraz, E.; de Paula, Q. A.; Liu, Q.; Reibenspies, J. H.; Darensbourg, M. Y.; Farrell, N. P. Thiolate bridging and metal exchange in adducts of a zinc finger model and PtII complexes: biomimetic studies of protein/Pt/DNA interactions. *J. Am. Chem. Soc.* **2008**, *130*, 6272-6280.

144. Hsieh, C.; Ding, S.; Erdem, Ö F.; Crouthers, D. J.; Liu, T.; McCrory, C. C.; Lubitz, W.; Popescu, C. V.; Reibenspies, J. H.; Hall, M. B. Redox active iron nitrosyl units in proton reduction electrocatalysis. *Nature communications* **2014**, *5*, Art. No. 3684.

145. Holloway, L. R.; Clough, A. J.; Li, J. Y.; Tao, E. L.; Tao, F.; Li, L. A combined experimental and theoretical study of dinitrosyl iron complexes containing chelating bis (diphenyl) phosphinoX (X= benzene, propane and ethylene): X-ray crystal structures and properties influenced by the presence or absence of π-bonds in chelating ligands. *Polyhedron* **2014**, *70*, 29-38.

146. Martin, R.; Taylor, D. Bending of linear nitric oxide ligands in four-coordinate transition metal complexes. Crystal and molecular structure of dinitrosyldithioacetylacetonatocobalt (-I), Co (NO) 2 (SacSac). *Inorg. Chem.* **1976**, *15*, 2970-2976.

147. Gaughan Jr, A. P.; Corden, B. J.; Eisenberg, R.; Ibers, J. A. Crystal and molecular structure of dinitrosyl-bis (triphenylphosphine) ruthenium-hemibenzene, Ru (NO) 2 (P (C6H5) 3) 2.1/2C6H6. *Inorg. Chem.* **1974**, *13*, 786-791.

148. Bhaduri, S.; Sheldrick, G. Dinitrosylbis (triphenylphosphine) ruthenium. *Acta Crystallographica Section B: Structural Crystallography and Crystal Chemistry* **1975**, *31*, 897-899.

149. Haymore, B. L.; Ibers, J. A. Linear vs. bent nitrosyl ligands in four-coordinate transition metal complexes. Structure of dinitrosylbis (triphenylphosphine) osmium (-II) hemibenzene, Os (NO) 2 (P (C6H5) 3) 2.1/2C6H6. *Inorg. Chem.* **1975**, *14*, 2610-2617.

150. Mingos, D.; Ibers, J. A. Crystal and molecular structure of dinitrosylbis (triphenylphosphine) iridium perchlorate,[Ir (NO) 2 (P (C6H5) 3) 2][ClO4]. *Inorg. Chem.* **1970**, *9*, 1105-1111.

151. Kaduk, J. A.; Ibers, J. A. Crystal and molecular structure of dinitrosylbis (triphenylphosphine) rhodium perchlorate,[Rh (NO) 2 (P (C6H5) 3) 2][ClO4]. *Inorg. Chem.* **1975**, *14*, 3070-3073.

152. Wittkamp, F.; Nagel, C.; Lauterjung, P.; Mallick, B.; Schatzschneider, U.; Apfel, U. Phosphine-ligated dinitrosyl iron complexes for redox-controlled NO release. *Dalton Transactions* **2016**, *45*, 10271-10279.

153. Smith, R. C.; Protasiewicz, J. D. A trans-spanning diphosphine ligand based on a m-terphenyl scaffold and its palladium and nickel complexes. *Organometallics* **2004**, *23*, 4215-4222.

154. Alyea, E. C.; Meek, D. W. Four-and five-coordinate nickel (II) complexes with monodentate phosphines. *J. Am. Chem. Soc.* **1969**, *91*, 5761-5768.

155. Zhang, C.; Wang, H.; Klein, A.; Biewer, C.; Stirnat, K.; Yamaguchi, Y.; Xu, L.; Gomez-Benitez, V.; Vicic, D. A. A five-coordinate nickel (II) fluoroalkyl complex as a precursor to a spectroscopically detectable Ni (III) species. *J. Am. Chem. Soc.* **2013**, *135*, 8141-8144.

156. Lozano, A. A.; Sáez, M.; Pérez, J.; García, L.; Lezama, L.; Rojo, T.; López, G.; García, G.; Santana, M. D. Structure and magnetic properties of carbonate-bridged five-coordinate nickel (II) complexes controlled by solvent effect. *Dalton Transactions* **2006**, 3906-3911.

157. GuyáOrpen, A. Synthesis of the 17-electron cations [FeL (L′)(NO) 2] (L, L′= PPh 3, OPPh 3): structure and bonding in four-co-ordinate metal dinitrosyls, and implications for the identity of paramagnetic iron dinitrosyl complex catalysts. *Journal of the Chemical Society, Dalton Transactions* **1996**, 3491-3502.

158. Harris, E. D. Cellular copper transport and metabolism. *Annu. Rev. Nutr.* **2000**, *20*, 291-310.

159. Dokken, K. M.; Parsons, J. G.; McClure, J.; Gardea-Torresdey, J. L. Synthesis and structural analysis of copper (II) cysteine complexes. *Inorg. Chim. Acta* **2009**, *362*, 395-401.

160. Venelinov, T.; Arpadjan, S.; Karadjova, I.; Beattie, J. Properties of the copper (II)-histidine complex obtained after dialysis of human plasma with histidine. *ACTA PHARMACEUTICA-ZAGREB-* **2006**, *56*, 105.

161. Sigel, H.; McCormick, D. B. Structure of the copper (II)-L-histidine 1: 2 complex in solution. *J. Am. Chem. Soc.* **1971**, *93*, 2041-2044.

162. Speisky, H.; Gómez, M.; Carrasco-Pozo, C.; Pastene, E.; Lopez-Alarcón, C.; Olea-Azar, C. Cu (I)–Glutathione complex: A potential source of superoxide radicals generation. *Bioorg. Med. Chem.* **2008**, *16*, 6568-6574.